THESIS FOR THE DEGREE OF DOCTOR OF PHILOSOPHY

IN

MACHINE AND VEHICLE SYSTEMS

Perspectives of Aerodynamic Drag and Cooling Airflow for Heavy-Duty Trucks - Reconsidering European Total-Length Legislation

HELENA MARTINI

Department of Applied Mechanics
CHALMERS UNIVERSITY OF TECHNOLOGY
Gothenburg, Sweden, 2016

Perspectives of Aerodynamic Drag and Cooling Airflow
for Heavy-Duty Trucks -
Reconsidering European Total-Length Legislation

Helena Martini

Department of Applied Mechanics

Chalmers University of Technology

SE-412 96 Gothenburg

Sweden

Telephone +46 (0)31-772 1000

This document was typeset using LaTeX.

Perspectives of Aerodynamic Drag and Cooling Airflow for Heavy-Duty Trucks - Reconsidering European Total-Length Legislation

Helena Martini
Department of Applied Mechanics
Chalmers University of Technology

ABSTRACT

Increasing fuel prices and constantly evolving emission legislation forces the vehicle industry to develop new methods for propelling vehicles and to optimize existing technology. Trucks constitute a significant proportion of the transportation system; consequently it is of great importance to ensure as low an impact as possible on the environment.

The length legislation for trucks in Europe regulates the total length of a vehicle combination, from the front of the cab to the trailing edge of the trailer. The European Cab Over Engine (COE) tractive units are, compared to the conventional designs with a hood, not preferred aerodynamically due to its flat front and relatively sharp edges. If elongating the nose of the COE cab, creating a so-called Soft Nose (SN), potential for improved aerodynamic properties is seen. To improve the transport efficiency, some countries in Europe allow vehicle combinations of up to 25.25m; the aerodynamic properties of these longer vehicles have however not been in much focus historically. This thesis deals with perspectives of aerodynamic drag and cooling airflow for heavy trucks, under the circumstances of reconsidered total length legislation. The potential for design changes of different parts of a complete truck-trailer combination have been evaluated. Computational Fluid Dynamics (CFD) was the main tool for obtaining the results; measurements were used to verify the methods.

The results presented in this thesis showed that there are many areas on a complete truck-trailer combination where substantial drag reductions may be acquired. For longer vehicle combinations, the gap between the cargo-units and the chassis level of the trailer units were large sources of drag, especially in yawed wind-conditions. By design changes of these areas, drag was reduced by significant amounts. Working with the front-end of the COE cab, an elongation of the grille area could result in both improved aerodynamic properties, but also cooling airflow can be enhanced if also considering the layout of the components in the under hood. Without a ducting system, guiding the flow from the grille towards the cooling module, or a movement of the cooling module by the same magnitude as the SN elongation, a large portion of the airflow in the under hood leaked around the cooling module and reduced the cooling capacity. The main conclusion to be made is that there still is much room for aerodynamic improvements on a truck-trailer combination when reconsidering the total-length legislation. Ideally, the tractive units and trailers should be developed as a whole, to maximize the possible aerodynamic reductions.

Keywords: aerodynamic drag, truck-trailer combinations, CFD, cooling airflow, soft nose, under-hood design, inlet duct, outlet duct

LIST OF PUBLICATIONS

This thesis concludes the research carried out from 2009 to 2016 at Chalmers University of Technology. The thesis is based on the following publications, referred to by Roman numerals in the text:

I Martini H., Bergqvist B., Hjelm L., Löfdahl L., *Influence of Different Truck and Trailer Combinations on the Aerodynamic Drag,* SAE Technical Paper 2011-01-0179, SAE World Congress, 2011

Martini and Bergqvist designed the study. Martini performed the simulations, analyzed the results and wrote the first version of the manuscript. The paper was reviewed and revised together with the co-authors.

II Martini H., Bergqvist B., Hjelm L., Löfdahl L., *Aerodynamic Effects of Roof Deflector and Cab Side Extenders for Truck-Trailer Combinations,* SAE Technical Paper 2011-01-2284, SAE Commercial Vehicle Engineering Congress, 2011

Martini and Bergqvist designed the study. Martini performed the simulations, analyzed the results and wrote the first version of the manuscript. The paper was reviewed and revised together with the co-authors.

III Martini H., Bergqvist B., Hjelm L., Löfdahl L., *Aerodynamic Investigation of Gap Treatment- and Chassis Skirts Strategies for a Novel Long-Haul Vehicle Combination,* SAE International Journal of Commercial Vehicles 5 (2), pp. 616-627, 2012

Martini and Bergqvist designed the study. Martini performed the simulations, analyzed the results and wrote the first version of the manuscript. The paper was reviewed and revised together with the co-authors.

IV Martini H., Gullberg P., Löfdahl L., *Comparative Studies between CFD and Wind Tunnel Measurements of Cooling Performance and External Aerodynamics for a Heavy Truck,* SAE International Journal of Commercial Vehicles 7 (2), pp. 640-652, 2014

Martini and Gullberg designed the study. Martini performed the simulations, analyzed the results and wrote the first version of the manuscript. The paper was reviewed and revised together with the co-authors.

V Martini H., Gullberg P., Löfdahl L., *Aerodynamic Analysis of Cooling Airflow for Different Front-End Designs of a Heavy-Duty Cab-over-Engine Truck,* Submitted to SAE International Journal of Commercial Vehicles, 2016

Martini and Gullberg designed the study. Martini performed the simulations, analyzed the results and wrote the first version of the manuscript. The paper was reviewed and revised together with the co-authors.

VI Martini H., Gullberg P., Löfdahl L., *Perspectives of Aerodynamic Drag and Thermal Management for an Elongated Heavy-Duty Cab-over-Engine Truck with Ducted Cooling Air Inlets and Outlets,* Submitted to SAE International Journal of Commercial Vehicles, 2016

Martini and Gullberg designed the study. Martini performed the simulations, analyzed the results and wrote the first version of the manuscript. The paper was reviewed and revised together with the co-authors.

ACKNOWLEDGEMENTS

To *Emilia* and *Vidar*, my little sunshines. When I started the work behind this thesis, you were not even born. Despite the fact that you haven't been around for so many years, I hardly remember not having you in my life. You have made my life joyful and happy, and your contribution to this thesis is not insignificant. To *Johan*, my dear. Thanks for your never-ending support, for always being there, in good times and times of doubt. Without you, this would not have been possible. To *mum* and *dad*, for always being there and for having believe in me, all the way from childhood until where I am today. Last but certainly not least, I would like to thank the rest of my dear *family* and my *friends* for all your support during my years at Chalmers.

NOMENCLATURE

A_f	Vehicle projected frontal area	m^2
C_D	Drag coefficient	$-$
C_L	Lift Coefficient	$-$
c_p	Pressure coefficient	$-$
C_p	Specific heat, at constant pressure	$J/kg\,K$
$c_{p,tot}$	Coefficient of total pressure	$-$
C_v	Specific heat, constant volume	$J/kg\,K$
C_μ	Empirical coefficient	$-$
DC	Drag Counts	$-$
e_0	Total energy	m^2/s^2
F_L	Lift force	N
F_{tot}	Total resistance	N
f_r	Rolling resistance coefficient	$-$
f_p	Porous resistance source term	kg/m^2s^2
g	Gravitational acceleration	m/s^2
k	Turbulent kinetic energy	m^2/s^2
L	Length	m
m	Mass	kg
$\dot{m}$	Mass flow rate	kg/s
P_i	Inertial resistance	kg/m^4
P_R	Power	W
P_v	Viscous resistance	kg/m^3s
Pr	Prandtl number	$-$
p	Pressure	Pa
p_∞	Free-stream pressure	Pa
q	Heat flux	W
R	Specific gas constant	$J/kg\,K$
Re	Reynolds number	$-$
t	Time	s
T	Temperature	K
u	Local velocity	m/s
U	Velocity	m/s
y^+	Dimensionless wall distance	$-$

Greek Letter Symbols

α	Angle	$°$
Δ	Denotes difference	$-$
δ_{ij}	Kronecker delta	$-$
ε	Dissipation	m^2/s^3
λ	Thermal conductivity	W/mK
μ	Dynamic viscosity	kg/ms
μ_t	Turbulent viscosity	kg/ms
ν	Kinematic viscosity	m^2/s
ρ	Density	kg/m^3
τ	Viscous stress	N/m^2
ω	Specific rate of dissipation	$1/s$

ABBREVIATIONS

AC	Air Condition
CAC	Charge Air Cooler
CAD	Computer Aided Design
CFD	Computational Fluid Dynamics
CO	Continuosly Open
COE	Cab Over Engine
CV	Control Volume
DES	Detached Eddy Simulation
DNS	Direct Numerical Simulation
EGR	Exhaust Gas Recirculation
EMS	European Modular System
EU	European Union
EVM	Eddy Viscosity Model
FVM	Finite Volume Method
GCW	Gross Combination Weight
GTT	Group Trucks Technology
HD	Heavy Duty
HS	Horizontal Slots
ID	Inlet Duct
LES	Large Eddy Simulation
LL	Loading Length
MRF	Multiple Reference Frame
NRC	National Research Council
OD	Outlet Duct
OEM	Original Equipment Manufacturer
PID	Property Identification
RANS	Reynolds Averaged Navier Stokes
RSM	Reynolds Stress Model
RTT	Reynolds Transport Theorem
SN	Soft Nose
TTT	Top Tank Temperature
US	United States
UTM	Underhood Thermal Management
VFL	Vehicle Feature Laboratory

x

Contents

Paper VI

1   Introduction

Transportation of goods by trucks constitute a substantial part of the total transportation system over the world. In Europe, the average usage of road transport was 75% in 2013 for inland transports [1]. The remaining percentages constituted rail freight and maritime freight, comprising 18% and 7%, respectively. Since the road transports make such a large part of the total freights, it is of interest to optimize their operation to ensure a safe and efficient transportation method.

The environmental debate has increased significantly in scope and importance over recent years. The overall trend for the crude oil prices the past 50 years has been a constant and rapid increase [2]. The increasing oil prices in combination with more strict emission legislation has meant that the entire vehicle industry had to optimize the existing technology for propelling vehicles, but also to develop new methods for propulsion, which does not rely on fossil fuels. Figure 1.1 shows the development of crude oil prices since 1910.
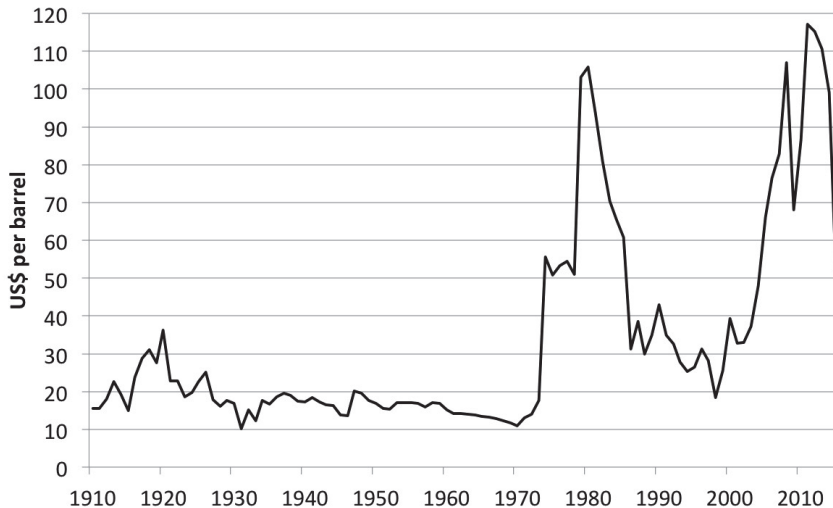
Figure 1.1: Development of crude oil prices over the past 50 years in US\$ per barrel, deflated using the consumer price index for the United States [2].

In 1992, regulations regarding emission levels were introduced by Directive 88/77/EEC, in an attempt to limit the harmful effect of emissions from fossil fuel transports. Since its introduction in the early $1990's$, the permitted

levels of the emissions have developed into lower and lower levels [3]. Figure 1.2 shows the development of emission levels for mono-nitrogen oxides (NO and NO_2, commonly referred to as NO_X) and Particulate Matter (PM) for trucks with a Heavy Duty (HD) diesel engine.
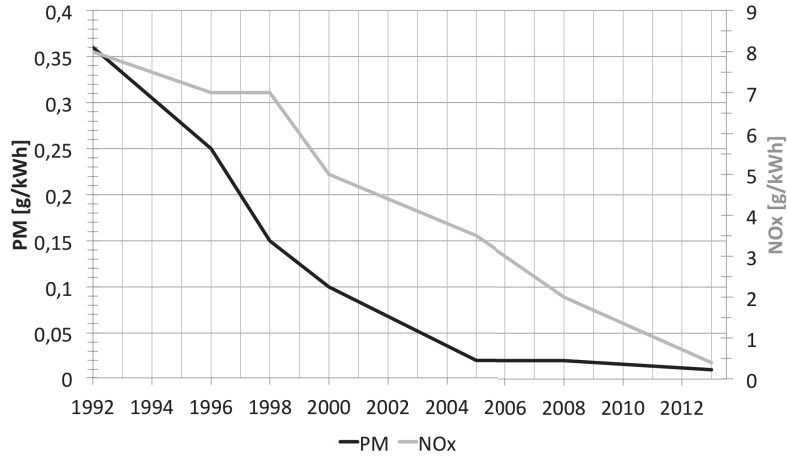
Figure 1.2: Development of emission legislation, for HD Diesel engines in Europe [3].

There are several factors influencing the fuel consumption of a vehicle. Equation 1.1 shows the forces acting on a vehicle in motion, according to Wong [4].

$$F_{tot} = m\frac{dU}{dt} + f_r mg\cos\alpha + mg\sin\alpha + \frac{1}{2}\rho A_f C_D U^2 \qquad (1.1)$$

In Equation 1.1 the first term denotes the resistance of acceleration of the vehicle, due to inertia. The second term is the contribution from rolling resistance; where the rolling resistance coefficient, f_r, is often considered as a constant since it is relatively constant with increasing vehicle speeds [4]. The third part is the contribution from gravitational forces acting on a vehicle when experiencing an inclined road. The last term is the aerodynamic resistance, which is dependent on: the air properties, the frontal area of the vehicle, the velocity of the vehicle and a dimensionless coefficient, C_D. C_D is called the drag coefficient and is used for determining the aerodynamic resistance acting on an object. Sometimes, the product of $C_D A_f$ is also considered, to compare the aerodynamic resistances of different vehicles, since the frontal area is a crucial factor which could increase the aerodynamic resistance significantly. In the strive for a more energy-efficient vehicle, the above described areas are the ones that have to be considered.

1.1 Project Background

Looking into the history of trucks, there was a time where aerodynamics of trucks was not a prioritized area. Trucks were just considered as large, bluff, heavy objects which, compared to passenger cars, travelled at low vehicle speeds. Hence the aerodynamic properties were not considered as especially important; the rolling resistance was considered a larger issue due to its large weight. However, truck aerodynamics is an area which has gained in importance the latest years. Long-haul trucks commonly operate at highway speeds, in some countries up to speeds of $130km/h$ [5]. This emphasizes the importance of aerodynamics of trucks, since major fuel saving may be acquired by proper considerations of the design and layout of the truck-trailer combination. As can be seen in Equation 1.1, the part of the total driving resistance corresponding to the aerodynamic resistance is not increasing linearly with vehicle speed. There is a quadratic behaviour of the aerodynamic resistance, which implies that as the vehicle speed increases, the aerodynamic drag related to the vehicle increases in importance. Hence it is of great interest to reduce this resistance as much as possible, since the aerodynamic drag is directly connected to the fuel consumption of the vehicle. Figure 1.3 shows the relationship of the power required to overcome aerodynamic drag and rolling resistance as a function of vehicle speed.
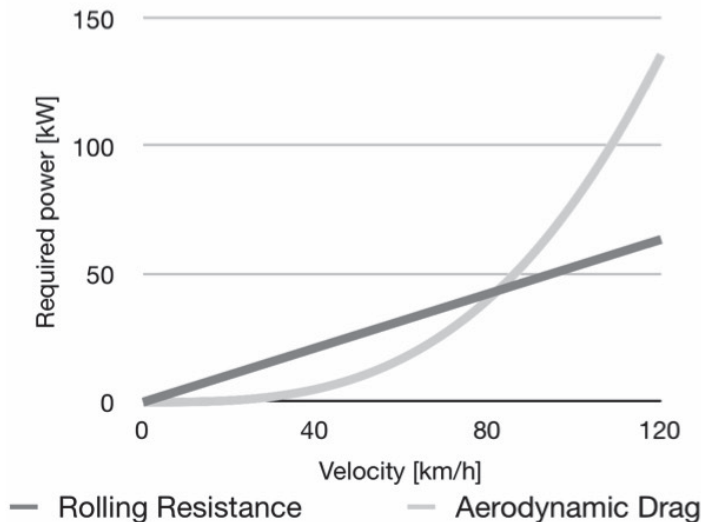
Figure 1.3: Power required for a 40-tonne vehicle combination to overcome the aerodynamic drag and rolling resistance, as a function of the vehicle speed.

As Figure 1.3 shows, the aerodynamic resistance increases in relative magnitude at higher speeds. Above approximately $80km/h$, the aerodynamic drag is a larger contributor to the total driving resistance than the rolling resistance. For heavy trucks, which in the European Union (EU) most commonly operate at speeds in the range of $80 - 90km/h$ [6], it means there is great potential for substantial fuel reductions if the aerodynamic properties can be improved. In the United States (US), trucks are often allowed to drive at higher speeds than

in Europe. The legislation differ between the states in the US; speed limits up to $75mph$ ($\approx 120km/h$) are allowed in some states [7].

The fact that the aerodynamic properties are important also for trucks has been concluded and this area of research has earned its importance. But, there is another issue with truck aerodynamics that still has not been pushed far enough yet, despite its great impact on the overall aerodynamic properties for trucks: the relation between drag improvements made on the tractive unit, the trailer unit, and their combined effect on the entire vehicle. An issue today is that tractive units and trailers are most commonly developed by separate Original Equipment Manufacturer's (OEM's), with no or very little collaboration between these two. The problem with the overall aerodynamics is then evident. The aerodynamic properties of an entire vehicle combination is very dependent on the design of the trailer that is used. The same tractive unit can produce very different overall drag results with different trailers attached to it. What is changed downstream along the trailer, affects the total flow field locally and possibly also globally around the vehicle. The fact that design optimization of the tractive unit makes less sense if a different trailer than the one used in the optimization process is used afterwards, also emphasizes the difficulties faced in the truck industry.

The European Modular System (EMS) is a standardized system for truck-trailer combinations. The use of longer vehicle combinations according to the EMS was the product of a common effort from mainly: Volvo Trucks and the Swedish road authorities, together with the Swedish government, and the EU Commission [8]. The EMS was formed in the 1990's when the EU was formed. The intent of the system was to let the EU member countries keep their own national rules regarding maximum vehicle length. Since the length legislation was different in different countries in Europe, it was decided that the EU countries should adapt to a modular system. The EMS includes several types of tractive units and trailers, together forming different vehicle combinations depending on how these modules are combined. For Sweden and Finland the modular system implied that vehicle combinations up to $25.25m$ could be used, which included a tractive unit, one short and one long module. The remaining countries in EU could use combinations of up to either $16.5m$, for a vehicle combination with a tractive unit and one long module, or $18.75m$, for a vehicle combination with a tractive unit with two short modules. The result of implementing a system where $25.25m$ combinations are allowed was that two $25.25m$ combinations could replace three conventional EU combinations, and the same amount of cargo would be transported, both with respect to volume and weight. The purpose was hence to maximize the load carrying capacity of each vehicle by extending the total length of the vehicle combination, at the same time reducing the number of vehicles on the roads. Several studies have shown that both the fuel consumption and emission levels [9, 10], as well as the logistics system [11, 12], would benefit from the longer vehicle combinations. One opposition against the $25.25m$ combinations would be the possible higher road wear. However, studies have shown that using longer vehicle combinations will not necessarily lead to increased road wear. It may even lead to a decreased road wear for vehicle combinations in some driving conditions as a consequence of lower axle loads per tonne [9].

There is various legislation limiting the maximum length of the vehicle combinations, depending on which part of the world that is considered. The present legislation in Europe regulates the total length of the entire vehicle combination, i.e. from the very front of the cab until the end of the trailer unit, while the legislation in North America limits the length of the trailer unit only. The trailers used on the respective market have been designed according to these legislation with the aim of carrying as much freight as possible simultaneously. The European legislation, limiting the entire length of the vehicle combination, has then lead to the use of Cab Over Engine (COE) tractive units. These cabs have a rather flat front and the engine is mounted below the cab. In North America, where only the trailer unit length is regulated, tractive units of conventional design with a hood are most commonly used instead. The overall shape of a COE tractive unit is not ideal; the conventional cab design would be preferred from an aerodynamic perspective [13]. Even though there are no federal regulations in the North America regarding the length of the tractive units, the states may have different regulations regarding the overall length for particular vehicle combinations [14]. Figure 1.4 shows the two discussed designs for tractive units, the COE and conventional trucks [15].

(a) COE design. Volvo FH16 model.   (b) Conventional design. Volvo VN model.
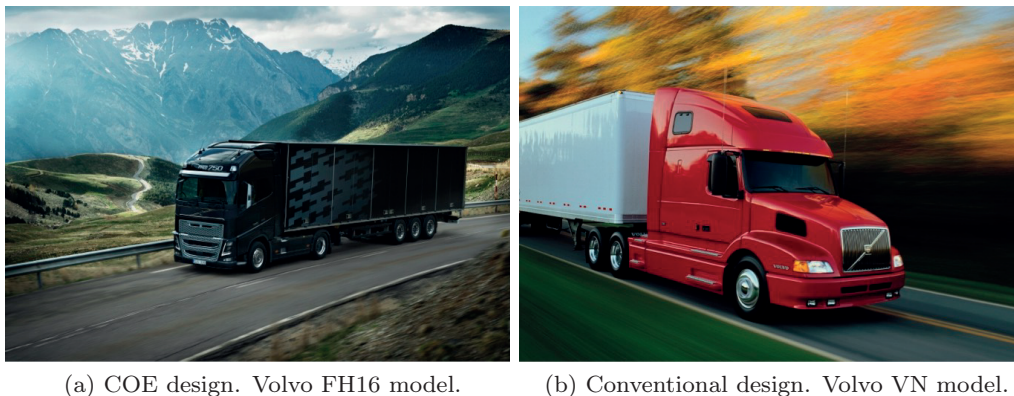
Figure 1.4: COE and conventional tractive units [15].

The non-aerodynamic nature of the COE tractive units may however change in the future. The EU recently introduced a new directive, which would allow for slightly longer vehicles. The extra distance added should be dedicated for aerodynamic and safety improvements of the vehicle. The directive, (EU) 2015/719, states that extension of the total length of the vehicle is allowed for both the front and the rear of the vehicle, in order to make room for these improvements. There is however a stipulation in the directive that if the added devices extends $500mm$ from the original, unmodified vehicle, or if the cab shape is elongated beyond the limits for Directive $96/53/EC$, these vehicles need to be type approved before they can be released onto the market [16].

The area of thermal management and cooling airflow is one major part within the truck development process, which is included in the total aerodynamic performance for a vehicle. Ensuring safe and reliable operation of the truck, it is

of outmost importance to assure sufficient cooling airflow through the heat exchangers in the under-hood area. However, as important it is to ensure sufficient cooling performance at critical driving conditions, it is also of great interest to try to minimize the drag penalty from the cooling airflow, when not all cooling capacity is needed for the specific driving scenario. The cooling airflow goes hand in hand with the external aerodynamic properties and they depend very much on each other. If considering a design change of a tractive unit, the cooling airflow must also be considered and evaluated for different driving scenarios.

Over the years, the engine power for vehicles have increased significantly and hence the cooling demand has increased in corresponding magnitude. At the same time, more focus has been put on the aerodynamic development of vehicles and low-drag vehicle designs have been aimed for. In the strive for a vehicle with low aerodynamic drag, the nose of passenger cars have tended to be moved downwards, resulting in smaller areas available for cooling air intakes [17]. Similar trends have been seen for trucks, where a significant increase in engine power only have resulted in a small increase of the heat exchanger core area. To fulfil the cooling requirements, either the velocity of the air through the cooling module have to be increased, or it requires the development of more efficient heat exchangers. Proper considerations of the cooling airflow in the under-hood compartment hence have to be made in order for the cooling system to be able deliver sufficient amount of cooling.

1.2 Project Objectives

What is limiting the aerodynamic development of trucks today is, to a large extent, the total length legislation that is present. This legislation limit what can be achieved geometrically with the truck and trailers and hence represent the outer boundary conditions that have to be considered. But, as already indicated, the design of the truck and trailer models today have great potential for aerodynamic improvements and hence fuel consumption reductions, if the legislation to some extent was disregarded or changed. Hence the importance of studying and showing the actual gains by a changed total length legislation can be stated.

The work performed within the frames of this thesis have included both thermal management- and external aerodynamic aspects of HD trucks. The main objective of this thesis was to study and quantify the possible reductions in aerodynamic drag by changing the design of the exterior and under hood layout of the truck, under the circumstances of changed total length legislation. The design changes made to the vehicle combinations considered both the rearmost part of the vehicle, as well as changes of the frontal design of the truck and its implications on both external aerodynamics and thermal management. The final question to be answered is: on a complete truck-trailer combination, where is the potential for largest improvements to be found in terms of reduced aerodynamic drag, allowing the present total length legislation to be changed?

2 Theory

This chapter will give an overview of different areas within vehicle aerodynamics important for the understanding of the thesis. Firstly, the area of truck aerodynamics will be treated, including the basic phenomena of the flow around the vehicle as well as different drag-reducing devices commonly used to improve the aerodynamic properties. The cooling airflow for truck applications will then be described. In the end of the chapter, previous research within areas related to the scope of this thesis will be overviewed.

2.1 Aerodynamics of Trucks

Vehicles, such as trucks, produce aerodynamic resistance as they move through the air. It was discussed in the previous chapter that the aerodynamic drag is an important parameter of the total driving resistance, especially for trucks operating at highway speeds.

The Reynolds Number is a dimensionless number of the ratio of inertial forces and viscous forces. It can also be translated into the relation between the pressure and friction forces acting on a body [18]. The Reynolds Number is expressed as in Equation 2.1. In the equation, the shear stress of the fluid has been rewritten as: $\tau = \mu \frac{\partial u}{\partial y}$, proportional to the velocity gradient near the body.

$$Re = \frac{Pressure\ Forces}{Shear\ Forces} = \frac{p - p_\infty}{\tau} \sim \frac{\rho U^2}{\mu \frac{U}{L}} \sim \frac{\rho U L}{\mu} \tag{2.1}$$

In Equation 2.1, the relationship between the dynamic viscosity, μ, and the density, ρ, can be written as $\nu = \frac{\mu}{\rho}$, where ν is the kinematic viscosity. Looking at Equation 2.1, it can be seen that as the Reynolds Number increases by increasing the speed of the flow field, the pressure forces will be more dominant, hence diminishing the effect of the shear forces. If considering the boundary layer, a higher Reynolds number will result in a thinner boundary layer relative to the body, hence the effect of viscosity becomes less important. However, considering the aerodynamic drag force of a truck, considerably separated flow is found and the viscous effects are therefore important.

The aerodynamic drag force can be split into two parts, denoted as pressure drag and friction drag. Pressure drag is defined as the part of the aerodynamic drag originating as a consequence of the pressure difference between the front and rear of the vehicle. Friction drag is defined as the part of the aerodynamic drag due to the shearing action of the air against the vehicle surface. For a

bluff body, such as trucks and vehicles in general, the pressure drag component is considerably larger than the friction drag and only a small portion of the total drag is due to friction [19]. It can further be said that the pressure drag component constitutes between 75% to 95% of the total drag, depending on the type of bluff body that is considered [19].

Trucks, in general, have drag coefficients approximately double that of passenger cars [17]. A key feature for trucks is that they have large frontal areas compared to passenger cars, typically in the range of $8 - 11.5m^2$ [20]. Due to its load carrying nature, where as much cargo space as possible is desired, trucks also have very large side areas. As a consequence of the large ratio of side area vs. frontal area, the aerodynamic properties change in side-wind conditions. Therefore it is not enough to only consider drag coefficients at 0° yaw, or still air conditions, in order to determine the aerodynamic drag for a truck [17]. Barnard [5] also states that the gap between the tractive unit and the trailer produces high aerodynamic resistance, especially in yawed-wind conditions.

Considering aerodynamics of heavy trucks, the greatest concern is the aerodynamic drag. One could also study the aerodynamic lift acting on the truck and trailer, but the magnitude of this parameter is very low compared to the weight of the vehicle combination. For a 40-tonne vehicle combination operating at a highway speed of $80km/h$, with a lift coefficient value of $C_L = -0.05$, this would result in a lift force of $F_L = -150N$. This would result in an downward force corresponding to approximately $15kg$. The insignificance of the lift force for loaded trucks are therefore evident. The cross-wind stability is neither considered as a large issue due to the vehicle combination weight. The cross-wind itself, however, is a crucial parameter for the aerodynamic drag and needs to be studied for drag purposes, as already indicated in this thesis. Other important areas related to the fluid motion around the vehicle combination are aero-acoustics, dirt deposition and visibility aspects.

Figure 2.1 shows a schematic picture of a standard Volvo FH tractor - semi-trailer configuration, divided into three areas with approximate numbers of their impact on the total aerodynamic drag. The percentages have been extracted by normalizing their respective cumulative aerodynamic drag value to the total value of C_D for the combination.
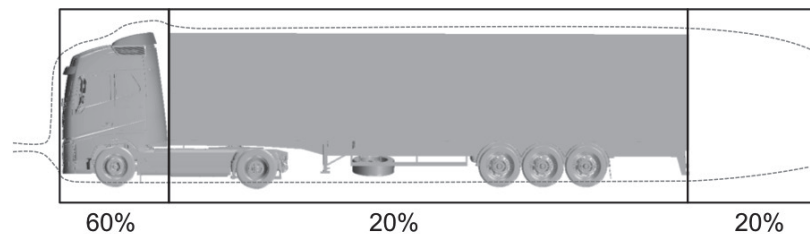

| 60% | 20% | 20% |

Figure 2.1: Schematic figure of the impact of three main areas of a complete vehicle combination on the total C_D value.

According to Figure 2.1, the largest contributor to the total C_D value is the front part of the vehicle. The part of the tractive unit from the grille until the leading

edge of the trailer unit constitutes approximately 60% of the total accumulated drag of the vehicle; the main contributor being the stagnation region in the front. The trailer unit (including a part of the chassis of the tractive unit) and the base wake each constitute approximately 20% of the total C_D value. The largest regions of flow losses, however, do not follow these proportions: the C_D value is coupled to the pressure field on the vehicle surface, while the flow losses are related to the total pressure field around the vehicle. For comparison, the main areas of flow losses around a truck and trailer are found in the base wake, at chassis level along the vehicle and in the gap between the cab and cargo-unit or between two cargo-units.

To be able to reduce the aerodynamic drag for trucks, it has become customary nowadays to add devices to the vehicle with the purpose to better guide the flow around the vehicle body, to reduce the size of the separated regions. The next subsection will treat descriptions of the function of a few common drag-reducing devices for trucks, as well as the main design criteria considered within the truck industry.

2.1.1 Drag-Reducing Devices

There are three main design parameters considering the aerodynamics of tractive units. These are the *corner radius*, the *wedge shape* and the *rake angle* of the wind-screen. The corner radius may be the parameter that earliest was considered; much of the early research for improving truck aerodynamics focused on this. One example is the work performed by Saltzman and Mayer [21], who discussed and agreed on the impression in the truck industry that a drag coefficient value of 0.25 was achievable. The authors also presented previous work carried out at NASA, where front- and rear edge rounding could lead to drag reductions of 73%. Figure 2.2 shows an example of the front-edge rounding conducted in the study.
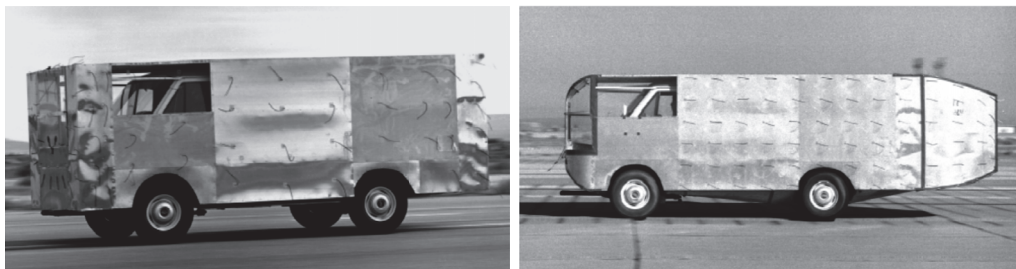
(a) NASA baseline model.   (b) NASA model with rounded front edges and tapered rear-end.

Figure 2.2: Example of front- and rear edge rounding of a truck model, performed by NASA [21].

Historically, relating to the front corner radius of the tractive unit, a common way of linking the flow from the front of the vehicle towards the sides was to

introduce so-called corner vanes. These were used to reduce the aerodynamic drag of the vehicle by postponing separation, in a time in history when the front corner radii were not very large for trucks in general. Nowadays, these corner vanes can still be found on the trucks on the market, however they serve a different purpose: to improve the dirt deposition on the doors, handles and foot steps. Figure 2.3 shows a picture of a Volvo FH cab, where the corner vanes have been integrated in the head lamps [15].

Figure 2.3: Corner vanes on a production type Volvo FH. The vanes are integrated with the head lamps [15].

Considering the wedge shape and rake angle of the tractive unit shape, these parameters are also important for the overall aerodynamic performance and truck OEM's are constantly managing the trade-off between aerodynamic design and packaging space, as well as length- and width requirements for the tractive unit. Even though considerable drag reductions may be achieved by working with the main design parameters, there is still room for improvements at other locations on the truck and trailer units. A description of a few common add-on devices are shown below.

The *roof deflector* is one of the most effective devices of reducing the aerodynamic drag of a truck and trailer model. The roof deflector is placed on the cab roof to guide the flow from the cab onto the trailer roof, preventing the flow to stagnate on the trailer front face. A visual reference is shown in Figure 2.4.

The *cab − side extenders* is another device, which, like the roof deflector, guides the flow from the tractive unit to the trailer unit. The side deflectors are, as the name implies, placed on the sides of the tractive unit, at the rearmost part of the cab, covering a bit of the gap between the tractive unit and the trailer. Especially at yawed wind-conditions, the side deflectors are efficient in reducing drag by preventing the cross-flow of air through the gap. The cab-side extenders are shown in Figure 2.4.

Chassis skirts is another device which is commonly used nowadays, for tractive units as well as for trailers. Its function is to keep the flow attached longer along the sides of the body, preventing interaction with the irregular chassis structure. The devices are, just as the side deflectors, especially efficient in side-wind conditions since they block a large part of the flow which otherwise would interact with the chassis parts. The chassis skirts are displayed in Figure 2.4.

The roof deflector, side deflectors and chassis skirts have become very common devices on trucks today. They are so common that they are often referred to together as a 'full aerodynamic package'. Figure 2.4 shows a picture of a truck with all these aerodynamic devices added.
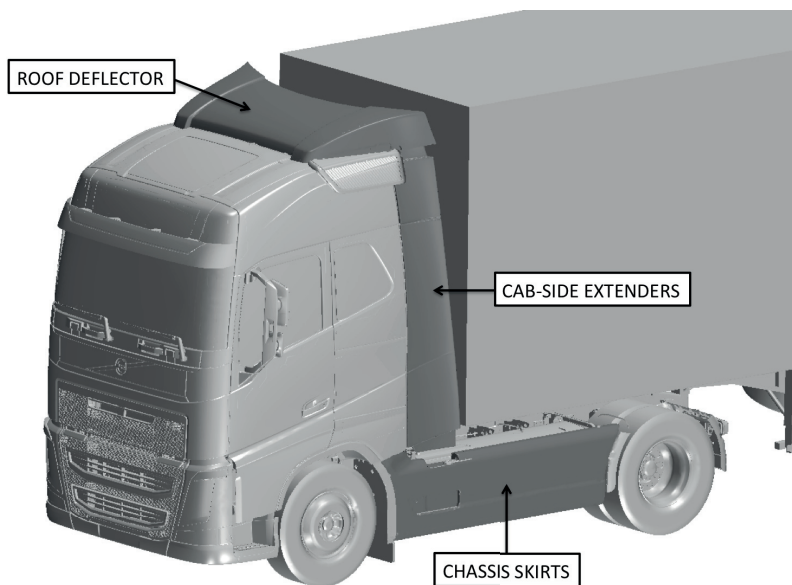
Figure 2.4: Tractor and semi-trailer model with a 'full aerodynamic package': roof deflector, cab-side extenders and chassis skirts. The aerodynamic devices are displayed in dark grey.

The trailer units have a large potential for aerodynamic improvement. Their design may have suffered even more than the tractive unit from neglected aerodynamic properties historically. For example, the very bare underbody of the trailer is not a desired feature with respect to aerodynamics, especially in side-wind conditions. The overall shape of the trailer is basically a box, to be able to store the goods as efficient as possible inside the cargo space. There have been quite a few attempts, however, to work with the overall shape of the trailer unit and reduce the part of the drag originating from the trailer unit. Examples are chassis skirts, boat-tailing of the rear-end of the trailer body and a teardrop-shaped trailer body. Several studies published through the years have shown the efficiency of such devices.

Considering a *boat tail* at the rear end of the trailer body, it is an efficient way of reducing the base wake area by preventing the large separation bubble to

form at the end of the cargo space. The boat tail makes the flow stay attached longer, attaching to the boat tail device that directs the flow towards the centre of the base wake. The base pressure is hence increased by the use of a boat tail and this is the main reason for the drag reduction obtained with this device [22]. The designs of these boat-tails can be different, from large plates directing the flow towards the base wake, to more solid devices with the shape of a bubble that fills up the base area. There are some practical issues with the boat-tail. Since the device is mounted on the rear face of the cargo area, it comprises just the area where the loading and unloading of the trailer is usually made. Another issue is the length legislation, which possibly makes it difficult to fit a boat-tail within the maximum length of the vehicle.

Figure 2.5 shows a tractor - semi-trailer model fitted with chassis skirts for the trailer and a type of base treatment with similar function as a boat tail, here referred to as base plates.
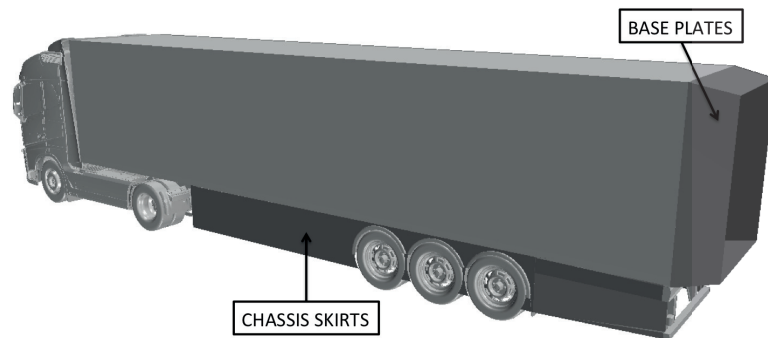
Figure 2.5: Tractor and semi-trailer model with trailer-mounted chassis skirts and a version of a boat-tail: base plates. After Lenngren and Håkansson [23].

The above described areas of aerodynamic improvements of trucks and trailers, mainly concerns the general shape of the cab. Since the $1970's$, the C_D values of tractor - semi-trailer combinations have been reduced by approximately 35% [13], thanks to proper consideration of overall cab shape and usage of roof deflectors, cab side-extenders and chassis skirts. Considering the tractive unit, most of the 'easy' improvements have been done, and to further improve the aerodynamic properties, other areas on the entire truck and trailer combination also have to be included. There are many other areas with great potential for drag improvements. Examples of other areas for heavy trucks that historically have not been considered as much as the cab shape, are the underbody and wheel flows and the under-hood flow including the flow through the heat exchangers. These areas are also large sources of drag and need to be developed in order to further decrease the fuel consumption.

2.1.2 Evaluation Methods for Trucks

There exist several methods of investigating the aerodynamic properties of vehicles; among them are: numerical simulations, wind-tunnel tests and on-road testing. Numerical simulations in the form of Computational Fluid Dynamics (CFD) is a relatively fast and efficient method for determining the aerodynamic behaviour of a vehicle. The method also enables an almost unlimited ability to analyze data later in time, in a different way than before. It has been shown that the results obtained from simulations are accurate if the simulations are performed in a proper manner.

Wind-tunnel tests have historically been important for testing aerodynamic properties, but for such large vehicles as trucks the size of the tunnel is a problem. Due to its size, both with respect to length and width, trucks often create too much blockage in normal wind-tunnels [17]. There are just a few tunnels in the world where a full-size tractor with semi-trailer may be installed that give good results of the test data. Hucho [17] states that reduced-scale wind-tunnel tests are an alternative, but that it takes a model of 1 : 2.5 scale in order to achieve good results, avoiding Mach number problems and achieving a reproducible level of details of the model. It will be appreciated the problems that vehicles measuring $25.25m$ will give instead of the more conventional $16.5m$. For longer vehicle combinations it is even more difficult to perform wind-tunnel measurements. There would both be limitations in the test section length of the wind tunnel, but also the width of the test section when yawing the vehicle combination. It may not be possible at all today if full-size vehicle combinations should be tested, making reduced-scale testing a necessity.

On-road testing is an alternative to wind-tunnel measurements, where the fuel consumption is measured on a test track or on a specific route. Alternatively coast-down testing, where the vehicle is accelerated up to a certain speed, after which neutral gear is selected and the vehicle is slowed by the forces acting on it. The measured variable is the vehicle speed as a function of time, resulting in, for example, the drag coefficient being calculated from the data obtained. The difficulty with on-road testing is that the error margin is rather large due to variations in weather conditions etc. and in order to be able to draw proper conclusions from the tests, differences in results between test cases have to be large.

2.2 Cooling Airflow

Underhood Thermal Management (UTM) is an important area within the development process of new vehicles. With the constant increase of engine horse power, and the introduction of new systems in need of cooling air, UTM just increases in importance. The cooling module of a heavy truck commonly consists of a number of heat exchangers: an Air Condition (AC) condenser, a Charge Air Cooler (CAC) and a radiator. The purpose of an AC condenser is to ensure the climate comfort in the cab compartment. The CAC cools the air exiting the

turbocharger, before it enters the engine for the combustion process. The radiator's task is to cool the coolant flowing through the engine block, preventing the engine from overheating. All these three components need the cooling air flowing through the under-hood area in order to completely fulfil all cooling requirements. In addition to the heat exchangers, there is also a cooling fan added behind the cooling module, to be used for critical cooling situations where not sufficient cooling air can be achieved just by the air passing through the engine bay as a consequence of the ram air. Between the fan and the radiator a fan shroud is mounted, ensuring that the air flow pulled by the fan is actually coming from the radiator and not entering from the sides of the cooling module. Figure 2.6 shows a picture of a cooling module for a heavy truck, including the above described components.
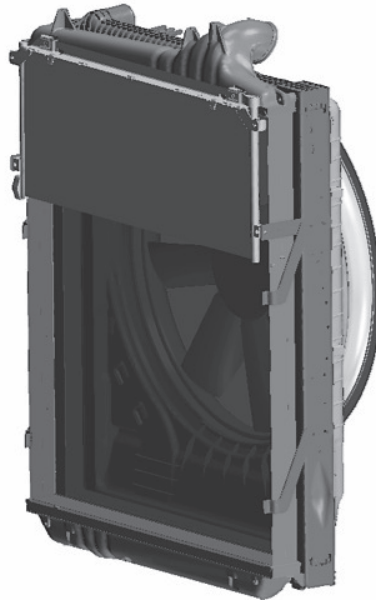
Figure 2.6: Cooling module components for a heavy truck: AC condenser, CAC and radiator. The cooling fan and fan shroud are also shown in the picture.

Figure 2.7 shows a schematic picture of the cooling circuit for a typical heavy truck. There are two different cooling circuits displayed in the model, one for the radiator and one for the CAC. The radiator circuit includes a coolant pump, which transports the coolant through the system. The coolant flows through the engine, and will be heated up due to the combustion process. The coolant exits the engine and reaches the thermostat, which will open if the temperature of the coolant is high enough and let the coolant enter the heat exchanger. If the coolant temperature is too low, the thermostat will not open and the coolant will flow through the engine once again. This process will continue until a temperature of sufficient magnitude is achieved to open the thermostat. The CAC circuit starts at the turbocharger, where the charge air is compressed; resulting in a temperature- and pressure increase of the charge air. To increase

14

the efficiency of the combustion process the compressed charge air enters the heat exchanger, where temperature is decreased and density is increased. After the combustion process, the hot exhaust gases are expanded in the turbine. The useful work resulting from the expansion is then used to drive the compressor. Nowadays, additional thermal management systems are sometimes introduced, such as Exhaust Gas Recirculation (EGR), which requires additional cooling.
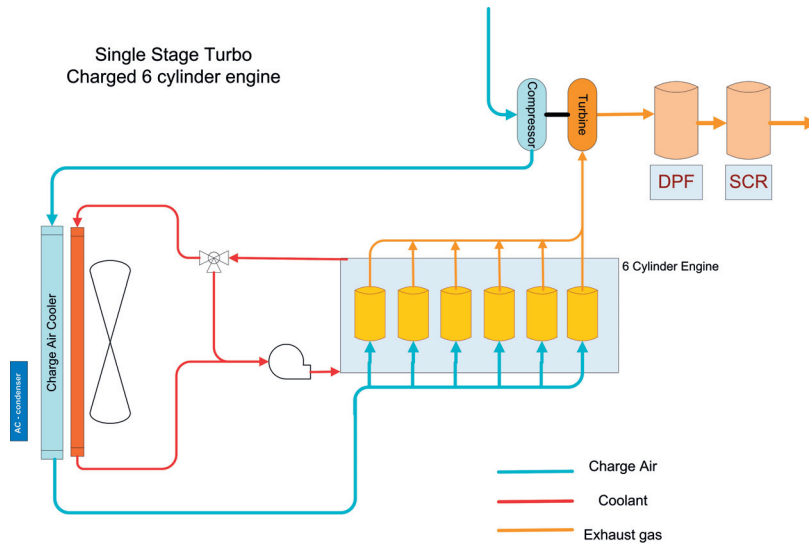
Figure 2.7: Schematic figure of the cooling circuit.

For a full-load operating condition, a cooling module of a heavy truck typically have a heat rejection of $8kW$ for the AC condenser, $80kW$ for the CAC and $220kW$ for the radiator. These values are dependent on the surrounding temperature and the driving condition [24].

It is of major importance for functional reasons to ensure sufficient cooling airflow for any given cooling situation that the vehicle can be subjected to. But, for many driving conditions, not all the available cooling air flowing through the under hood is needed. The irregular under hood of a heavy truck is a known source of aerodynamic resistance. Hence there are possibilities for shutting the entire, or parts of, the cooling airflow in order to reduce the aerodynamic resistance originating from the under-hood area. These kind of arguments have lead to the implementation of grille shutter devices, which controls the amount of air entering the under-hood area and hence the amount of air flowing through the heat exchangers. Several studies [25][26] have indicated that there are potential reductions in drag to be expected with a controlled cooling airflow. The benefits of restricting the amount of cooling airflow entering the under-hood area are not only limited to reducing the aerodynamic drag. The cold start behaviour; the noise level related to the combustion engine; and the fact that the cooling module is better protected from external, possible harmful objects, can be improved with a grille shutter system. Also, the cooling performance can be improved in some cases by directing the flow towards the cooling package, via a duct [26].

The term *cooling drag* is defined as the difference in aerodynamic drag between an open- and closed-grille configuration, and is referred to as the part of the total aerodynamic drag originating from the under-hood flow. By controlling the air flowing through the under hood, the cooling drag proportion can be minimized. The cooling drag for a heavy truck can be up to 8% of the total aerodynamic drag for a vehicle combination [27]. This aerodynamic resistance is a consequence of the external interference of the cooling air, occurring at both the inlet and outlet of the cooling air, as well as the internal momentum losses in the under hood [28]. The proportion of cooling drag for a vehicle combination usually differs depending on which evaluation method used. CFD most commonly over-predicts the cooling drag component, compared to wind tunnel tests where a cooling drag value of 4% is customary. The reason for CFD to over-predict the cooling drag component is partly ascribed to the fact that in CFD, it is possible to perfectly seal the grille intakes of the surface model, preventing any leakage of air through the grille, which in wind tunnel tests is more difficult to achieve. Another explanation is ascribed to the difference in boundary conditions used for CFD and wind tunnel measurements. For CFD, rotating wheels and moving ground is commonly used to simulate on-road conditions. For wind tunnels, however, it is not customary to offer these test conditions for full-scale trucks. The difference in flow field for a moving ground- compared to a stationary ground case is significant, also for the cooling airflow. The absence of moving ground commonly decreases the amount of cooling airflow into the under-hood, hence reducing the cooling drag dependence.

The cooling module for heavy vehicles is commonly found in the front of the vehicle, behind the grille and in front of the engine. The cooling airflow can then be controlled by a grille-shutter system to avoid unnecessary flow losses. There are, however, other solutions to the cooling drag issue. The cooling module could be moved to another location on the vehicle where the ram effect is less significant. Moving the cooling module would put different requirements on the propulsion system; today the engine and cooling fan are mechanically engaged, which may not be the case if reconsidering the cooling module position. There could however be potential for other cooling module locations for hybrid- and electric vehicle configurations, where electrically or hydraulically driven fans can be installed instead. A relocated cooling module also has advantages in terms of ergonomics for the driver: if alternative systems for propelling the vehicle are introduced and the cooling module is relocated, the cab compartment could be lowered, improving the entering and exiting of the cab [29].

2.3   Preceding Work

Most of the work considering aerodynamics of trucks have focused on the tractor - semi-trailer combination, much due to the common use of this vehicle combination. There are however many other vehicle combinations that are present on the roads, with different demands, needs, and aerodynamic properties. The largest differences between the aerodynamics of longer vehicle combinations compared to the conventional tractor - semi-trailer are the extra gap between the cargo-units and the larger exposed side area and irregular undercarriage, especially

in yawed-wind conditions. All these factors are known to increase the drag coefficient and it would be logical to assume that longer vehicle combinations generally show larger drag coefficient values. However, it must be remembered that longer vehicle combinations makes it possible to reduce the number of vehicles on the roads and thereby the fuel economy may be improved. It is still of considerable interest improve the aerodynamic properties of these longer vehicle combinations to minimize the damaging effects of fossil fuel on the environment.

Gilhaus, Hau, Künstner and Potthoff [30, 31] performed several studies during the 1970's and 80's which dealt with the aerodynamics of truck-trailer combinations. Yaw angle dependence, also in combination with different roof deflectors and cab-trailer gaps was investigated. Gilhaus et al [30] showed a schematic figure of the flow field around a tractor with semi-trailer and a truck with trailer and it was revealed that the gap between the two cargo-units for the truck with trailer was disturbing the flow field and gave rise to losses in this region. The study by Gilhaus et al [30] also included methods for improving the flow structure in the gap between two cargo-units.

Göhring and Krämer [32, 33] carried out aerodynamic studies for different kinds of trucks, both wind tunnel measurements and road tests were performed. The studies included investigations of different trailer heights, front-edge rounding and roof deflector configurations. The results from the investigations showed that substantial drag reductions may be achieved with proper considerations of the analyzed parameters.

An area which is rather closely related to the aerodynamics of longer transport concepts is convoy driving. A study carried out by Watkins and Vino [34] shows the effects of vehicle spacing on the aerodynamic properties. It has earlier been shown that the inter-vehicle spacings have a considerable effect on drag. Today discussions regarding Intelligent Transport Systems (ITS) are in progress. In these systems, technologies such as distance sensing and fly-by-wire makes it possible for vehicles to operate in close formation, suggesting that drag reductions may be achievable. Watkins et al [34] found that for two Ahmed bodies in tandem with 30° slant back angles the results changed considerably with the distance between the two bodies. The authors concluded that due to the interest of new transport systems, such as ITS, further work is required to fully appreciate the interaction effects, in order to better understand the function of two bodies in tandem.

An investigation by Browand and Hammache [35], examined the interaction of two truck shapes in tandem, both for block-shaped objects that approximately resemble trucks, and more realistic truck models with wheels and tractor-trailer gap. The results showed that drag reductions between $10-40\%$ may be achieved for closely spaced block-shaped objects. Browand et al [35] found that the magnitude of the drag reductions were highly depending on the separate drag coefficients of the trucks, and also how the truck models were arranged. The authors also claim that the results obtained from the more realistic truck models were more modest; a total drag reduction of $15-20\%$ was achieved.

Cooper [22] investigated aerodynamic development strategies for trucks and analyzed their efficiency. For example, Cooper examined the efficiency of tractor and trailer chassis fairings on a tractor-semi-trailer and he found that chassis skirts attached to both the tractor and the trailer yielded substantial drag reductions, especially in yawed-wind conditions since they help to block the flow which otherwise would interact with the irregular shaped chassis. For the scale-model tests performed, it was found that the double-trailer combination with added skirts to the entire truck and trailer model, showed larger drag reductions obtained over the entire range of tested yaw angles compared to the tractor - semi-trailer model tested. Cooper [22] also reported that by a combined system of roof deflector and cab side extenders, aerodynamic drag reductions in the range of $0.15 \leq \Delta C_D \leq 0.25$ can be achieved in a wind-averaged scenario. By rounding the edges of the front-end of the tractive unit or use simple front-edge fairing, drag reductions of $0.15 \leq \Delta C_D \leq 0.20$ can be expected. Compared to the early tractive units with squared edges, which had C_D values of approximately $0.8 - 1.0$ in the wind-averaged measure, the magnitudes of these possible reductions are evident.

A study by Castellucci and Salari [36] investigated tractor-trailer gap flow and the influence of cab side-extenders for different sizes of the tractor-trailer gap. It was found that for a Reynolds number of 7 million and an incoming flow angle of 6°, cab side-extenders could reduce drag by 2.80%. The authors found that the major drag reduction was experienced by the trailer.

Schoon and Pan [37] investigated practical devices for reducing drag on heavy trucks. The investigation revealed that a 23% aerodynamic drag reduction may be achieved for a tractor-semi-trailer combination by utilizing trailer skirts, base-plates in combination with lengthened side-extenders and air fairings.

Håkansson and Lenngren [23] made a computational analysis of different drag-reducing devices for trailer units. Different base treatment strategies were evaluated, as well as undercarriage fairing and gap treatment devices in the area between the tractor and trailer. The results from the investigation showed that the undercarriage and base region are individually the two most beneficial areas to place the drag-reducing devices, if only making aerodynamic changes to the trailer itself. A combination of trailer chassis skirts and a frame extension in the rearmost part of the trailer (like a boat tail) resulted in a drag reduction of $114DC$ in an averaged wind-condition. One of the conclusions was that it would be preferable if the tractor and trailer units were developed together in order to achieve larger fuel savings. The gap between the tractor and trailer would be redesigned to obtain a smooth transition between the cab and leading edge of the trailer.

The approach of ducting the cooling inlets and outlets for aerodynamic and thermal management purposes is not new, at least not for passenger vehicles. According to Barnard [38] there was a shift in the late $1970's$ towards using some kind of ducted inlet system for the cooling air. Fully ducted cooling airflow systems have traditionally mostly been seen within the motorsport community. A fully ducted cooling system gives the opportunity to control the velocity of the flow through the radiator core, something that is valuable for reducing the

aerodynamic drag. Barnard [38] further discusses the design of outlet ducts and states that by constructing the duct so that the exit area is smaller than the radiator core area would result in a less design-dependent outlet flow path due to a favourable pressure gradient in the duct.

Kuthada and Wiedemann [39] performed investigations of the cooling airflow system for a passenger vehicle. In the study, the authors compared the aerodynamic drag development along the vehicle for an open-grille configuration and one closed-grille configuration. One of the conclusions from this study was that the drag changes associated with the cooling system were seen mostly locally, in the under-hood area. The authors found that after one third of the vehicle until the end of the vehicle, the drag development curves were similar for the two configurations, i.e. the drag reduction obtained in the under-hood region was maintained downstream until the end of the vehicle.

Baeder et al [40] performed comprehensive experimental and numerical studies of a modified SAE body, with different approaches for exiting the cooling air entering the under-hood area. For the configurations with opened cooling airflow, the cooling air could either exit under the vehicle at 45° or 90° relative to the horizontal plane, or at 0° into the base wake area. The results from the study for a SAE squareback model showed that the configuration where the cooling air exited at 0° relative to the horizontal plane, the aerodynamic drag was reduced and also a higher air mass flow rate through the radiator was achieved, compared to its corresponding 45° and 90° configuration. For the SAE notchback model, the 45° results showed the largest drag reductions, but still the 0° configuration had the largest mass flow rate through the radiator.

There have been studies performed for truck applications where attempts of moving the cooling module to alternative positions have been investigated. Larsson et al [41] performed computational studies where the cooling module of a heavy vehicle was moved from its original, frontal position to other parts of the vehicle, and the cooling performance of such a concept was studied. The vehicle considered was a semi-generic HD rigid truck, and two different rear-mounted cooling module installations were evaluated in terms of cooling performance. The rear-mounted cooling modules were placed behind the rear wheels of the truck, below the cargo unit area. The results from the study showed that a rear-mounted cooling module resulted in a lowered aerodynamic resistance and less recirculation of cooling air compared to the reference cooling module position. The authors also concluded that the results were highly dependent on the detailed design of the inlet to the cooling channel. Larsson et al [42] continued the study of the rear-mounted cooling module installations and made a few design changes to the cooling air channels. In the second study, the authors found that for two of the rear-mounted installations, the combined resistance in terms of aerodynamic drag and power required by the fan was lower than for the front-mounted configuration. Even though the fan operation increased for the rear-mounted cases, the aerodynamic winnings were larger than the addition in fan power.

3 Methodology

The work behind this thesis was mainly based on a computational approach. By the use of CFD, the flow field around the vehicle was simulated. CFD is a method based on the Finite Volume Method (FVM). This chapter will describe the function of the numerical method as well as the details of the set-up in the softwares.

3.1 Governing Equations

The methodology is built on the governing equations of fluid flow. These are the continuity equation, momentum equations and energy equation, and they are referred to as the Navier-Stokes equations [43]. The equations are conservation laws, based on the Reynolds Transport Theorem (RTT) . RTT is a fundamental theorem, used to analyze quantities in a Control Volume (CV) instead of analyzing separate masses. For a fix CV, the theorem describes the rate of change of a variable per unit time within the CV, and the flux of the variable passing into and out from the CV [44].

The Navier-Stokes equations are non-linear, partial differential equations. Hence, to directly solve the these equations for a high Reynolds number flow, with all its time dependent properties, would not be practical. There are however examples of low-Reynolds number applications where the entire Navier-Stokes equations have been solved.

For a compressible fluid, the Navier-Stokes equations can be written as in Equations 3.1-3.3 [45].

Continuity Equation:

$$\frac{\partial \rho}{\partial t} + \frac{\partial}{\partial x_j}\left[\rho u_j\right] = 0 \tag{3.1}$$

Momentum Equation:

$$\frac{\partial}{\partial t}\left(\rho u_i\right) + \frac{\partial}{\partial x_j}\left[\rho u_i u_j + p\delta_{ij} - \tau_{ji}\right] = 0 \tag{3.2}$$

Energy Equation:

$$\frac{\partial}{\partial t}\left(\rho e_0\right) + \frac{\partial}{\partial x_j}\left[\rho u_j e_0 + u_j p + q_j - u_i \tau_{ij}\right] = 0 \tag{3.3}$$

21

The viscous stress, τ_{ij}, is defined as in Equation 3.4 for a Newtonian fluid. μ is the dynamic viscosity of the fluid.

$$\tau_{ij} = 2\mu \left(\frac{1}{2} \left(\frac{\partial u_i}{\partial x_j} + \frac{\partial u_j}{\partial x_i} \right) - \frac{1}{3} \frac{\partial u_k}{\partial x_k} \delta_{ij} \right) \tag{3.4}$$

To solve the energy equation, it is also needed to define the density of the fluid, ρ. This can be done with the ideal gas law, which defines ρ as a function of the temperature and pressure. The ideal gas law can be seen in Equation 3.5, where p_{abs} is the absolute pressure ($p_{abs} = p_{static} + p_{ref}$), R is the specific gas constant and T is the temperature [46].

$$\rho = \frac{p_{abs}}{RT} \tag{3.5}$$

To close the system of equations, a few more parameters have to be defined. These are q_j, and e_0. The heat flux, q_j, is given by Fourier's law in Equation 3.6.

$$q_j = -\lambda \frac{\partial T}{\partial x_j} \equiv -C_p \frac{\mu}{Pr} \frac{\partial T}{\partial x_j} \tag{3.6}$$

where Pr is the laminar Prandtl number, defined in Equation 3.7. C_p denotes the specific heat at constant pressure and λ is the thermal conductivity.

$$Pr \equiv \frac{C_p \mu}{\lambda} \tag{3.7}$$

The total energy, e_0, is defined in Equation 3.8.

$$e_0 \equiv e + \frac{u_k u_k}{2} = C_v T + \frac{u_k u_k}{2} \tag{3.8}$$

The above described system of equations are valid for compressible flow, i.e. flows where considerable changes in density are seen. For some of the applications treated in this thesis, the flow can be considered as both isothermal and incompressible and hence simplifications can be made to the Navier-Stokes equations. Due to incompressibility the density variations in the equations can be neglected. For an isothermal flow case, there are no temperature changes in the flow field and hence there is no need to model the energy equation.

As described above, the Navier-Stokes equations are non-linear partial differential equations, which are difficult for engineering purposes to solve directly. There are different methods that can be applied to solve the Navier-Stokes equations, depending on the specific application to be considered. There are the Reynolds-Averaged Navier-Stokes (RANS) approach, the Large Eddy Simulation (LES) and Detached Eddy Simulation (DES), to mention a few. The Direct Numerical Simulation (DNS) is an approach where the entire Navier-Stokes equations are solved directly, with no involvement of turbulence models.

The DNS approach is an extremely expensive method in terms of computational resources and is, as of today, therefore not often seen for industrial purposes.

One of the most widely used approaches for analyzing flow phenomena is to take the time average of the Navier-Stokes equations, a method that is called RANS. The RANS method will be described in the next subsection.

3.1.1 RANS

The RANS equations are obtained by taking the time average of the Navier-Stokes equations. The method of time-averaging the equations is called Reynolds decomposition, and it is accomplished by dividing the unsteady transport parameters into one mean and one fluctuating part (denoted with a 'bar' and 'prime', respectively), see Equation 3.9 where Φ denotes any of the dependent variables. Equation 3.10 shows the expression of the time-averaged variable.

$$\Phi_i = \overline{\Phi}_i + \Phi_i^{'} \tag{3.9}$$

$$\overline{\Phi}_i = \frac{1}{t} \int\limits_0^t \Phi_i \, dt \tag{3.10}$$

By substituting Equation 3.9 into the Navier-Stokes equations described in Equation 3.1-3.3 and using them in the incompressible, isothermal Navier-Stokes equations gives the following resulting expressions for the continuity and momentum equations, shown in Equation 3.11-3.12.

$$\partial_i \overline{u_i} = 0 \tag{3.11}$$

$$\rho \partial_0 \overline{u_i} + \rho \partial_j \left(\overline{u_j u_i} \right) + \rho \partial_j \left(\overline{u_j^{'} u_i^{'}} \right) = -\partial_i \overline{p} + \mu \partial_j \partial_j \overline{u_i} \tag{3.12}$$

The result of the time averaging is a simplification of the Navier-Stokes equations, where only averaged variables are included and the turbulence is present via an additional term. These turbulence terms, often referred to as the Reynolds stresses, need to be modelled since not all of them can be solved directly. This is what is modelled with turbulence models. The theory behind turbulence modelling will be treated in the coming subsection.

For the compressible Navier-Stokes equations, the time averaging of the variables is slightly different. For this averaging, often denoted as the Favre-averaging, a density-weighted averaging decomposition is introduced and applied to u_i and e_0, while a regular time-averaging decomposition is applied for ρ and p as in Equation 3.9. The density-weighted decomposition can be described as in Equations 3.13-3.14 [47].

$$\tilde{\Phi} = \frac{\overline{\rho \Phi}}{\overline{\rho}} \tag{3.13}$$

$$\Phi = \tilde{\Phi} + \Phi^{''} \tag{3.14}$$

The Favre-averaging procedure gives rise to a few more unknown variables after substitution into the Navier-Stokes equations. With a few assumptions of the fluid and the flow, the Favre-averaged Navier Stokes equations together with turbulence models results in a closed system of equations and can be solved numerically.

3.1.2   Turbulence Modelling

There are different ways of modelling turbulence. Two methods are the Reynolds Stress Model (RSM) and the Eddy Viscosity Model (EVM). The RSM solve transport equations for each component in the Reynolds stress tensor. The EVM is a model, which connects the Reynolds stresses with the velocity gradients by means of a turbulent viscosity, μ_t. By the Boussinesq assumption, it is stated that the Reynolds stress tensor, τ_{ij}, is proportional to the mean strain rate tensor, S_{ij}^*[48]. The Boussinesq assumption can be written as:

$$\tau_{ij} = 2\mu_t S_{ij}^* - \frac{2}{3}\rho k \delta_{ij} \tag{3.15}$$

Equation 3.15 can be rewritten as:

$$-\rho \overline{u_i' u_j'} = \mu_t \left(\frac{\partial U_i}{\partial x_j} + \frac{\partial U_j}{\partial x_i} - \frac{2}{3}\frac{\partial U_k}{\partial x_k}\delta_{ij} \right) - \frac{2}{3}\rho k \delta_{ij} \tag{3.16}$$

One of the most common Eddy Viscosity Models is the so-called Two-Equation approach, where two extra transport equations are solved to model the turbulent properties of the flow. There are several Two-Equation models, for example the $k - \varepsilon$ model and the $k - \omega$ model. They both contains two extra transport equations, one for the turbulent kinetic energy, k, and one for the dissipation of turbulent kinetic energy, ε, or the specific dissipation rate, ω. ω is defined as the dissipation rate per unit turbulent kinetic energy [46]:

$$\omega \sim \frac{\varepsilon}{k} \tag{3.17}$$

Furthermore, there are several forms of the $k-\varepsilon$ and $k-\omega$ models. The realizable $k - \varepsilon$ model, implemented by Shih et al [49] has been shown to perform well for industrial approaches. The model predicts drag satisfactorily and due to its implementation the model is stable, and fast convergence is experienced [50]. This model is widely used for automotive applications [20], motivating the usage of this model in this thesis. The key features for the realizable $k-\varepsilon$ model compared to the standard $k-\varepsilon$ model is that it contains a different formulation of the dissipation ε, which is based on the dynamic equation of the mean-square vorticity fluctuation, together with a new eddy viscosity formula involving a parameter C_μ [50].

The work performed in this thesis were mainly based on the realizable $k - \varepsilon$ model and a version of the standard $k - \varepsilon$ model. In the software used for the simulation part of the work, a realizability coefficient has been added to the standard $k - \varepsilon$ model, denoted as the Durbin Scale Limiter. This realizability option has been implemented to overcome the effect that an unexpectedly large growth of turbulent kinetic energy is experienced in stagnation point flows. The Durbin Scale Limiter proposes a lower limit of the turbulent time scale, which imposes the 'realizability' constraint on the eddy viscosity formula [46].

3.1.3 Porous Media Formulation

Throughout all work performed included in this thesis, the models used for the simulations were highly detailed and included all the under-hood components, such as: cooling package including the AC condenser, CAC and the radiator; the engine; and the cooling fan. The cooling module and its components were important parts within the complete vehicle analysis and it was desired to capture the effect of air flowing through the cooling module. The heat exchangers consists of very fine geometry, such as small fins and tubes. To completely resolve all these small structures is a complex task and it would lead to extremely large meshes, which would not be practical for complete-vehicle simulations. Another approach is to model the cooling package components (AC, CAC and radiator) as rectangular volumes with the exact outer measures as the 'real' heat exchangers, and apply a porous media formulation. The porous media formulation assigns a resistance over the cooling module components, to simulate the pressure drop over the heat exchangers [46].

The porous media formulation included parameters which defined the effects of the porous media on the flow field downstream the heat exchanger. The parameters are included in source terms in the momentum equation. The parts that should be modelled as porous media are assigned their own flow region, where co-efficients of flow resistance are added. These co-efficients are then used to calculate the porous source term in the momentum equation. The porous source term is defined as in Equation 3.18.

$$f_p = - \left(P_v + P_i \left| u \right| \right) \cdot u \tag{3.18}$$

In Equation 3.18, P_v and P_i are the viscous and inertial resistance tensors, respectively. The values of the inertial and viscous resistance were obtained by pressure drop measurements over each heat exchanger component; the specific values were obtained from the manufacturer.

3.2 Numerical Set-up

The overall work flow of the CFD process can be divided into three main steps: $pre-processing$, $solving$ and $post-processing$. The pre-processing

part includes Computer Aided Design (CAD) cleaning and generation of surface models, as well as creation of surface mesh and volume mesh inside the computational domain. The solving includes an iterative solving process in the simulation software, where the equations of fluid flow are solved numerically, while the post-processing is the analysis of the results from the simulation, by plotting certain parameters in the flow field or graphs of the development of specific scalars.

This subsection will further on describe the set-up of the computational cases in the simulation softwares. Two main softwares have been used in this work; for pre-processing, ANSA by Beta CAE Systems [51] have been used. The simulations and part of the post-processing have been performed in STAR-CCM+ by CD-adapco [52]. Additional post-processing has also been done with FieldView by Intelligent Light [53].

The CAD geometries of the tractive units, a Volvo FH tractor unit and a rigid truck, as well as the semi-trailer, were available. There were however other models needed for the simulations, that were not available at start. CAD data was not given from the manufacturers for the missing parts, hence these models had to be generated in another way. By using drawings from existing products, the digital geometries of the other models used in the simulations were built from scratch. The models that were generated were a dolly, a link, a centre-axle carrier, a cargo-box for the rigid truck, as well as a special trailer unit used for wind-tunnel measurements. The geometries of the EMS modules were created by viewing drawings from NÄRKO [54] and Parator [55]. However, there were numerous variations of each trailer, dolly and link, with different positions of wheel axles, different heights and lengths. When applicable, one of the most common configurations of the modules was chosen to be used in the studies. The geometry of the trailer unit used for the wind-tunnel measurements was generated by using drawings from internal reports at Volvo Group Trucks Technology (GTT).

Throughout the work behind this thesis, two different cab designs have been used in the analyses. This was a consequence of a design change at Volvo GTT and the launch of the new Volvo FH in 2012. It should be emphasized that no comparisons have been made, within the frames of this thesis, where the aerodynamic drag for the separate cab designs have been compared to each other. For the analyses covered in this thesis, only the differences in C_D between two configurations have been considered and the absolute values of each vehicle combination have been of less interest. It can however be mentioned that the absolute C_D values for two vehicle combinations with the old and the new cab design are similar.

3.2.1 Correlation of CFD Method with Experimental Data

As mentioned previously; performing wind-tunnel measurements for full-scale trucks is a difficult task. Performing numerical simulations of the same truck is not really a simple thing either, but the challenges faced are of different kinds.

Independently of the type of aerodynamic evaluation method used, it is of outmost importance to ensure that the method used is accurate and captures the actual effects of the flow. The choices of models to use for the simulations have been correlated with test data. Prior to starting evaluating the cooling capacity and external aerodynamics properties for different front-end designs, correlation studies were conducted. Both the approach for simulating the external aerodynamics, as well as the method for cooling performance analysis, have been correlated with respective measurements performed by Volvo GTT [56]. In the correlation study, full-scale wind tunnel measurements were correlated with CFD, where simulations were run with a truck in the National Research Council (NRC) wind tunnel [57]. Different turbulence models were tested and evaluated, and the truck and trailer was simulated at different yaw angles of the wind. Similarly, the cooling performance simulations were correlated with chassis dynamometer data from the Volvo Vehicle Feature Laboratory (VFL) climatic tunnel. For the cooling performance simulations, four different operating points were evaluated, all of them were steady-state points commonly used for characterizing cooling performance. The results from the simulations showed in general good agreement with measured data and the differences between CFD and measured data were stated. The correlation study can be further studied in the paper by Martini et al [58], and the simulation set-up will be described in more detail in the following subsections.

The methodology used for Papers $I - III$ [59, 60, 61] differs slightly from the one used in the latter part of the project. At the time when the simulations for Papers $I - III$ were conducted, the methodology used was based on the 'best practice' available. The deviations from the methodology described in this section can be further studied in the respective paper [59, 60, 61].

3.2.2 Pre-processing

The creation of new geometries of the missing geometries, the CAD cleaning and initial surface meshing was performed using the software ANSA [51]. The models were wrapped, re-meshed and volume meshed in STAR-CCM+ [52].

Generation of Surface Models

For the main part of the simulations, where specific geometries were to be analyzed in terms of aerodynamic properties and cooling capacity, open-road conditions were aimed for. This means that the computational domain used in the simulations was designed to be sufficiently large not to affect the flow field around the vehicle. The extension of the open-road domain was based on recommendations from Z. Chronéer, Volvo GTT [62]. The extension of the calculation domain was 2.5 times the combination length upstream, 5 times the combination length downstream, 12 times the vehicle width in lateral direction and 5 times the vehicle height in vertical direction. The size was held constant for all open-road simulations, with the domain size dimensioned for the longest vehicle combination tested.

Simulations have also been run where the calculation domain should resemble an actual wind-tunnel geometry; the complete study can be found in [58]. In the case where the Volvo VFL geometry was used, this geometry was available from Volvo GTT. Correlation studies have also been performed for test results from the NRC wind tunnel in Canada [57], where full-scale wind tunnel tests have been performed. For these simulations, the geometry of the test section was available from NRC, but the rest of the parts were drawn manually according to drawings and photos of the wind tunnel. Upstream of the test section, a contraction area was created, and upstream of this contraction a symmetrical elongation of the tunnel was created, in order for the flow field to stabilize before entering the contraction area. Downstream of the test section a diffusor was created, followed by a symmetrical elongation of the diffusor downstream. Both the contraction area and the diffusor were created to resemble the actual geometry of the NRC wind tunnel.
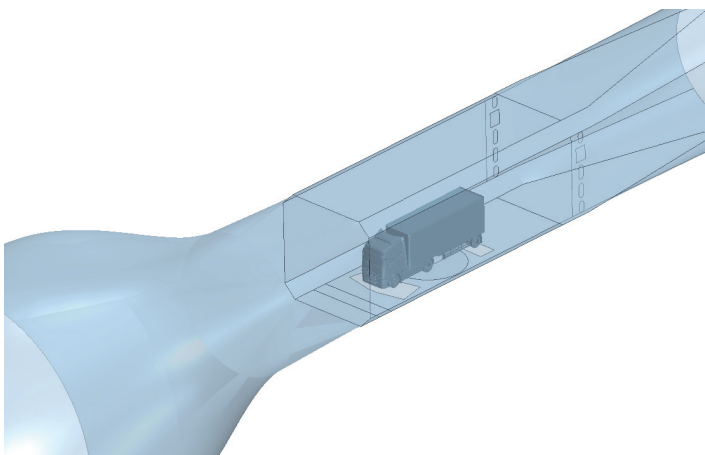
Examples of the computational domains used for the simulations can be seen in Figure 3.1.
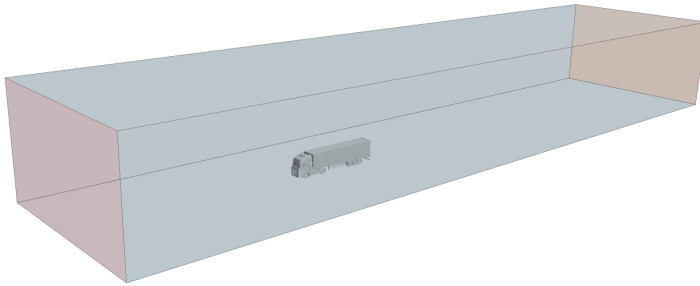
(a) Domain used for open-road conditions.
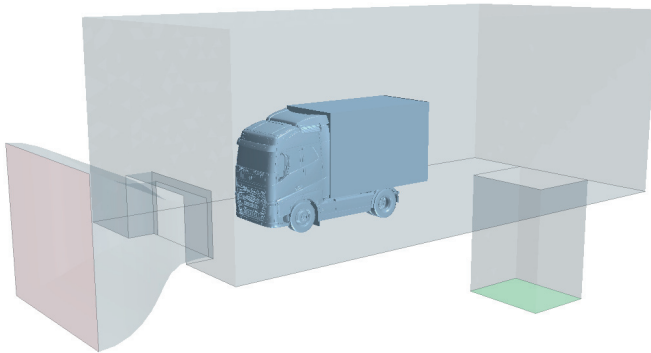
(b) Volvo VFL tunnel.

(c) NRC wind tunnel. The entire domain is not displayed in the figure.

Figure 3.1: Computational domains used for the simulation models.

Surface Mesh

In order to be able to build a volume mesh between the model and the computational domain, a surface mesh needed to be generated for all parts of the model. The geometry of the vehicle is by the transition from CAD to surface mesh approximated by a triangular representation of the surface. It is of great importance to ensure a good quality of the surface mesh used, since this is what will be used in the simulation later on. Both the quality of the cells themselves, as well as the cell density is important for the quality of the results. Poor representation of the surface of the model will hence yield simulation results of low accuracy.

For the computations acquired in this thesis, the initial surface meshing was performed in ANSA, and the file of the surface mesh was exported to STAR-CCM+. In STAR-CCM+ the surface mesh was re-generated and this was performed in two steps: firstly, the vehicle model was wrapped in order to obtain a closed geometry without any small holes etc.; in the second step a surface mesh was applied to the wrapped surface. This surface mesh was then used as the reference, to build the volume mesh from.

The surface meshes of the vehicle models were controlled by setting minimum and target lengths of the surface cells, to be able to refine certain parts of the model that require smaller cells to be used. The entire vehicle model was divided into several smaller parts, called Property Identifications (PID's), to better be able to control the resolution of the surface/volume mesh in this region. Different PID's can also be assigned different boundary conditions etc. in the simulation software, so for example for the computational domain walls, the wheels of the truck and trailer models and the cooling module, need to be distinguished by dividing the model into smaller components to be able to control the set-up of the model and assign proper boundary conditions.

Volume Mesh

The volume meshes were hexahedral dominant, using the STAR-CCM+ Trimmer model. The model uses automatic curvature and proximity refinement and the mesh could be aligned with a user defined coordinate system. This type of mesher uses the Octree method; which is an approach where the computational domain is divided into cubes, which are refined until the desired user-defined resolution is reached. The cells are bisected for each subdivision and the result is a mesh with a smooth variation in cell size [23]. The final volume mesh mainly consists of hexahedral cells, with trimmed cells closest to the surface of the model. Visually, the trimmed cells look like hexahedral cells with one or more corners that are cut off, but they are truly polyhedrals [46].

Another feature of the trimmer mesh is that the mesh can be locally refined in wake regions, by applying the STAR-CCM+ Trimmer Wake Refinement model. By the use of this method, the mesh is locally refined downstream of selected surfaces; the size of the mesh is controlled by setting desired refinement size and

growth parameter. Additionally, the resolution of the calculation domain was controlled by a number of refinement boxes that were added around the vehicle model with different levels of refinement. An example of the extension of these zones can be seen in Figure 3.2. There was one refinement zone in the front grille area to resolve the forward stagnation region, and for the cases with two cargo-units there was an additional refinement zone in between the units. Also the areas around the rear-view mirrors, at ground level along the entire vehicle and the base wake were controlled by refinement zones.

The work behind this thesis has been conducted during a relatively long period of time. During this time, available computer capacity has increased substantially, enabling a higher mesh density for the simulations. For a standard simulation of a tractor - semi-trailer model, the cell count has increased almost by a factor of 3. It should be noted that awareness of this discrepancy has been conducted in the analysis of the results. Only results that are truly comparable, i.e. where the mesh set-ups are identical will be discussed.

Generally, the simulations run at any non-zero yaw angle, resulted in slightly increased number of volume cells. This was a consequence of the adjustment of the refinement zones on the leeward side of the vehicle, to account for the larger wake areas on this side of the vehicle.

Examples of the mesh resolution can be seen in Figures 3.2 and 3.3, both further from the vehicle and near the vehicle surface.
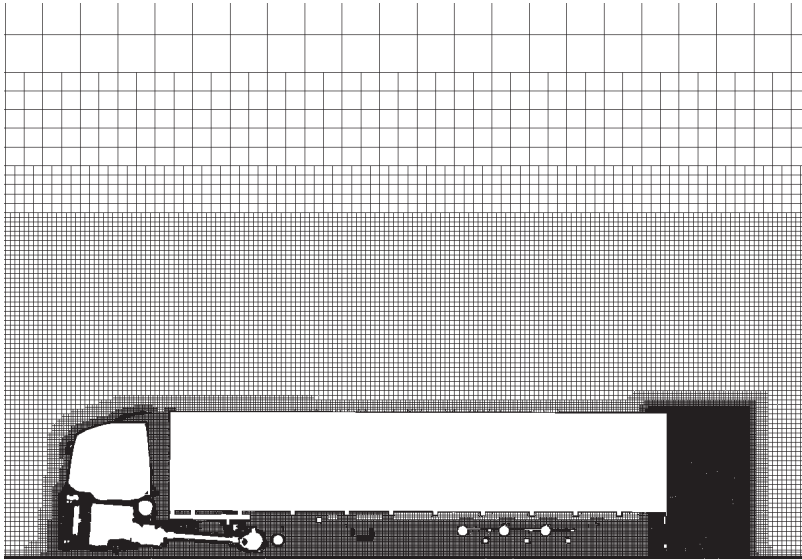

Figure 3.2: Volume mesh around the model, shown in a plane along the centre-line. The entire calculation domain is not visualized.
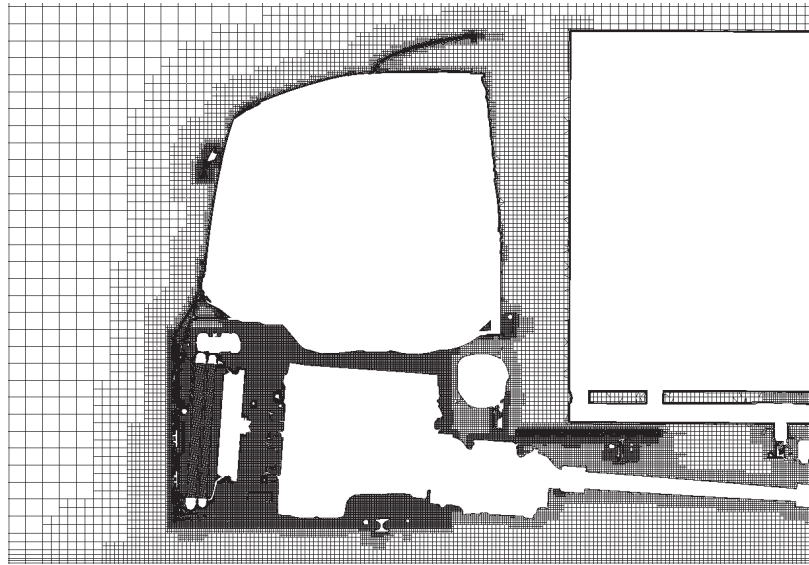
Figure 3.3: Example of the volume mesh near the vehicle model, shown in a plane along the centreline.

Grid Dependency

Grid dependency studies were conducted throughout the work. The presented grid dependency study was performed for one of the COE models in the later part of the work. Different grid refinement levels were evaluated and the absolute values of C_D were monitored and compared to each other; it was then straightforward to see how the aerodynamic drag force prediction was varying with mesh density and a desired level of resolution was found. Figure 3.4 shows the variation of C_D with number of cells in the simulation model. Each C_D value was compared to the C_D value for the configuration where the desired level of resolution was found (marked with a cross in the graph).
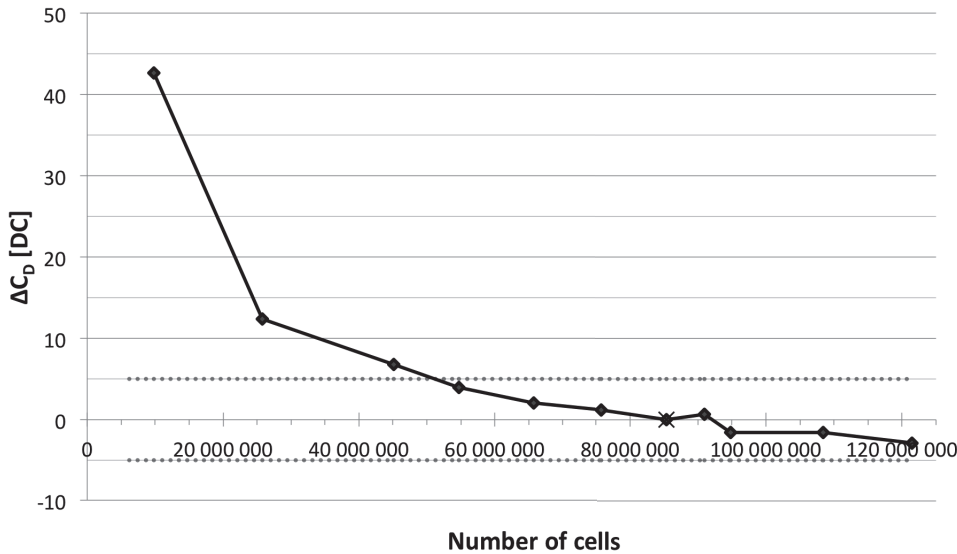
Figure 3.4: Mesh dependency study; ΔC_D as a function of number of cells in the simulation model.

According to Figure 3.4, it was clear that the absolute levels of C_D were different depending on the mesh resolution. Though, it was found that for a grid resolution above $55 millions$, the variation of C_D was very small and the curve flattened out considerably. The variation in C_D compared to the chosen refinement level was $\pm 2DC$ for mesh sizes between $65 - 120 millions$. The desired level of refinement was found at $85 million$ cells and the rest of the configurations were set up accordingly.

Mesh preparation for yawed wind-conditions

As mentioned previously, the aerodynamic properties change significantly in yawed wind conditions and it is therefore not sufficient to simulate only straight-ahead wind conditions. Therefore, the concept evaluation studies were performed by simulating the flow field at two different flow angles. This was chosen so as to limit the number of simulations; even though it would be preferable to use a larger number of flow angles to achieve a wider perspective of the aerodynamic behaviour in different conditions. It is known that the European average angle of the wind relative to the vehicle direction is between 0° and 5° [63] and therefore it was decided to simulate the flow at both these angles. Performing the analysis in such manner, the change in the flow field around the vehicle could be seen by comparing the 0° and 5° results. Another feature is that it enabled the possibility to, if desired, averaging the drag coefficients and thereby obtain a value of the drag coefficient that somewhat represents average wind conditions.

For the simulations run at yawed-wind conditions, a slightly different meshing approach was employed. The entire calculation domain, that is the virtual wind-tunnel, was rotated at the same degree as desired to simulate. Each case was

meshed with the new wind-tunnel orientation as the mesh coordinate system, with the result that the mean flow would stream axially in and out from the computational cell. An example of the mesh of one of the 5° yaw cases is shown in Figure 3.5. The mesh is displayed in a plane parallel to the ground, at a height of $2500mm$ above ground. Also note the wake refinement areas growing downstream, aligned with the computational domain.
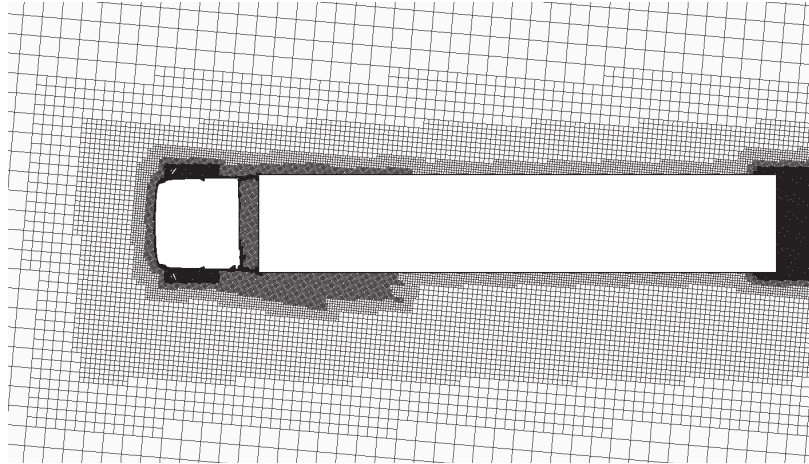

Figure 3.5: Example of one of the volume meshes used for 5° yaw simulations, visualized in a plane parallel to the ground at a height of $2500mm$. Note that the entire calculation domain is not visualized in the figure.

Near-Wall Treatment

In order to accurately account for the viscous effects near the wall, it is a necessity to add so-called prism layers closest to the vehicle surface. The prism cells are needed in order to predict the forces and heat transfer on the walls, but also to determine separation. The separation point is a critical parameter, since it further affects values of aerodynamic drag and pressure drop. In order to obtain an accurate solution of the flow field, the velocity and temperature gradients normal to the wall needs to be resolved. Comparing the results from solutions with different mesh densities, the gradients for a finer mesh will be much steeper in the viscous sublayer for the higher-resolved mesh, compared to what would be indicated by a coarse mesh. By using the prism layer mesher, the viscous sublayer can either be resolved entirely, for $y^+ \sim 1$, or estimated more accurately by the use of wall functions for $y^+ > 30$ [46]. Both approaches have been conducted during the work building up this thesis, and the two approaches are described below.

Prism Layer Approach for $y^+ > 30$

On parts where mostly attached flow was predicted three prism layers were built, with a total height of $6mm$ and a growth rate of 1.2. The height of the first layer was hence set by the growth rate. For the parts where the flow was predicted to be highly separated, such as the chassis of the vehicle and trailers, one prism layer with a height of $1mm$ was used. The Two-Layer All y^+-wall treatment was used, which is recommended by STAR-CCM+. The Two-Layer approach is a model that offers considerable mesh flexibility. The model may be used for meshes solved for High-Reynolds number models, as well as for finer meshes (low-Reynolds number type) and it will also produce the least inaccuracies for meshes where $1 < y^+ \leq 30$. [46]. Figure 3.6 shows an example of the mesh structure for the prisms with a total height of $6mm$.
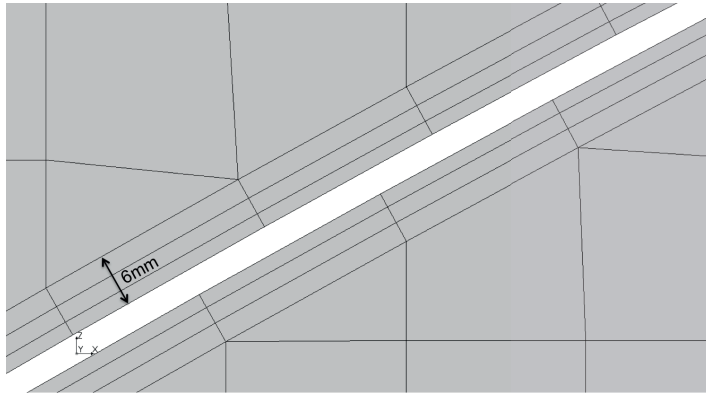

Figure 3.6: Prism structure, total height of $6mm$.

Prism Layer Approach for $y^+ \sim 1$

For this approach, the aim was to achieve y^+ values below 1 in regions where mostly attached flow was expected. This meant that 10 layers with a total height of $16mm$ was created; the near-wall layer was set to a height of $0.04mm$ and the layers were then built according to these specifications. As for the high-y^+ value approach, the parts of the model where mainly separated flow was predicted, one prism layer with a height of $1mm$ was generated. The Two-Layer All y^+-wall treatment was used in this method as well. Figure 3.7 shows a visualization of the mesh built with the approach of completely resolving the viscous sublayer.
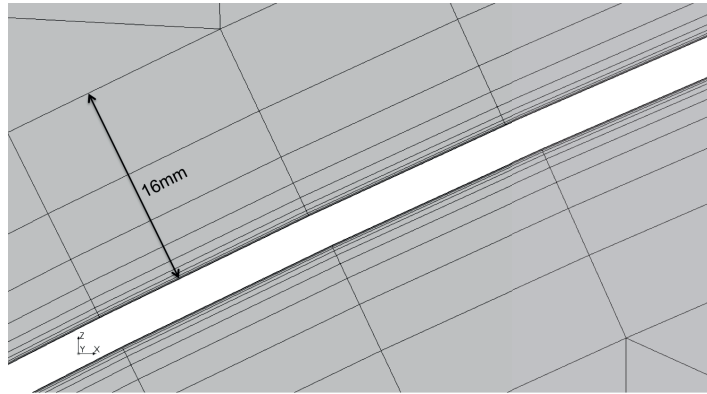
Figure 3.7: Prism structure, total height of 16*mm*.

3.2.3   Solving

The simulations were run in STAR-CCM+, versions 4, 5, 8 and 9 throughout the work.

The boundary conditions used for the computational domain and vehicle model are shown in Table 3.1, being valid for all simulations and yaw angles where open-road conditions were applied. Information about the cooling fan and how the rotation of this component was modelled is described in a coming subsection.

Table 3.1: Boundary conditions used in the computational model.

Surface	Boundary Condition
Inlet	Velocity-Inlet
Outlet	Pressure-Outlet
Tunnel ground	Moving wall - Translational velocity
Tunnel walls + tunnel roof	Wall - Slip condition
Wheels	Rotating wall - Rotation rate
Vehicle body	No-slip condition

The *velocity−inlet* boundary condition means that the velocity vector is defined directly on the inlet boundary, while the boundary value of the pressure is extrapolated from adjacent cells. The *pressure − outlet* boundary condition fixes the pressure on the outlet boundary. *Wall − slip* condition means that the face value of the velocity is computed by extrapolating the parallel velocity component in the adjacent cell. The *translational velocity* condition means that the tangential velocity is specified with a vector. The *rotation rate* condition used for the wheels is defined as a tangential velocity about a local reference frame. The *no − slip* boundary condition means that the velocity at the wall is explicitly set to zero.

Operating Conditions

Throughout the work, different operating conditions have been applied to simulate specific situations that occur for a long-haul truck during operation. The specific driving situations considered in this thesis distinguishes between 'highway driving'; a non-critical cooling situation where aerodynamic drag perspectives are of major interest, and a 'critical cooling condition'; where the most important task is to ensure sufficient cooling capacity at the specified situation. The two operating conditions are described in more detail below.

Highway Driving

For the analysis of different aerodynamic improvements of the truck-trailer combinations, a driving condition intended to simulate European highway driving was chosen as operating condition. For the isothermal simulations, a constant speed of $90km/h$ was set. The simulations which also included the cooling capacity analysis was simulated at $80km/h$ with an ambient temperature of 10°C, which corresponds to the average daily temperature in Europe [64].

For a part of the simulations, both external aerodynamics and cooling capacity properties were evaluated simultaneously. For these cases, it was also necessary to apply heat exchanger models and describe the operating condition for the cooling system components. The input values to the simulation models were obtained from test data from measurements performed at Volvo GTT and corresponded to a typical highway driving condition. Specific input values for the operating point were added in the simulation software, in terms of mass flow of air entering the CAC, target heat rejection of the radiator, volume flow of coolant in the radiator, fan rotational speed, and the inlet temperature of the charge air into the CAC.

Critical Cooling Condition

The above described driving condition, the 'highway driving', has formed the basis of the work throughout the thesis and this condition has been considered as the target condition to design for. However, for the applications where thermal management issues were considered, it was not sufficient to simulate the highway driving scenario. Even though the evaluated concept did result in satisfying cooling capacity for the highway driving, this is not right away also valid for more critical cooling situations. Therefore, for some cases also a set of simulations were run where critical cooling performance parameters were evaluated. The driving conditions used to characterize cooling performance were typical points where maximum engine power was exerted, the ambient temperature was high and the vehicle was operating at low vehicle speeds.

The free-stream velocity of the cooling air was set to $36km/h$ and the ambient temperature was 38°C. The cooling performance was evaluated at four different operating points, all of them critical for establishing sufficient cooling performance. The engine speeds of these operating points were $1100rpm$, $1300rpm$, $1500rpm$ and $1800rpm$. All four operating points are steady state points that are commonly used for characterizing the cooling performance [65]. In similar manner as for the external aerodynamics simulations with active heat exchanger models, specific values of heat the heat exchanger operation were added to the software. The values of the parameters were obtained from test data at Volvo GTT.

3.2.4   Heat Exchanger Modelling

As described in Chapter 3.1.3, the heat exchanger surface was modelled as porous media and the details about this can be found there. To include cooling performance analysis, a heat exchanger model was implemented in the simulation. The STAR-CCM+ Actual Dual Stream heat exchanger model [46] was used to evaluate the heat exchange between the hot and cold cores. The hot core is defined as the part of the heat exchanger where the coolant and charge air is flowing, whereas the cold core is defined as the part where air passes through the heat exchanger to cool the coolant and charge air. By defining heat exchanger interfaces between the hot and cold cores for the CAC and radiator, the heat exchange between the hot and cold cores was calculated. Via the interfaces, the heat exchanger model also used information about the specific heat exchanger components that were used. Files including the mass flow through the hot and cold cores, and the corresponding heat-transfer rate were therefore provided to the simulation model.

The Actual Dual Stream Heat Exchanger Model in STAR-CCM+ uses the flow and energy values that are obtained from the simulation itself, to compute the mean temperature difference and the heat transfer coefficient over the heat exchanger area.

3.2.5   Modelling Fan Rotation

For the simulations run with active heat exchanger models, the fan rotation needed to be considered in order to accurately predict the flow field in the under-hood area. There are several ways of modelling this rotation. For the work included in this thesis, the Multiple Reference Frame (MRF) model was used to model the fan rotation in the simulations. This model is a frozen rotor method. The user defines a control volume around the fan, and the model simulates the effect of rotation on a stationary mesh inside this control volume. The MRF method is used to obtain a steady-state approximation of the relative motion between different parts, a phenomenon which otherwise is highly transient. By this method, the run-time is reduced to a large extent and, if used properly the quality of the results are similar to far more time consuming approaches [52]. The size of the control volume, or MRF region, is a sensitive parameter for the

accuracy of the results. The choice of MRF region size was made in accordance with results from Gullberg et al [66].

For the isothermal simulations, where only the external aerodynamics was considered, there was no discernable need of rotating the fan. Hence, the cooling fan was stationary for these simulations.

3.2.6 Output Parameters

Depending on which type of simulation that was performed, different parameters were used to analyze the results. These are briefly described below.

Aerodynamic Drag

For the external aerodynamics simulations, the output parameter of most importance naturally was the C_D value of the analyzed configurations, where the ΔC_D values between two configurations were used to compare different cases. The ΔC_D values were most commonly referred to in the unit Drag Counts (DC), defined in Equation 3.19.

$$DC = 1000 \cdot \Delta C_D \qquad (3.19)$$

To compare two configurations with each other, it was also convenient to extract the accumulated drag along the entire vehicle, to see where differences in the aerodynamic behaviour occurred. The accumulation curve was created by taking the local drag value at discrete points along the vehicle surface, which were added to the previous extracted value.

Yet another approach for evaluating different configurations in terms of C_D, was to divide the total drag coefficient into fractions, originating from different parts of the vehicle. By adding up the local C_D values for different PID's of the model, partial C_D values were extracted for, for example, the cab and the tractive unit.

Radiator Top Tank Temperature (TTT)

For the simulations run with active heat exchanger models, to evaluate the cooling capacity the parameter of most interest was the TTT value. The TTT value is defined as the temperature of the coolant at the point it enters the heat exchanger, defined in °C. For the studies performed in this thesis, a TTT value below 100°C when the fan was disengaged, was the target value in order for a concept to be considered as a practically feasible.

Air Mass Flow Through Heat Exchangers

The mass flow of air, $\dot{m}$, through each of the cooling module components (AC condenser, CAC and radiator) was another parameter of interest to evaluate together with the TTT values, in the analysis of different layouts in the under hood.

4 Results

The results presented here are the product of the six papers appending this thesis [59, 60, 61, 58, 67, 68]. A summary of the findings from the mentioned publications are shown, to merge the results in order to find out where the most promising areas for improvements are found, in terms of reduced aerodynamic drag and improved thermal management. The terms and conditions for these improvements to be implemented would be a change of the European total length legislation, in order to make room for the geometrical changes needed.

Unless otherwise stated, the vehicle combination that the results are compared to was the tractor - semi-trailer configuration, often referred to as the 'standard European combination'.

4.1 Airflow Characteristics of Truck and Trailer Combinations

The results from the first paper appending the thesis [59] formed the basis for the succeeding studies and put the subject of truck-trailer aerodynamics in context. The aerodynamic properties of different truck and trailer combinations were evaluated and the results showed that there were significant differences in the flow field, depending on which vehicle combination that was considered.

The vehicle combinations analyzed were built up from different tractive units, cargo units and supportive structures such as dolly and link models. Figure 4.1 shows the six vehicle combinations with defined abbreviations. Each abbreviation is described in Table 4.1. More detailed information of the vehicle combinations and the modules they are built from can be seen in Appendix A.

Table 4.1: Abbreviations of modules used for assembling the vehicle combinations.

T	Tractor
R	Rigid
S	Semi-trailer
C	Centre-axle trailer
W	Swap body

(a) TS: Tractor - semi-trailer.

(b) TSC: Tractor - semi-trailer - centre-axle trailer.

(c) TWS: Tractor - swap body - semi-trailer. Commonly referred to as 'B-double' [8], or as 'Tractor - link - semi-trailer'.

(d) RW: Rigid - swap body.

(e) RWC: Rigid - swap body - centre-axle trailer. Also referred to as 'Truck - centre-axle carrier' in [8].

(f) RWS: Rigid - swap body - semi-trailer. Also referred to as 'Truck, dolly and semi-trailer' in [8].

Figure 4.1: Overview of the vehicle combinations used in the analysis.

By running simulations of the six different vehicle combinations described above, the aerodynamic properties for each combination were established. The results can be seen in Figure 4.2, for both 0° and 5° yaw of the incoming flow relative to the longitudinal axis of the vehicle.
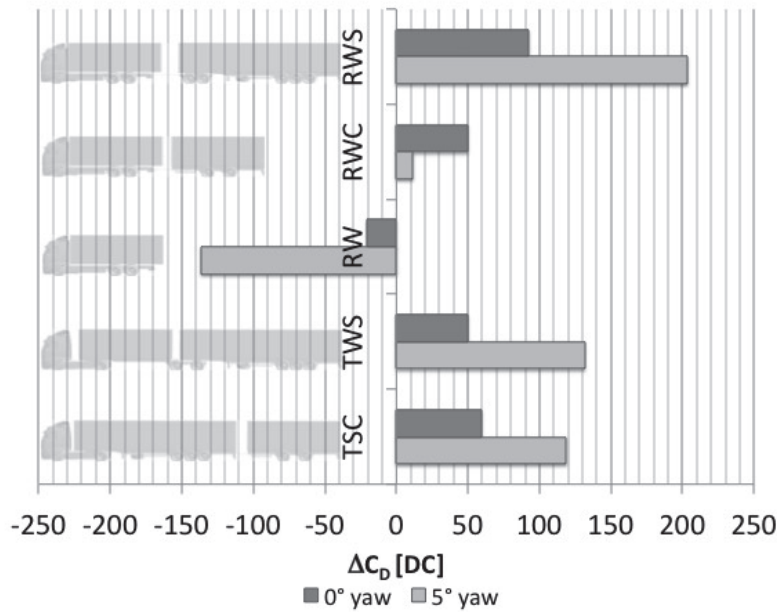
Figure 4.2: Differences in C_D values between the analyzed vehicle combinations for 0° and 5° yaw relative to the reference case, TS (not shown in the figure).

The results in Figure 4.2 revealed that the longest vehicle combinations, that is TSC, TWS and RWS, showed significantly higher drag levels compared to the reference configuration. This effect was particularly strong in 5° yaw conditions; but there was also a large difference between the 25.25m combinations. The rigid truck with a dolly and semi-trailer, RWS, showed a significantly larger drag increase compared to the other 25.25m combinations. This result can be explained by the size of the gap between the two cargo-units. RWS had a gap of almost 1.5m while the two other 25.25m combinations had a gap of under 1m. The impact of the gap size between the units hence seems important, and it will be discussed later.

It can be seen that the increase of C_D in yaw conditions is dependent on the length of the truck-trailer combination. Figure 4.3 shows the percentage increase of the drag coefficient for 5° yaw angle relative the value obtained at 0° yaw.
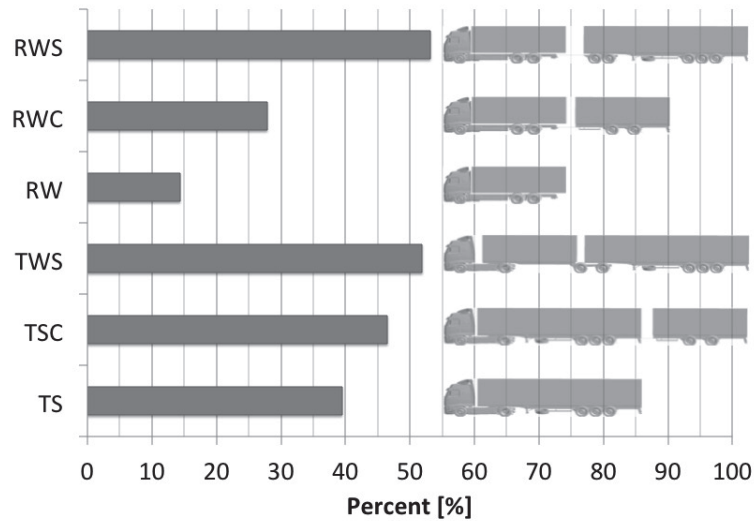
Figure 4.3: Percentage increase in C_D between 0° and 5° yaw angle of the wind.

The results in Figure 4.3 indicated that the three longest vehicle combinations, i.e. TSC, TWS and RWS, are more sensitive to yaw conditions than the other configurations. These configurations show an increase of approximately 50% in the aerodynamic drag coefficient. The shortest combination, RW, shows the lowest dependence of yaw conditions and only increases by approximately 15%. For the remaining configurations slightly contradictive results are obtained. RWC, the rigid truck with a swap body and a centre-axle trailer, has a longer total length than the reference case and should therefore, according to the previously mentioned trend, show a larger sensitivity to yaw conditions than the reference case. Though, RWC has double cargo units which means that it has an extra gap compared to the reference case, yielding a larger value of the drag coefficient at 0° yaw. One reason for the TS combination being more yaw-sensitive than the RWC is that the semi-trailer itself seems to be very sensitive to crosswinds. Its underbody design is rather bare which allows a large amount of air to flow underneath the semi-trailer body, yielding large energy losses in 5° yaw angle. It has been shown by Landman, Wood, Seay and Bledsoe [69] that when closing the gap between the truck and trailer and blocking the cross-flow by sealing the trailer sides with chassis skirts, the rate of drag increase with yaw angle decreases.

By visualizing isosurfaces of total pressure coefficient, $c_{p,tot}$, equal to zero, it is possible to detect areas of high energy-losses, for example separated flow regions, and areas with strong vortices. A smaller volume of the isosurfaces hence indicates that the losses are less. Figure 4.4 shows the isosurfaces of $c_{p,tot} = 0$ for two of the 25.25m combinations (TSC and RWS) at 5° yaw angle.
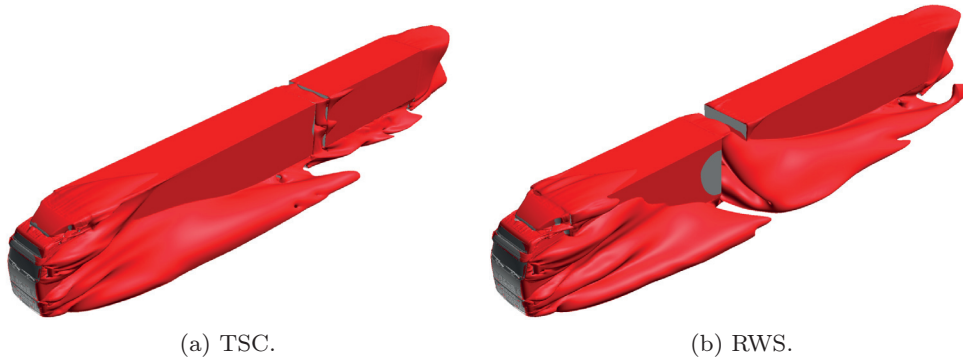
(a) TSC.
(b) RWS.

Figure 4.4: Isosurfaces of $c_{p,tot} = 0$ at 5° yaw.

Figure 4.4 shows that the energy losses associated to the RWS model were of a larger magnitude than for the TSC combination. In particular, the structure of the isosurfaces in the gap between the cargo-units are dissimilar. There was a strong cross-flow of air through the gap for RWS, which was not seen for TSC. This cross-flow appears to be the most important element, explaining why the aerodynamic drag increased so significantly for this vehicle combination. There is also an indication that the very exposed underbody of the semi-trailer may be responsible for the large field of energy losses at chassis level, both at the 1st unit for TSC, and the 2nd unit for RWS.

Drag Force Distribution

Dividing the total drag coefficient along the vehicle: starting with the front part, the gap region, and the rear part of the vehicle, see Figure 4.5, differences in drag accumulation between the configurations can easily be seen. The divisions were made so that: the front region ranged from the front of the tractive unit until the middle of the 1st cargo-unit; the gap region covered the gap and included the middle of each cargo-unit; and the rear region from the second half of the rearmost cargo-unit until the end of the vehicle combination. Figure 4.5 shows all values normalized with the front region partial C_D value for TS. It should be noted that since the cargo-units were of different lengths between the combinations, the lengths of the front region, gap region, and rear region were changing between the cases. The visualization here was included to highlight the aerodynamic behaviour over the gap region, marked in red in Figure 4.5.
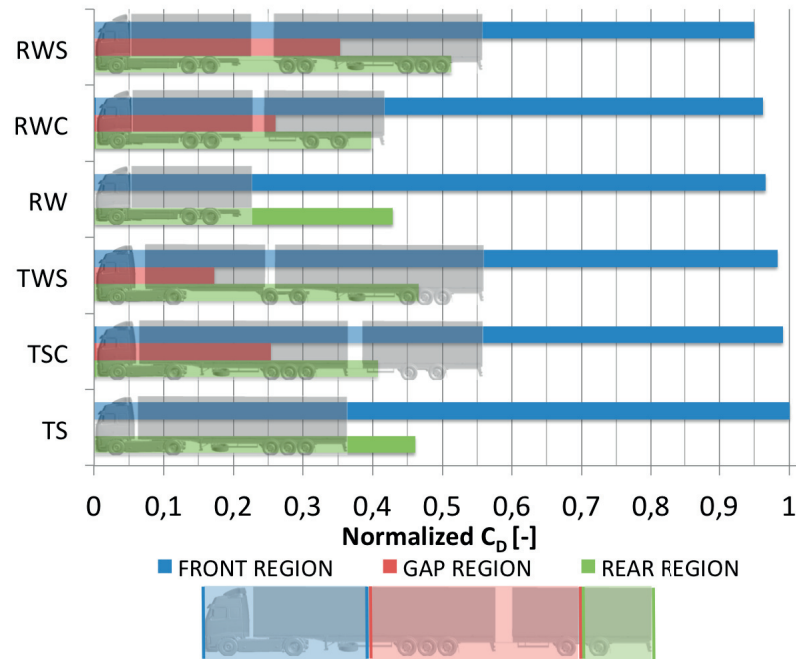
Figure 4.5: Normalized C_D values for the front region, gap region, and the rear region for each vehicle combination.

What is evident from Figure 4.5 is that the aerodynamic drag which was accumulated in the gap region reflects the size of the gap between the cargo-units. RWS showed the largest local drag accumulation in the gap region compared to the other cases, as a result of the size of the gap between the cargo-units. TWS, which had the smallest gap between the 1st and 2nd cargo-unit also showed the lowest contribution over the gap region. However, it should be noted that the part of the vehicle combination which gave rise to most of the drag was the front part. From Figure 4.5 it will be seen that the front region contributed more than three times the drag coefficient than the gap region for some of the cases.

Pressure- and Friction Drag Components

As discussed in the introductory chapter of this thesis, vehicles, and trucks especially, are strictly dominated by the pressure drag and just a small portion of the total drag is due to friction. However, the hypothesis for the different vehicle combinations evaluated was that the proportion of friction drag should increase with increasing vehicle length. Figure 4.6 shows the results of differentiating the pressure and friction drag components for each of the vehicle combinations.
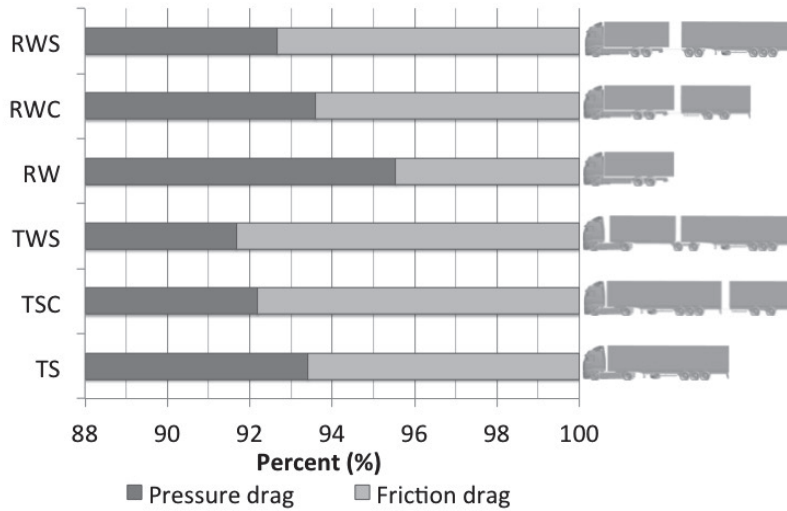
Figure 4.6: Balance of pressure drag and friction drag for the vehicle combinations included in the analysis, 0° yaw.

It was found that the longer vehicle combinations showed a considerable percentage increase in friction drag compared to the reference case; the friction term has almost doubled. The additional trailer box is the predominant factor of increasing friction drag for the longer vehicle combinations. The other parts, such as the chassis and the wheels of the trailers, have a negligible effect on the friction drag. The percentage increase of pressure drag with increasing vehicle length is not as large as the friction drag, but the absolute values of the pressure drag are many times higher.

Transport Efficiency

Comparing the aerodynamic drag coefficients of the different vehicle combinations to each other and from this value only draw conclusions about their suitability for certain driving conditions is close to impossible. Therefore, a simplified estimation of the transport efficiency was performed for each of the six vehicle combinations. In this manner a joint value of the performance of each vehicle combinations are obtained, making it possible to compare the cases with each other. The total driving resistance was calculated by adding the contribution from aerodynamic drag and rolling resistance. For the aerodynamic resistance, C_D values for 0° yaw and 5° yaw were used to calculate averaged drag coefficients, which is more convenient than using a value for a single yaw angle. However, using only two angles would not be enough to completely calculate a wind-averaged drag coefficient. Most commonly, a wide range of yaw angles would be measured to be able to calculate a wind-averaged drag coefficient, which also takes into account average wind conditions. In this study, a simplified method for calculating an average of two drag coefficients has been used to get an estimate of a wind-averaged drag coefficient. The averaged drag coefficient was calculated using a method within Volvo GTT, which includes

a weighting parameter taking into account the average angle of the incoming wind according to European measures. For the rolling resistance contribution, the unladen- and loading weights together with an estimation of the rolling resistance per tonne was used. One loading case and one driving condition were chosen to resemble a common transport scenario. The driving condition chosen was $90km/h$ on a level road, which can be considered as European driving conditions. The choice of loading case was made with respect to studies performed by Åkerman and Jonsson [9], which found that most long-haul transports are volume sensitive rather than weight sensitive; the entire volume of the cargo-unit is filled before the maximum weight limit is reached. By using data from [9] a loading case where 60% of the allowed loading weight and 100% of the total loading volume was used. The empty weights of each EMS module used in the analysis can be seen in Appendix B.

The results indicated that it was more efficient to use fewer, but longer vehicle combinations to transport the same amount of cargo. Figure 4.7 shows normalized power required per Loading Length (LL) for the six vehicle combinations. The values of the power requirements per LL have been normalized with the value for TS, and the LL is the combined total length of the cargo-units for each configuration. The $25.25m$ combinations TSC, TWS and RWS had identical LL's since the modules they were built from had the same sizes.
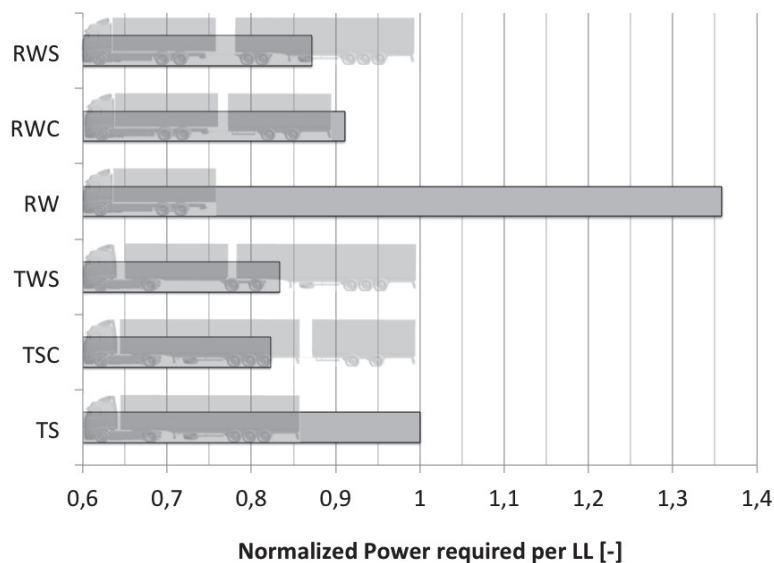

Figure 4.7: Normalized power required per LL for each of the vehicle combinations.

As can be seen, the relative power consumption is lower for longer vehicle combinations, and can therefore be considered to be more suitable for this driving condition than the other vehicles. It can also be concluded that RW, the shortest vehicle combination, is not very suitable for long-haul transports; it has an

almost 40% increase in power requirements per LL compared to TS, the reference case. Comparing the three 25.25m combinations it will be seen that RWS, the rigid truck with swap body and a semi-trailer, showed significantly higher relative power requirements than the other two 25.25m combinations. This result was not only a consequence of the larger aerodynamic resistance calculated for this configuration, but also because the unladen weight of this vehicle is larger.

From the transport efficiency analysis, it can hence be concluded that all the 25.25m combinations showed substantially better efficiency levels than the shorter combinations. This suggests that the idea of replacing three tractor - semi-trailer combinations with any of the longest vehicle combinations would be preferable from an transport efficiency point of view.

4.2   Cab-Mounted Aerodynamic Devices

Two common drag-reducing devices for tractive units, the roof deflector and cab extenders, were evaluated in terms of aerodynamic drag. The study was performed for three different vehicle combinations of different lengths and trailer configurations, to investigate the effect of these drag-reducing devices on the type of vehicle combination. Important aspects were to investigate the effect of devices downstream of the vehicle combinations, to see if these effects were different for different lengths of the vehicles.

For the simulations performed for the analysis, three different configurations of a rigid truck and cargo-units were evaluated: RW, RWC and RWS as described in Section 4.1. There were also three separate modifications of each of the three vehicle combinations; the configurations can be seen in Figure 4.8. More information about the specific truck and trailer models used for the analysis can be found in Appendix A.

(a) Configuration A.   (b) Configuration B.   (c) Configuration C.
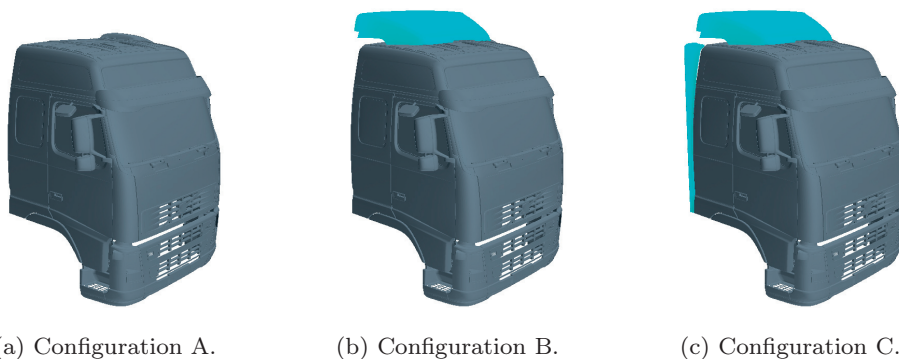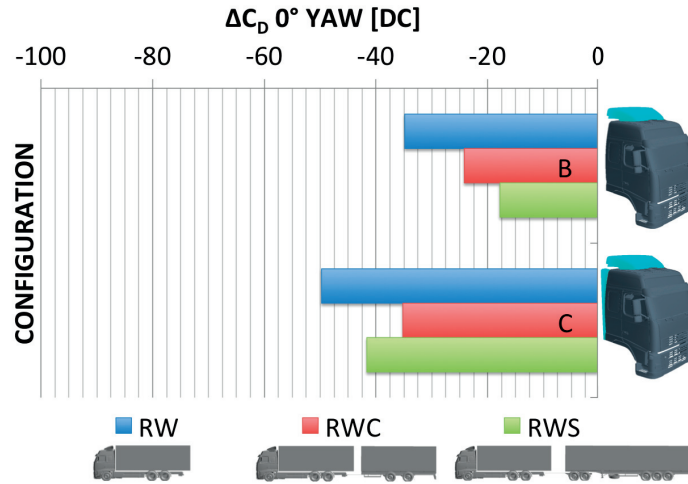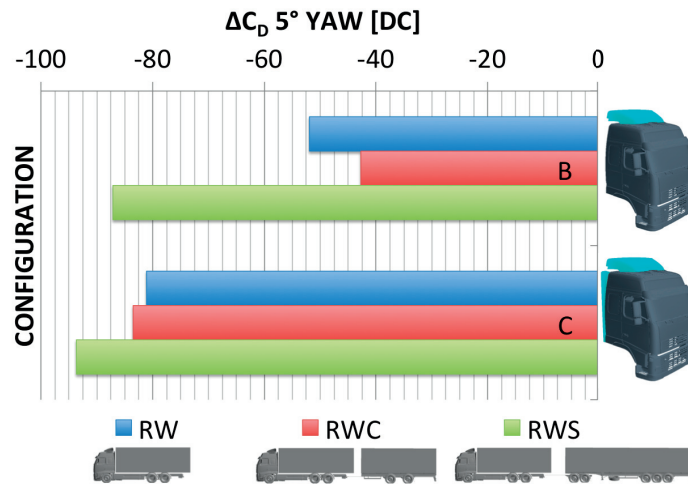
Figure 4.8: Configurations of roof deflector and cab side-extenders used for the RW, RWC and RWS.

It was seen that the effect of the drag-reducing devices were positive; both the cab side-extenders and roof deflector were efficiently reducing drag for the three vehicle combinations. The numerical results can be seen in Figure 4.9.
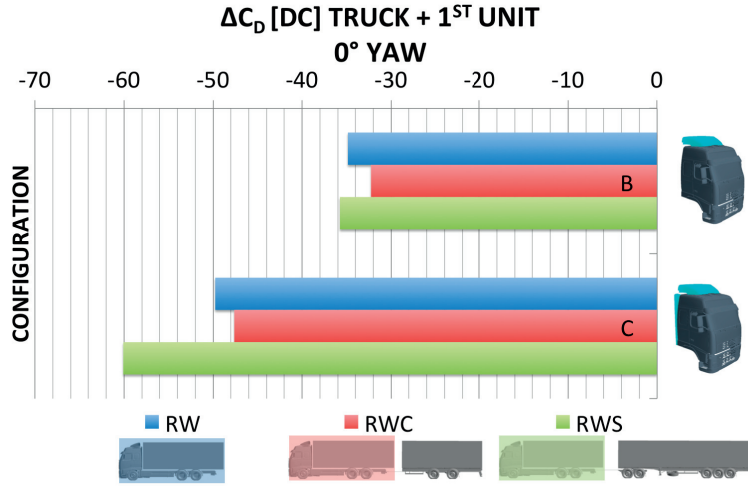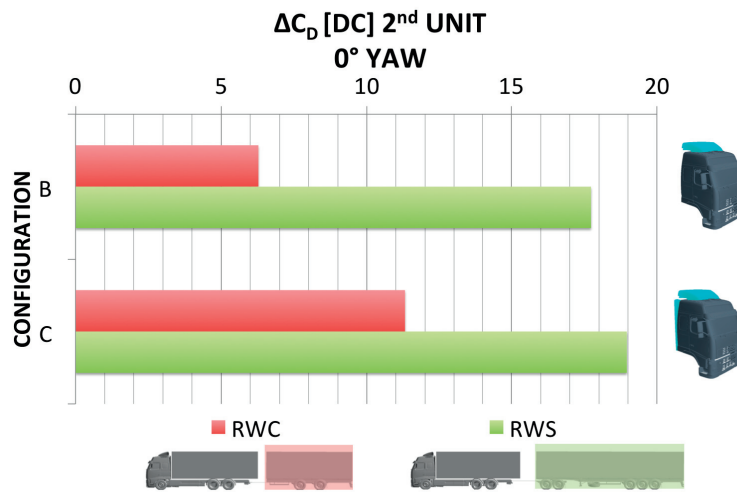

(a) 0° yaw.

(b) 5° yaw.

Figure 4.9: Difference in C_D values relative to the reference configuration (A), without any roof deflector and cab side-extenders.

That it is important to also consider the rearmost part of the vehicle became evident when the drag coefficient was split into sections. The total drag coefficient of the truck-trailer combinations was divided into two parts; one part from the tractive unit and the 1st cargo-unit and one part from the 2nd cargo-unit. These partial drag-coefficients were then related to drag coefficients for each reference case (i.e. configuration A for each of the vehicle combinations); see Figure 4.10. Naturally, since RW only had one cargo-unit, the differences in

drag coefficients shown in Figure 4.10a were the total reductions in C_D; being the same as presented in Figure 4.9.

(a) Difference in C_D originating from the truck and 1st cargo-unit.

(b) Difference in C_D originating from the 2nd cargo-unit.

Figure 4.10: Difference in partial C_D values relative to configuration A, 0° yaw.

What was discovered was that the largest effects were seen on the truck and 1st cargo-unit; the influence on the 2nd unit was smaller. There was a large reduction in the local drag coefficient for the truck and 1st cargo-unit for the cases with the aerodynamic devices. However, as drag was reduced locally for the truck and 1st cargo-unit, the local drag on the 2nd unit was somewhat increased. This again confirmed the significance of the gap between the units; the increase of drag on the 2nd unit can be explained by flow attachment. For the combinations without roof deflector or cab side-extenders the flow around the vehicle was already highly separated at the front part of the vehicle, which results in less air flowing through the gap, hitting the front part of the 2nd

unit; hence not affecting this part as much as if the drag-reducing devices were present. But, as has been shown earlier, the resulting effect was still an improvement compared to the original configurations.

In the study by Browand et al [35], two bluff bodies in tandem were analyzed. The total drag coefficients were split into two parts; one originating from the leading body, and one from the rear body, similar to this study in Figure 4.10. The results from Browand et al [35] showed that when the leading body had rounded front edges, the portion of the drag originating from the rear body was higher compared to when the leading body had a more abrupt shape. These results can be related to this thesis, where the results obtained from fully-detailed models have shown that the more aerodynamic devices that are added to the truck, the larger the proportion of drag coefficient on the 2nd cargo-unit.
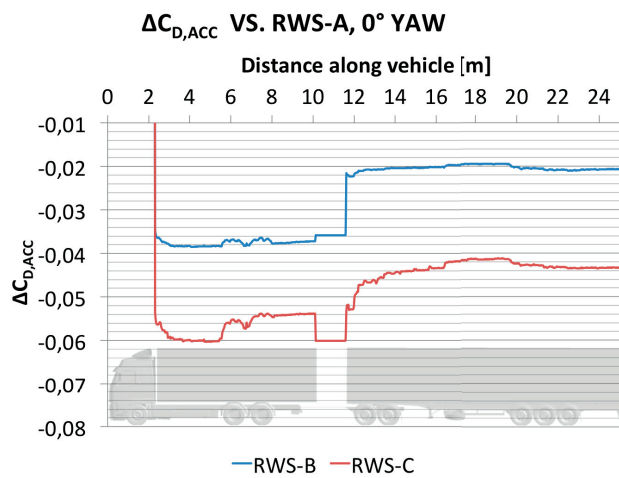
By calculating the difference in accumulated drag between two configurations it is straightforward to detect areas in the flow field where the aerodynamic properties change from the original case. Performing such an analysis for the three vehicle combinations with different configurations of the drag-reducing devices revealed interesting effects. All combinations were compared to each reference case, that is, RW-A, RWC-A and RWS-A, and the results are shown in Figure 4.11.
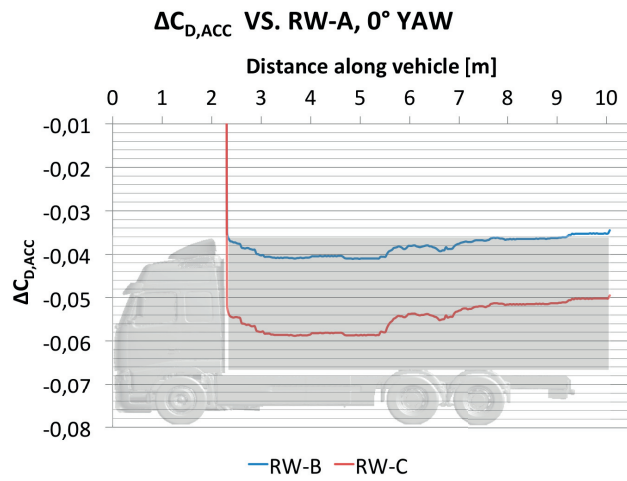
(a) RW.
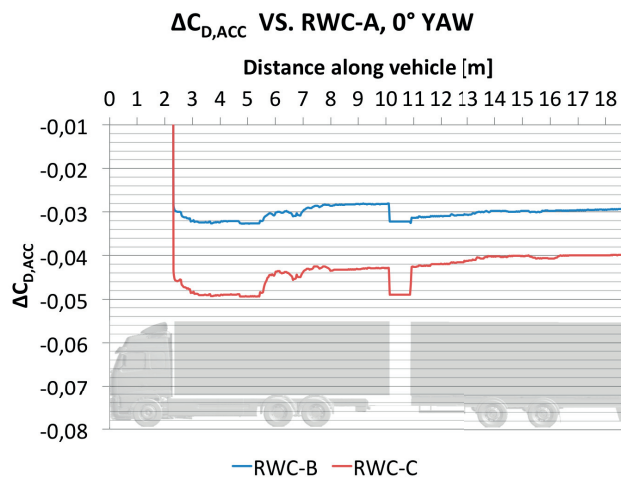
(b) RWC.

(c) RWS.

Figure 4.11: Difference in accumulated drag for configurations B and C compared to configuration A, 0° yaw. Note that the entire accumulation curve is not visualized; only the part from the first cargo-unit and further downstream.

The results showed that a lot of the drag reduction was lost downstream of the vehicle combination, especially for the two vehicle combinations with two cargo-units: RWC and RWS. From the end of the 1st cargo-unit until the end of the 2nd unit, $14DC$ were lost from the overall drag reduction for RWS-C, which means that more than 33% of the total drag reduction was lost in this region. The corresponding value for Case RWC-C was $6DC$, which corresponds to 17%. This implies it is very important to work to improve the flow around the rest of the vehicle, in order to maintain the positive effects that have been created in the cab area upstream. It should however be emphasized that the roof deflector and cab side-extenders reduce the total drag of the vehicle combination, but there is considerable potential for further developments, if also considering the parts of the vehicle behind the tractive unit.

Comparing the results from Figure 4.10a with the outcome from the investigation performed by Castellucci et al [36] shows that the results were similar. Castellucci et al [36] found that when adding side deflectors, the major drag reduction was experienced by the trailer, which in this investigation can be seen as the 1st cargo-unit. It has been noted above that the major drag reduction in this study was experienced by the truck and the 1st cargo-unit. However, bearing in mind the shape of the drag accumulation curves that were previously shown, it can be concluded that it is actually the 1st cargo-unit itself that experienced the greatest local drag reductions; as a consequence of directing a larger portion of the airflow away from the cargo-unit surface.

4.3 Trailer-Mounted Aerodynamic Devices

The motivation behind evaluating aerodynamic devices for the trailer unit came from the results previously discussed; that a considerable amount of the drag reductions obtained in the cab region with the commonly used roof deflector and cab-side extenders were lost downstream along the trailer. The trailer-mounted devices evaluated here focused on the chassis level and gap region between the cargo-units since these areas have been found to be two major sources of energy losses for a truck-trailer combination.

For the analyses undertaken in the thesis, the baseline vehicle for the investigations was a tractor model with two semi-trailers in tandem, creating a $31.60m$ combination with a Gross Combination Weight (GCW) of $80 tonnes$. This vehicle combination was a novel vehicle combination that was introduced on a trial basis, to be run between Gothenburg and Malmo in Sweden. The fuel efficiency of such a combination, where two conventional TS combinations were replaced with one tractor- semi-trailer - semi-trailer combination, has been evaluated in road tests by Volvo Trucks since 2012 [70]. The vehicle combinations with a tractor and two semi-trailers in tandem, supported by a dolly in between the trailers, will from here on be denoted as T2S.

Referring to Hjelm and Bergqvist [13] the truck operation can differ significantly and it is possible to distinguish between two distinct modes. The first operation mode is when driving slowly or standing still, for example when loading

or unloading, driving on and off ferries, etc. For this driving condition it is important to ensure sufficient ground clearance, and also to be able to manoeuvre the vehicle in confined places. The second mode can be seen as high-speed driving, typically highway driving. In these kinds of conditions only a small amount of manoeuvrability is needed and at the same time less ground clearance is required. In order to take advantage of this driving condition one could use altering designs of the entire vehicle combination; for example via adjustable gap-size between the cargo-units. An adjustable gap between the cargo-units could be a satisfying solution if it is not be possible to make a permanent solution by covering the gap. Hence both methods were investigated in this thesis.

4.3.1   Ideal Design Changes

Different methods for improving the aerodynamic drag for the T2S were investigated; the designs being rather ideal to see their potential. The different modifications made to the T2S model are shown in Figure 4.12, the abbreviations used for the different drag-reducing strategies are shown in Table 4.2.

Table 4.2: Abbreviations of modifications made to the T2S model.

CG	Covered Gap
EG	Eliminated Gap
CS	Chassis Skirts

(a) T2S with covered gap between semi-trailers (CG).

(b) T2S with eliminated gap between semi-trailers (EG).

(c) T2S with chassis skirts for the semi-trailers (CS).
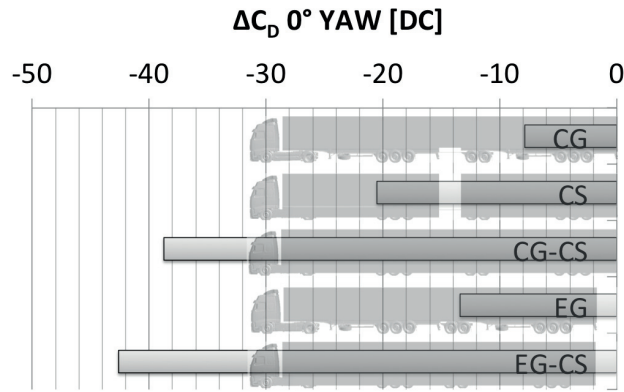

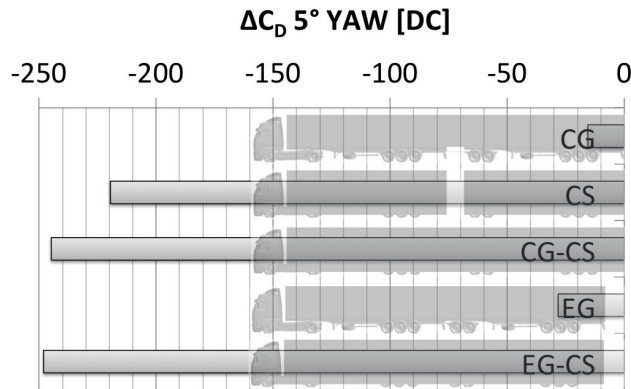(d) T2S with covered gap and chassis skirts for the semi-trailers (CG-CS).

(e) T2S with eliminated gap and chassis skirts for the semi-trailers (EG-CS).

Figure 4.12: Modifications made to the T2S model, to the chassis- and gap regions.

The results from the simulations run with the different drag-reducing devices is shown in Figure 4.13.

ΔC$_D$ 0° YAW [DC]

(a) 0° yaw.

ΔC$_D$ 5° YAW [DC]

(b) 5° yaw.

Figure 4.13: Difference in C_D between the cases with different drag-reducing strategies compared to the T2S without any gap treatment or chassis skirts.

The results presented in Figure 4.13 showed that there were large C_D reductions to be expected by using the different gap- and chassis skirts approaches. Especially large were the magnitudes of the drag reductions in 5° yaw. For both simulated yaw angles, it was found that the combined effect of gap treatment and chassis skirts for the semi-trailers yielded better results than adding the individual contributions together. Hence this indicated that an even better flow field was obtained with the combined approach and that the devices used in the two areas were cooperating in a favourable manner.

Another finding was that it seemed more efficient to eliminate, rather than covering, the gap between the two cargo-units. The same effect was seen for the combined solution with chassis skirts and gap treatment, where EG-CS showed a larger drag reduction than CG-CS.

As mentioned above, the results from the 5° yaw simulations showed that the drag reductions were considerably larger than in 0° yawed wind. This effect was particularly strong for the combinations with chassis skirts. The drag reductions for cases with gap elimination or gap coverage was approximately double the amount compared to 0° yaw, but compared to the chassis skirts configurations those results were rather modest. For a combined solution of chassis skirts and gap elimination the drag reduction was in the range of $250DC$, which is very significant. The reason for the results of the chassis skirts being more prominent was that, in yawed-wind conditions, the chassis skirts covered the main part of the irregular chassis of the semi-trailer units. Since the vehicle combination was more than $30m$ long, the effect of such a device became very large.

To further emphasize and understand the flow field around the different T2S models, the accumulated drag along the vehicle was plotted for two of the configurations, for both evaluated yaw angles. Figure 4.14 shows the drag accumulation for T2S and the CG-CS configurations. All cumulative C_D values were normalized with the resulting value obtained for the T2S configuration at 0° yaw.
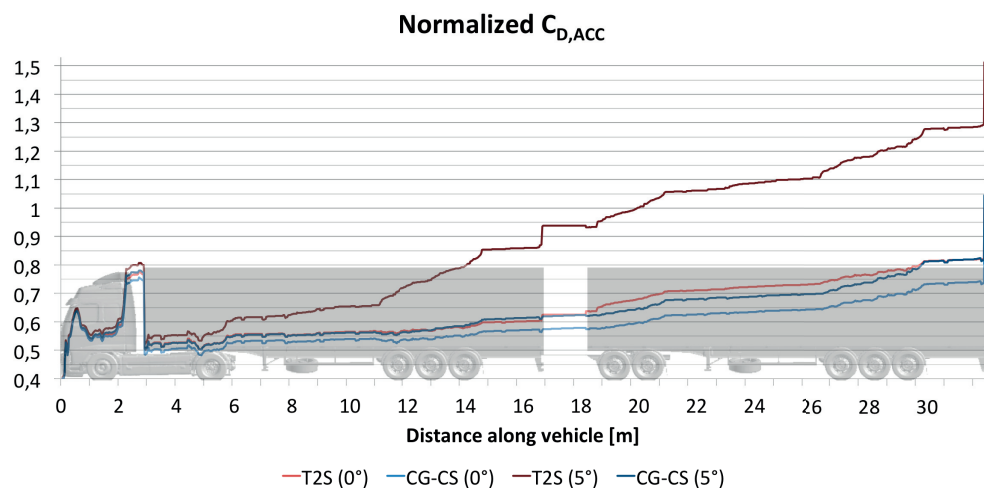

Figure 4.14: Normalized accumulated C_D along the vehicle for the T2S and CG-CS configurations.

The results in Figure 4.14 really shows the sensitivity to yawed-wind conditions for this kind of vehicle combination. It was seen that the T2S model at 5° yaw showed very steep drag increases, especially along the trailer units. The area around the semi-trailer wheels seemed to accelerate the drag accumulation; an area that was significantly improved by the addition of chassis skirts. Another interesting phenomenon was that the resulting C_D value obtained for T2S at 0° yaw was very similar to the corresponding value for CG-CS at 5° yaw. The potential for introducing drag-reducing devices in the gap region and at chassis level of the trailers was very prominent.

4.3.2   Practical Device for Improving the Gap Region

The coverage, or elimination of the gap between the semi-trailers are ideal solutions of the gap treatment. In order to achieve an understanding of the performance of a more realistic solution of this problem, a so-called gap fairing system was also investigated. The device had smooth, rounded edges and it was mounted on the front face of the trailer. The purpose was to reduce the high-pressure area at the edges of the trailer, and instead guide the flow onto the trailer roof and sides, hence improving the re-attachment of the flow. For visual reference, the gap fairing is displayed in Figure 4.15.
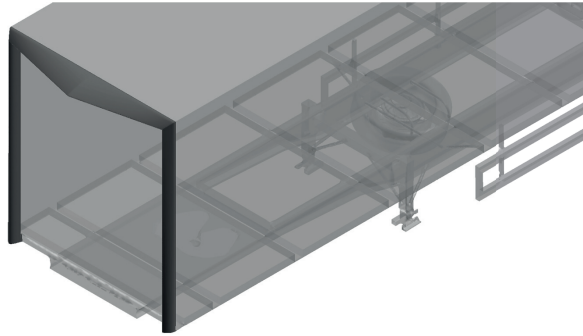

Figure 4.15: Practical gap fairing device, mounted on the semi-trailer front face.

The gap fairing device was tested in three separate configurations: for the 1st semi-trailer unit, for the 2nd semi-trailer unit, and for both semi-trailers simultaneously. The results from the simulations are shown in Figure 4.16. The abbreviations for the gap fairing configurations are explained in Table 4.3.

Table 4.3: Abbreviations of the gap fairing configurations evaluated for the T2S model.

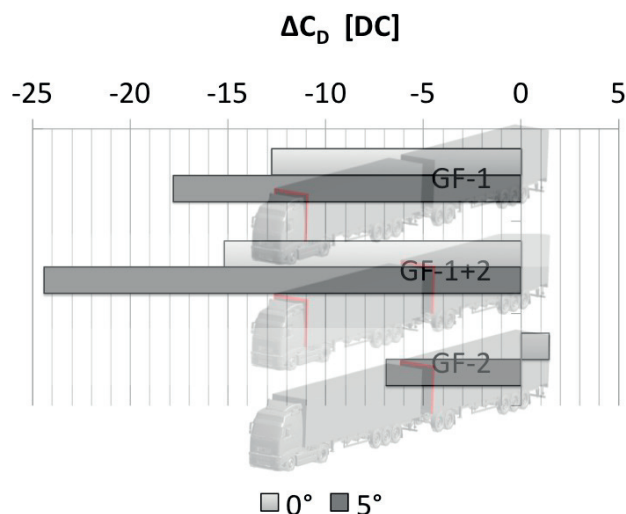| GF$-$1	Gap Fairing for 1st semi-trailer unit
GF$-$1$+$2	Gap Fairing for 1st and 2nd semi-trailer unit
GF$-$2	Gap Fairing for 2nd semi-trailer unit

Figure 4.16: Results from the gap fairing simulations for the T2S combination.

What can be concluded from the values of C_D for the simulations with included gap fairing systems, was that working with the 2nd semi-trailer only did not result in particularly large changes. It was more efficient to mount the gap fairing system on the 1st semi- trailer. However, if considering both trailer units, the combined solution with a fairing system on both trailer units was the most promising configuration; with a higher total drag reduction than the individual values. What differed between the front and rear gap fairing installations was that the gaps in which they operated were of different sizes. The gap between the cab and 1st semitrailer was $0.650m$, while it was $1.485m$ between the two trailer units. It appeared that the gap between the two trailer units was too large for this device to be efficient. This was also seen when analysing the flow structures in the gap region for these configurations; there were still significant areas of flow losses in this region due to the fact that air still had the possibility to flow into the gap and create substantial separated areas. The main drag reduction was hence due to the front gap fairing, and in this gap, which was significantly smaller, there was also help from the roof deflector and cab side-extenders, to guide the flow from the cab to the trailer roof and sides.

When adding the gap fairing to the semi-trailer front, it was seen that the high-pressure areas on the edges of the trailer front faces were substantially decreased. This effect was seen for both the front and rear semi-trailer units. Hence this implies that the flow was more smoothly guided towards the sides of the trailer. Visualizing the difference in accumulated drag for GF-1, GF-1+2 and GF-2 compared to the T2S combination without any devices it was straightforward to see where the changes in drag occurred along the vehicle. This can be seen in Figure 4.17.
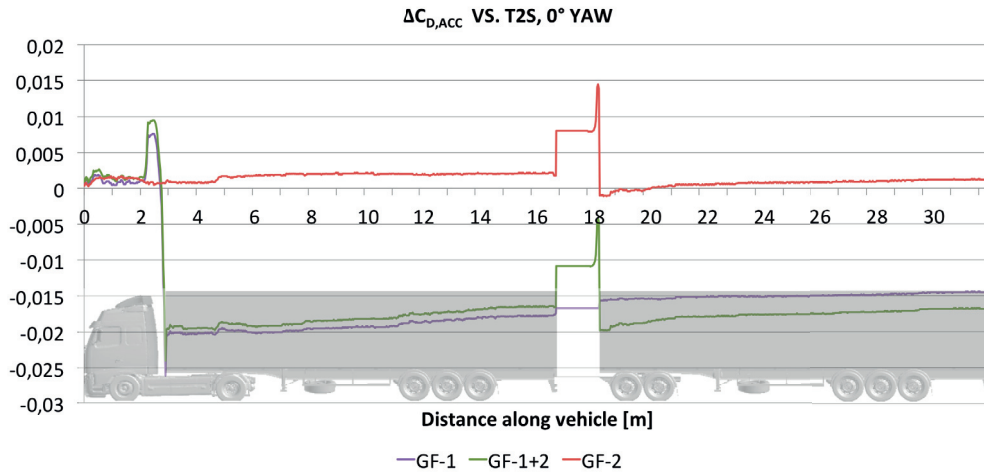
Figure 4.17: Difference in accumulated drag for GF-1, GF-1+2 and GF-2 relative to T2S, 0° yaw.

GF-2, the configuration with rear gap fairing only, resulted in a slight drag increase compared to the reference case. It can be seen that drag was recovered locally just after the gap fairing on the 2nd semi-trailer unit, but this drag decrease was gradually reduced towards the end of the 2nd semi-trailer, and the net effect was that there was a small drag increase. Though, the increase in drag of $1.5DC$ was very small and cannot be seen as a significant result, rather that the effect of the gap fairing system in this configuration was negligible. GF-1+2, the case with gap fairing system on both trailer units, showed the same trend along the 2nd trailer unit as GF-2; the drag decrease obtained in the gap between the trailer units was reduced towards the end, indicating that the flow was redirected in an unfavourable manner with the gap fairing and hence some of the drag reduction was lost downstream.

4.4 Influence of Cab Front-End Design on the Aerodynamic Properties

The COE cab, which is the most common type of tractive unit on the European market, is not the ideal design with regards to the aerodynamic resistance. There are large potential for drag reductions, working with an elongation of the grille area of the COE cab. As described in Section 1.1, there is a new EU proposal regarding extending the total length of vehicle combinations, to allow for aerodynamic and safety improvements [16]. The concept of elongating the COE grille area and hence generating a longer nose is often referred to as a Soft Nose (SN), where 'soft' implies that the structure should be deformable in a way as to minimize injuries for car occupants and pedestrians.

For the work included in this thesis, it was decided to evaluate an elongated COE cab in terms of aerodynamic drag, to estimate the possible winnings associated with such a concept. Two different SN concepts were evaluated; one $200mm$ and one $500mm$ elongation of the COE grille area. The COE cab and the SN $200mm$ are shown in Figure 4.18.

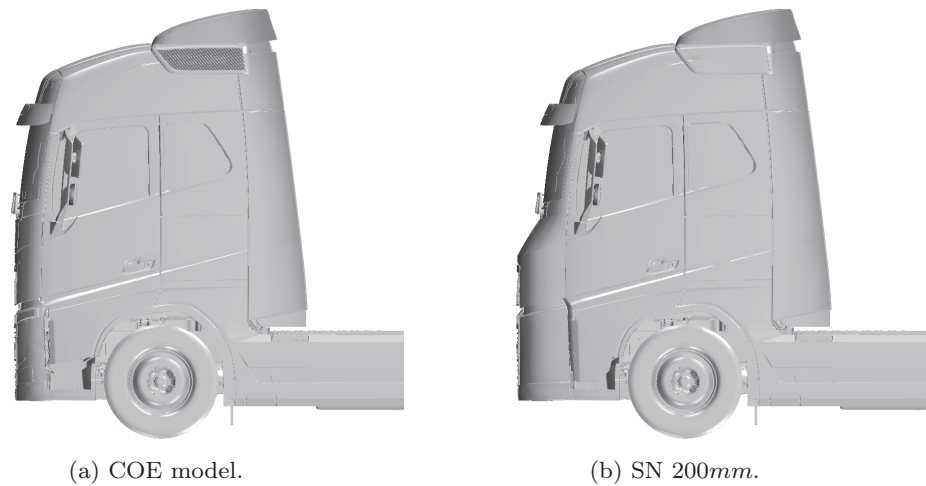(a) COE model.   (b) SN $200mm$.

Figure 4.18: COE and SN $200mm$ geometries, shown in a side view.

Running the simulations for the two geometries described in Figure 4.18 yielded the results in terms of C_D shown in Figure 4.19. Both open and closed grille configurations are displayed in the figure.
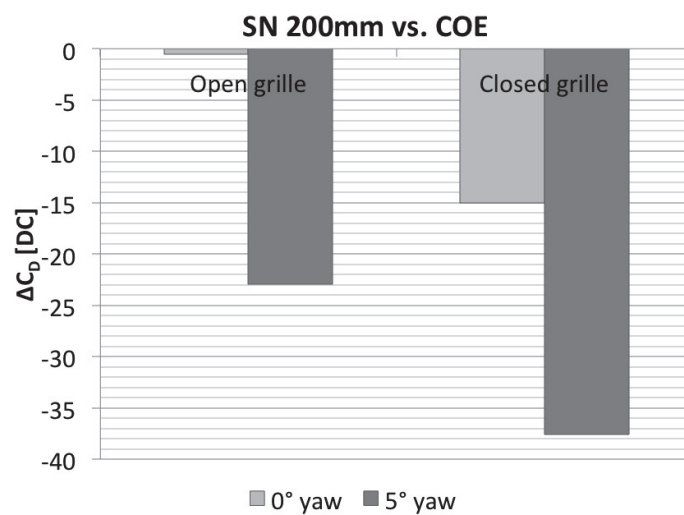

Figure 4.19: ΔC_D values for the SN 200mm model relative to the COE model, for open and closed grille-configurations.

The results in Figure 4.19 showed that the drag reductions obtained for the open-grille configurations were rather modest; the 0° yaw results showed almost identical C_D values for the SN 200mm and the COE model. The results in 5° yaw and the closed-grille results showed a bit larger potential. Since the closed-grille configurations showed far more potential for drag reductions, it was suspected that the under-hood flow for the SN 200mm was not ideal, and in order to understand the results the flow field was investigated. It was found that there was a large decrease in mass flow of air through the cooling module, see Figure 4.20.
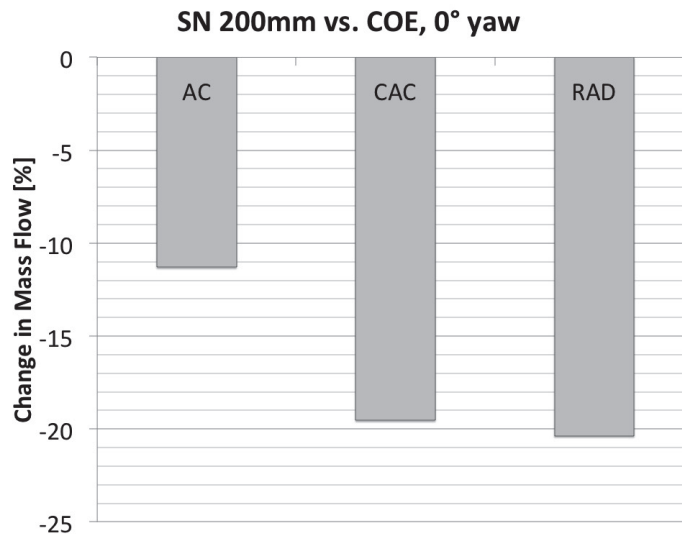

Figure 4.20: Percentage difference mass flow of air through each of the cooling module components; SN 200mm relative to the COE model.

As can be seen from Figure 4.20 there was a significant reduction of the flow through the cooling module and it was also seen that the flow through each of the cooling module components became smaller and smaller as moving downstream. The largest effect was seen for the radiator. What was also discovered was that, even though the mass flow through the heat exchangers was higher for the COE model, the mass flow through the grille was significantly lower for the COE model compared to the SN model. The COE model had approximately 45% lower mass flow compared to the SN model.

The large decrease of mass flow through the heat exchangers for the SN model related to the general layout of the under-hood components. When creating the SN 200mm model, only the exterior of the cab was changed. The under-hood components were kept in their COE position; hence there was a 200mm distance between the grille and the cooling module, leading to substantial leakage of air around the cooling module. This resulted in both reduced cooling capacity and that a large portion of the potential aerodynamic gains were lost by the unfavourable flow structures on the inside of the grille. To visualize these phenomena, Figure 4.21 shows the velocity magnitude in a z-plane 960mm above ground, cut through the grille and cooling package area.
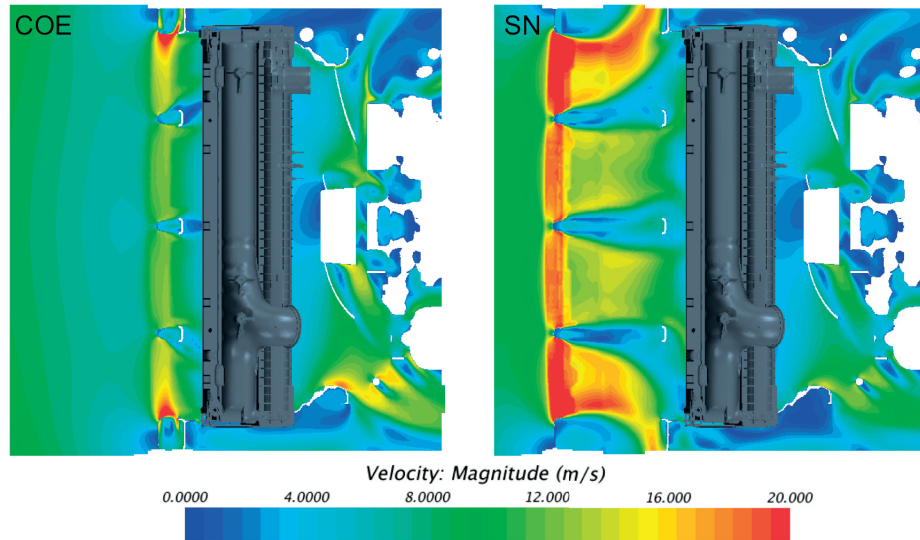
Figure 4.21: Velocity magnitude in a plane at $z = 960mm$, for the COE and SN $200mm$ models.

It can be seen from Figure 4.21 that the velocity magnitude was indeed much higher at the grille inlet for the SN model. Additionally, there was a substantial leakage of air around the sides of the cooling module, seen to the right in Figure 4.21; the air was flowing around the cooling module instead of flowing through it. This explains the reduced mass flow values for the SN $200mm$ model.

There were very small aerodynamic drag winnings associated with the SN $200mm$ model, given that the under hood was kept as the COE model. With these results as a reference, a new SN $200mm$ model was created, where the cooling module and related components of the under hood were moved $200mm$ longitudinally towards the grille area. This resulted in a minimization of the distance between the grille and cooling module, which was one of the main reasons for the low potential for this geometry. The reason for moving the cooling module instead of keeping it at its original position and ducting the flow from the inlet to the cooling package, was that the longitudinal space between the cooling module and the engine should be used for introducing an outlet duct. This will be treated later in the thesis.

The movement of the cooling module, fan, and other related parts, resulted in that a longitudinal space was released behind the fan, before the engine. Figure 4.22 shows the cooling module including the re-circulation shields, fan and fan shroud, plus the engine and the SN $200mm$ geometry for the original and updated model, where the cooling module and related parts have been moved $200mm$ longitudinally towards the grille. The intention of the figure is to show the cooling module displacement.
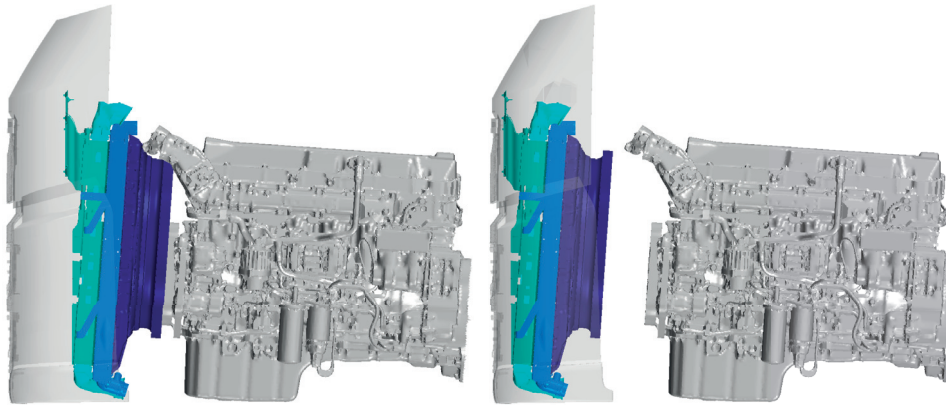
Figure 4.22: Displacement of the cooling module, fan and related geometry for the SN 200mm model. The left picture shows the original cooling module position, the right picture shows the 200mm displacement longitudinally. Note that not all parts that have been moved are displayed in the figure.

By the movement of the cooling module towards the grille of the SN model, the results were significantly improved. The results can be seen in Figure 4.23, where the C_D values were compared to the COE model; CM denotes Cooling Module and the configuration of the respective case can be seen in the pictures below the graph.
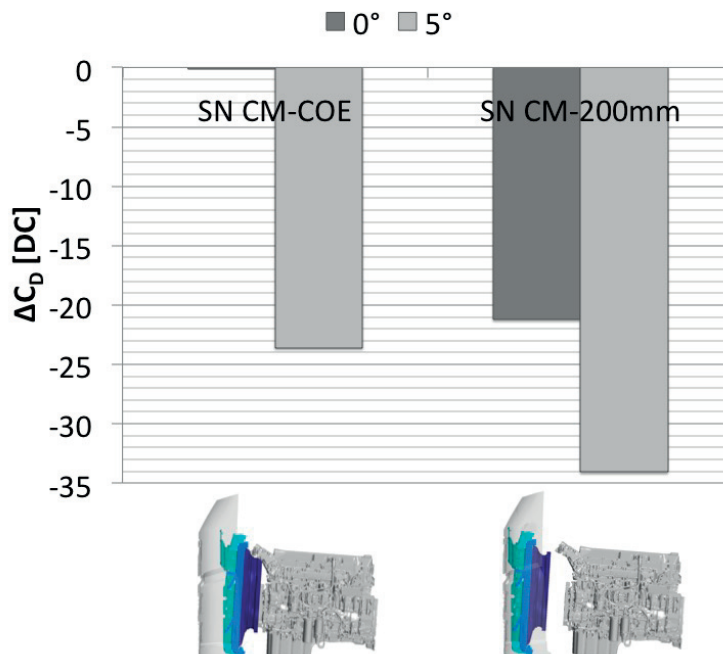

Figure 4.23: ΔC_D values for the SN 200mm models relative to the COE model, for the two different cooling module positions.

According to the results in Figure 4.23, there was a large benefit from an aerodynamic perspective of moving the cooling module towards the grille area. C_D was lowered by $22DC$ compared to the COE configuration at 0° yaw, and compared to the SN $200mm$ model the magnitude is almost as large. The benefits at 5° yaw were also significant, with a $34DC$ reduction for the SN configuration with moved cooling module. At the same time as the aerodynamic drag was reduced when moving the cooling module, it was also seen that the cooling capacity was improved significantly. The $200mm$ movement of the cooling module yielded a decrease of TTT of 10° and an increase of mass flow of air through the radiator of $0.75kg/s$ at 0° yaw compared to the original SN $200mm$ model.

It can be concluded that there was potential for aerodynamic drag reductions with the SN model compared to the COE model. The magnitudes shown so far were however rather modest and implies that proper consideration of the under-hood design has to be made. The elongation itself was also rather small and it can be suspected that a properly-designed longer nose could result in even better results considering aerodynamic drag. Therefore, an additional SN was evaluated, with a $500mm$ elongation from the COE grille area. For comparison, the SN $200mm$ and SN $500mm$ geometries are shown in Figure 4.24. For the SN $500mm$ nose, the cooling module and related geometry was moved $500mm$ longitudinally, in a similar manner as for the SN $200mm$ model. Something to keep in mind when changing the exterior shape of the cab is that the turning ability changes. The $500mm$ nose evaluated in this thesis most certainly does not comply with the turning circle requirements for this kind of vehicle. The intention of the study performed here was to show the potential of the elongation as such.

(a) SN 200*mm*.
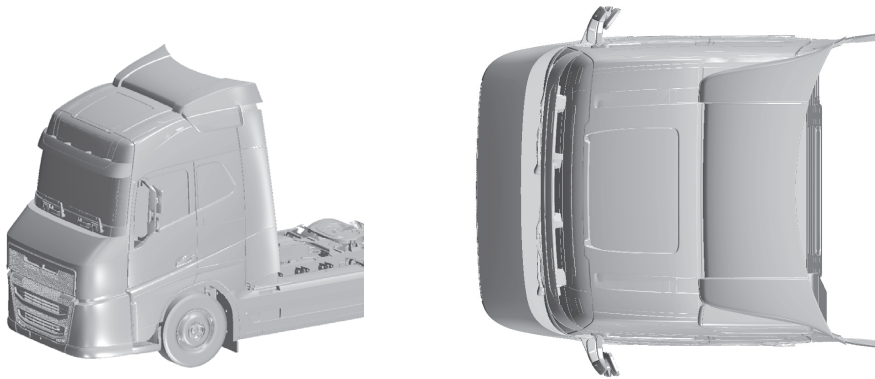
(b) SN 500*mm*.

Figure 4.24: Geometries of the two SN models; the pictures to the right show the cab seen from above.

Figure 4.25 shows the C_D reduction for the two evaluated SN models compared to the COE configuration at both evaluated yaw angles.
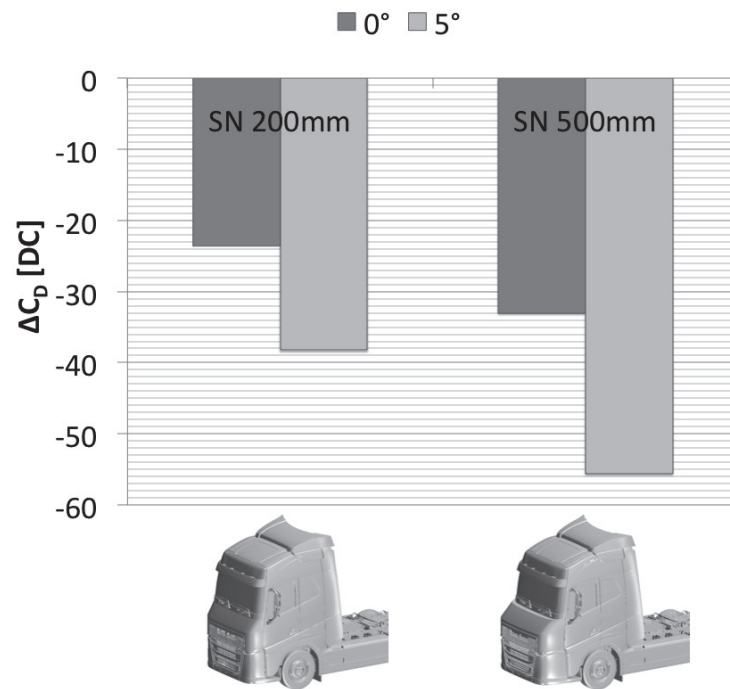
Figure 4.25: Difference in C_D relative to the COE model, for the SN $200mm$ and $500mm$ models, at 0° and 5° yaw.

The results in Figure 4.25 clearly shows the benefit of having a more rounded front of the cab, compared to the COE model. Especially good were the results from the 5° yaw simulations, where the C_D values were decreased by as much as $56DC$ for the $500mm$ nose. The results of the aerodynamic drag indicates that a significantly improved flow field was generated around the vehicle with a smoother shape of the cab front.

To explain the significant decrease in C_D for the SN models at yawed-wind conditions, planes of the velocity magnitude were visualized along the vehicle. Figure 4.26 shows the COE model and the SN $500mm$ model at 5° yaw, on the leeward side.
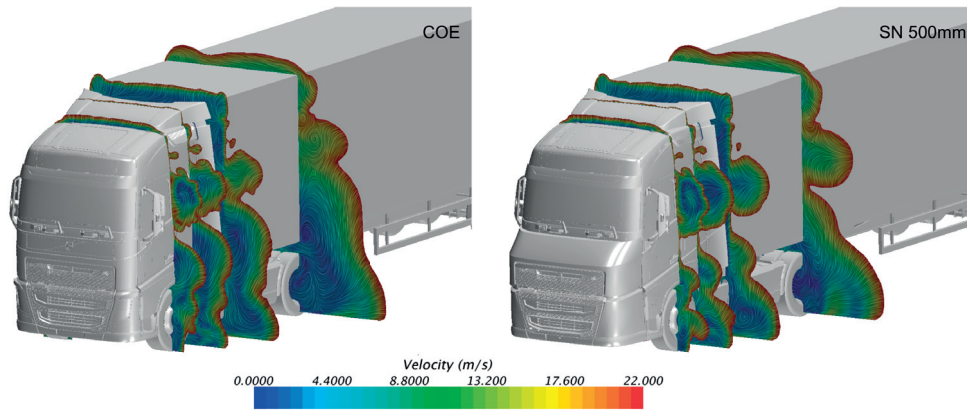
Figure 4.26: Planes of velocity magnitude at different locations along the vehicle, $5°$ yaw and leeward side. The planes are cut at $22m/s$.

It can be seen in Figure 4.26 that the flow was highly redirected when introducing the nose: a larger portion of the flow was directed above the nose and interacted with the rear-view mirrors, compared to the COE model. As a consequence, the SN model showed larger separated areas in this area. However, the low-velocity areas at chassis level were significantly decreased for the SN model. Overall, it seemed straightforward by looking at the figures that the total amount of flow losses were decreased by the addition of the nose. The effects were seen around the entire vehicle, and not only in the region close to the cab. For the $5°$ cases, the windward side also showed significant differences in flow structure. Figure 4.27 shows similar pictures for the COE and SN $500mm$ models at $5°$ yaw on the windward side.
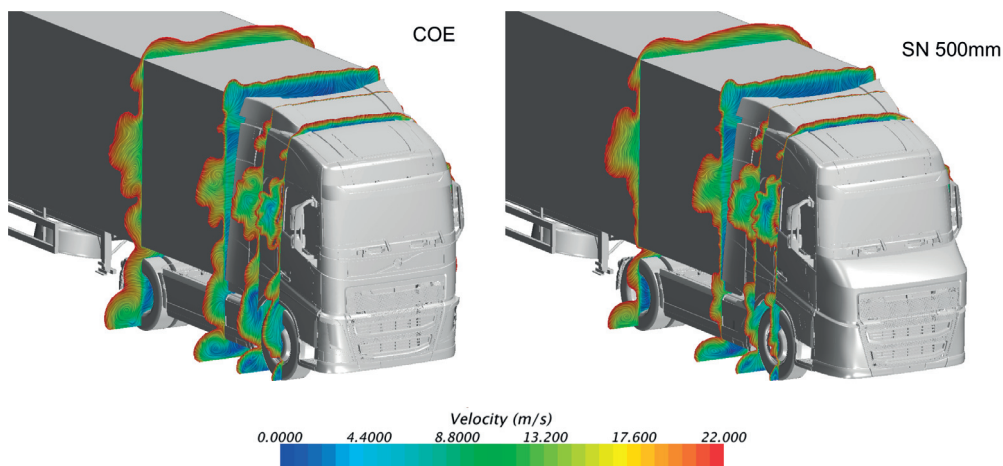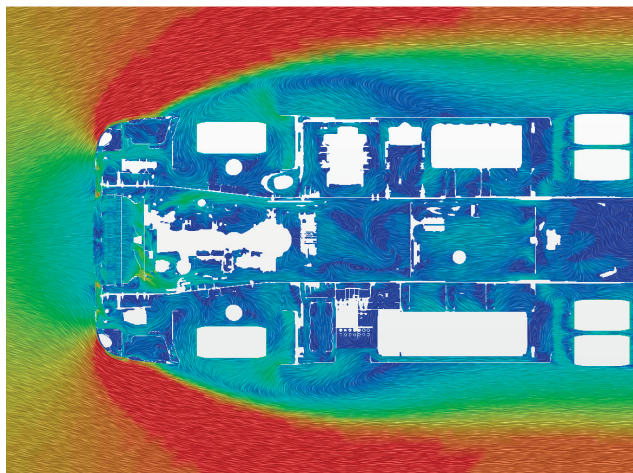

Figure 4.27: Planes of velocity magnitude at different locations along the vehicle, $5°$ yaw and windward side. The planes are cut at $22m/s$.

As Figure 4.27 shows, there were also significant changes in the flow field on this side of the vehicle, when adding the nose. The flow changes around the rear-view mirrors were not as significant as for the leeward side. The flow structures

in this region were more similar to the COE model. At chassis level, however, large differences were found: a large portion of the flow losses from the lower part of the cab and downstream was reduced with the SN $500mm$ model.

The trends seen for the 5° yaw cases were also seen for the simulations run at 0° yaw angle. The extension of the regions was however smaller, explaining the difference in magnitudes between 0° and 5° shown in Figure 4.25. Figure 4.28 shows vectors of the velocity magnitude in a plane $930mm$ above ground for the COE, SN $200mm$ and SN $500mm$ models at 0° yaw.

(a) COE.
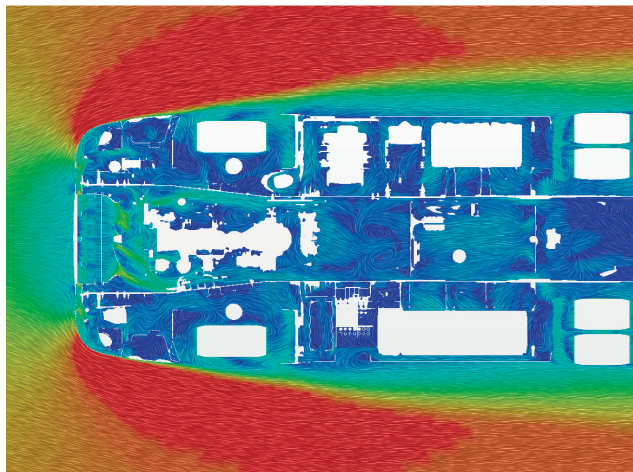
(b) SN 200*mm*.
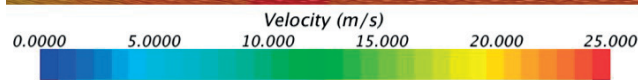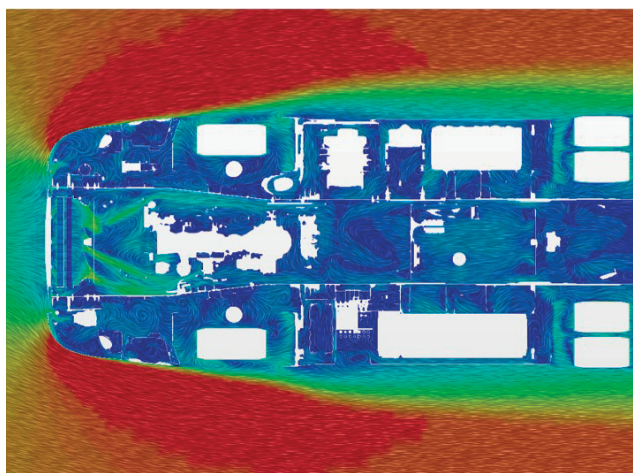
(c) SN 500*mm*.

Figure 4.28: Planes of velocity magnitude at a height of 930*mm* above ground. Note that the entire domain is not visualized in the figure.

The results in Figure 4.28 shows that, as elongating and hence smoothening the shape of the cab, the flow stayed attached longer along the sides of the vehicle. The flow seems to be attached until reaching the front wheels of the tractor, where it interacts with the irregular flow originating from the wheels. It can be concluded that, for the specific nose designs studied here, the longer the nose, the better the attachment of the flow around the corners and along the sides of the cab.

To further visualize the changes in the flow field resulting from the SN addition, the pressure coefficient (c_p) is displayed on the cab in Figure 4.29 for the three cab shapes. Note the narrow scale of c_p, which intends to visualize the differences in stagnation regions between the cases.
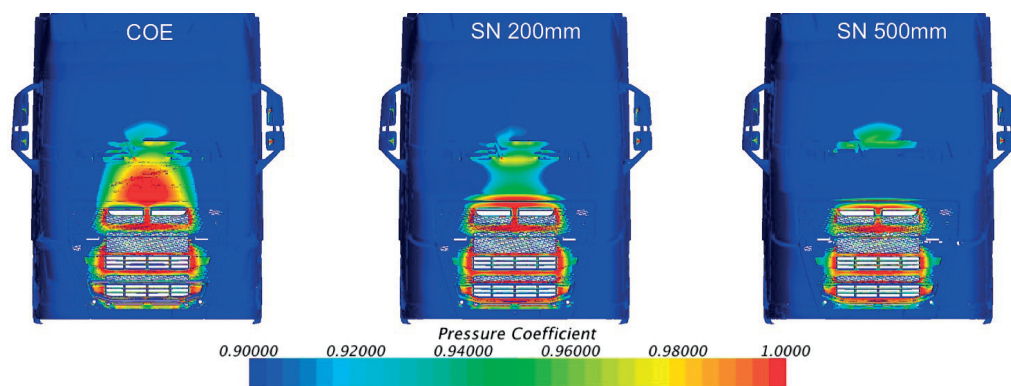
Figure 4.29: Contours of c_p displayed on the cab, seen from the front. The dark blue areas correspond to $c_p \leq 0.9$.

Figure 4.29 shows that there were significant changes in the stagnation regions between the different cab shapes. The COE model showed the most wide-spread stagnation region, and it was also positioned higher up on the front face compared to the other configurations. With the SN $200mm$ model the forward stagnation area was shifted downwards in the grille area and reduced in size. The smoother shape of the cab resulted in a smaller stagnation region; also the region itself was positioned a bit lower on the cab, as a consequence of the nose extension. This effect was further increased with the $500mm$ nose, where the stagnation region was decreased further in extension.

4.5   Influence of Under-Hood Design on the Aerodynamic Drag and Thermal Management

The results presented in the previous subsection mostly treated the exterior of the cab. In this section, results regarding different under-hood designs will be presented.

4.5.1   Potential for Grille Shutters

One discussion that is very active these days regards the possibility of closing of the entire or parts of the cooling airflow at driving situations where not all available cooling air would be needed. A typical situation for this kind of arrangement for a truck would be at highway driving: driving at constant speed and at low road inclinations. It was decided to investigate the possibility to close off the cooling airflow for a COE model and compare the results to the open-grille configuration, in terms of both aerodynamic drag and thermal management.

It was directly found that, for the given cooling situation used for the simulation, it was not possible to entirely close off the cooling airflow and still have enough amount of cooling air for the cooling module. The radiator TTT values obtained from the simulations were substantially higher than the permitted levels (target value of 100°C), hence meaning that it would not be possible to close off the entire cooling airflow at the tested operating condition. Therefore, it was decided to evaluate at which opening percentage of the grille that yielded TTT values within the permitted range. A number of simulations were hence run, with different grille designs and opening degrees of the grille area. What however must be kept in mind is the fact that CFD simulations tend to over-predict the cooling drag due to the 'perfect sealing' in the front that is possible with CAD, and the boundary conditions discrepancy between CFD and wind-tunnel measurements, which was also mentioned earlier in the thesis.

Two different approaches for opening the grille area were conducted: one where horizontal slots (HS) were opened in the grille area and one where the grille area was continuously opened (CO) from the top, with the same total percentages as with the slots. It should be noted that, in this context, the expression 'grille area' refers to the area of the grille where the CAC has been projected onto the front, creating an area where the two opening approaches were applied. The remaining parts of the cab front was covered, including the split line, and there was no grille mesh pattern left in the model. The two methods can be seen in Figure 4.30, where the rectangular light grey areas denote the grille area.

Figure 4.30: Approaches for the partially-opened grille-configurations. The HS are shown to the left, the CO to the right. The cases shown in the figure both corresponds to a grille opening percentage of 17.5%.

The results from the simulations with partially-opened grille-openings can be seen in Figure 4.31, where Figure 4.31a describes the relationship between C_D and mass flow of air through the grille area and Figure 4.31b shows the TTT values and the corresponding mass flows of air through the radiator for the respective cases. The ΔC_D values shown in Figure 4.31 are calculated as the difference between each HS and CO configuration compared to the COE model with conventional grille design at 0° yaw, used in the analysis in Section 4.4.
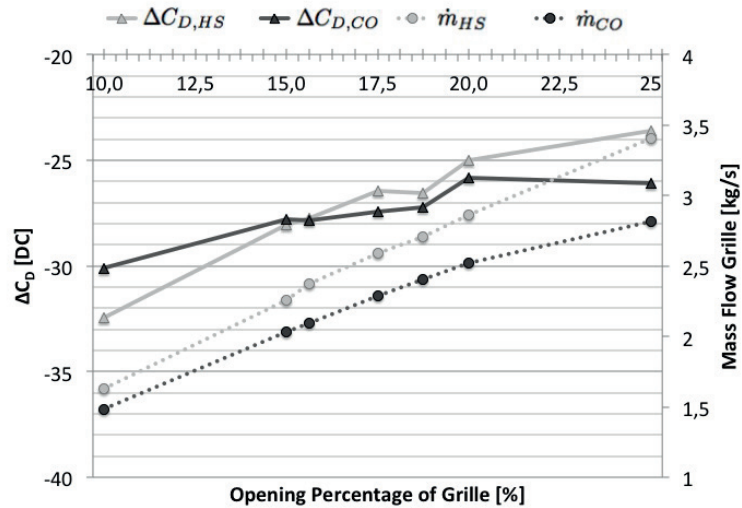
(a) Values of C_D and the corresponding mass flow of air through the grille area for different degrees of grille opening.
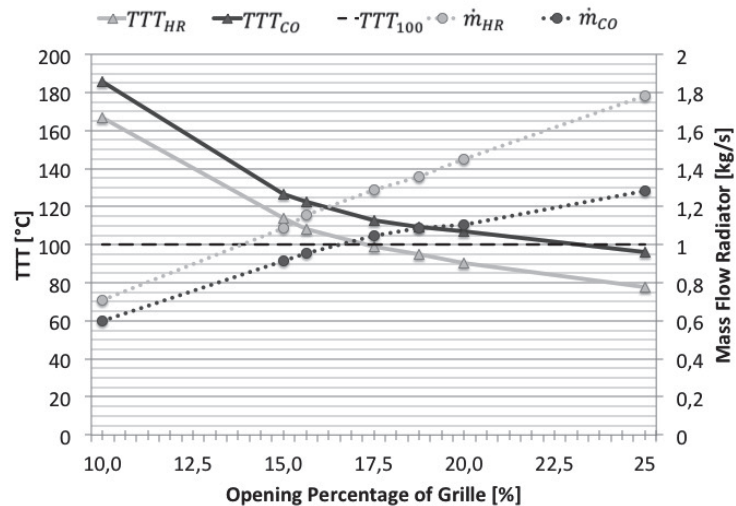
(b) Values of TTT and the corresponding mass flow of air through the radiator for different degrees of grille opening.

Figure 4.31: Results from the partially-opened grille-configurations, for the COE model.

By analyzing the results presented in Figure 4.31 it was seen that the two approaches for opening up the grille area produced significantly different results.

It was found that rather small differences in opening percentage had a large impact on the radiator TTT values. There was also a significant difference between the two methods: HS resulted in a lower opening percentage being acceptable compared to the CO approach. The fan speed was kept at a constant level of $392 rpm$, which is a typical speed for a fan in a 'wind-milling' condition. The wind-milling fan condition is defined as the speed of the fan when the fan is disengaged and its rotation is dependent on the oncoming airflow and the slipping of the fan clutch. No studies of the effect of different fan rotations were performed within this thesis, but the results would most likely be different with some degree of fan engagement.

It was found that it would be beneficial from a thermodynamic point of view to have HS, in terms of TTT values only. For the HS cases, TTT values were below the target level at 17.5% grille opening, while the corresponding value for the CO cases was 25%. However, the aerodynamic gains were very small; the C_D values for the HS with 17.5% were very similar to the 25% case for the CO arrangement. Hence the CO method would be preferable from a purely aerodynamic perspective. But, this method was seen to result in a very non-uniform temperature field in the engine bay compared to the scenario with HS. The HS approach was also thought as a more realistic representation, since air will, most likely, always leak through the grille cover construction over the entire grille area; and not, as for the CO case, be entirely sealed in the lower grille area.

To see the large effects; Figure 4.32 shows the aerodynamic drag changes for the COE model with HS 17.5% and the closed-grille configuration, compared to the COE model with open grille.
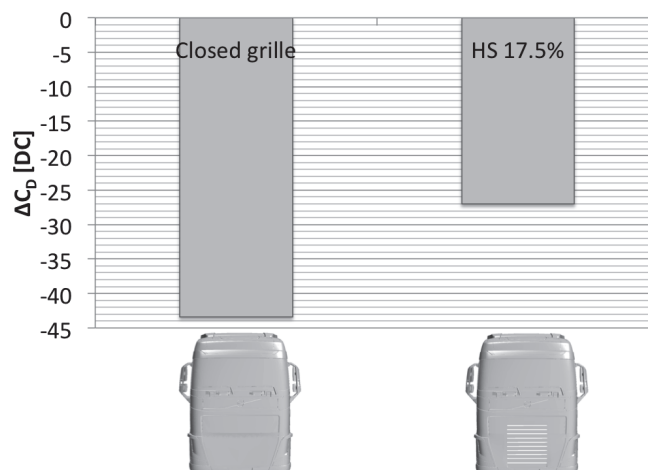

Figure 4.32: Difference in C_D for the closed-grille and the HS 17.5% configurations, relative to the COE open-grille configuration.

According to Figure 4.32, it can be seen that almost 40% of the drag reduction that was obtained with the entirely closed grille was lost as opening up the grille area by 17.5%. However, due to the fact that the perfectly sealed configuration simulated in CFD would never occur in reality, the 17.5% HS configuration would perhaps be a more realistic representation of a physical grille-shutter device.

4.5.2   Ducted Inlets and Outlets in a Soft Nose Concept

It has been shown that the displacement of the cooling module towards the grille area in the SN model was preferable from both an aerodynamic and thermal management point of view. What theoretically would be even better from a thermodynamic point of view would be to add an Inlet Duct (ID) between the grille and the cooling module, to guide the flow into the heat exchangers. Also, by moving the entire cooling module, fan and related parts forwards, an empty space is created between the fan and the engine. It would be interesting to investigate the possibility for exiting the cooling air via an Outlet Duct (OD) at different locations, to see how the cooling capacity changes and if the aerodynamic properties of the complete vehicle can be affected by such an installation. The coming subsections will treat the analysis of such inlet- and outlet ducts.

Inlet Duct

The analysis of ID addition was performed for both SN models ($200mm$ and $500mm$). The ID used for the $200mm$ nose is shown in Figure 4.33.
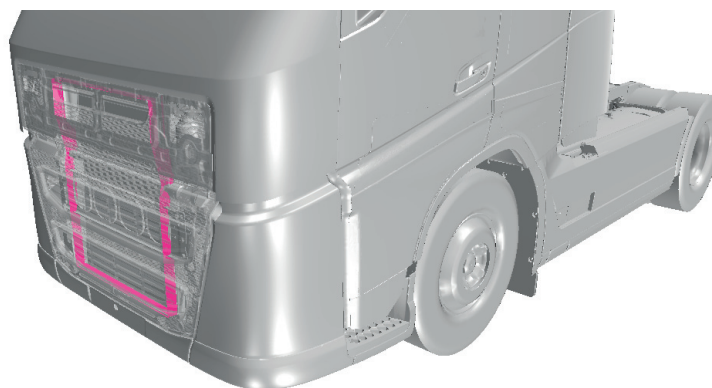

Figure 4.33: Geometry of the inlet duct used for the SN $200mm$ model. The duct is shown in pink and the grille area is made transparent, for clarification.

The results from the study where an ID was added can be seen in Figure 4.34, both for the $200mm$ and $500mm$ SN models.
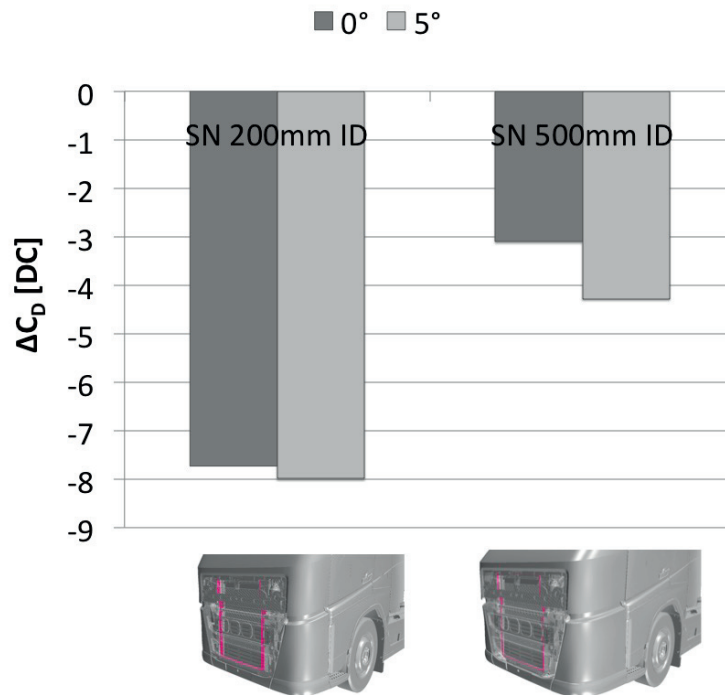
Figure 4.34: Difference in C_D when adding an ID. The SN models are related to the respective configuration and yaw angle without any ID, but with the cooling module moved $200/500mm$ towards the grille area.

It was seen from Figure 4.34 that the addition of an ID improved the flow field further, compared to the configuration where the cooling module was moved $200mm/500mm$ towards the vehicle front. It was found that for both yaw angles evaluated, the SN $200mm$ model seemed to benefit more from the ID addition than the SN $500mm$ model. The explanation for this phenomenon was the way the SN $500mm$ model was created; the geometry of the $500mm$ nose resulted in a tighter distance between the recirculation shields and the nose geometry compared to the $200mm$ model. Hence, less air was allowed to leak around the cooling module and the difference in flow field on the inside of the grille between the two SN $500mm$ models was small. It was seen that, for the SN $200mm$ model, there was an approximately 27% decrease in mass flow of air through the grille area when introducing the ID. For the SN $500mm$ model the corresponding mass flow through the grille area was similar between the ID configuration and the original; a 2% reduction in mass flow was obtained when adding the ID. The trends were seen for both 0° and 5° yaw.

To visualize the differences in mass flow in the grille area, Figure 4.35 shows the velocity magnitude shown in an x-plane just behind the grille, for the SN $200mm$ and $500mm$ models.

(a) SN 200mm, 0° yaw.

(b) SN 500mm, 0° yaw.
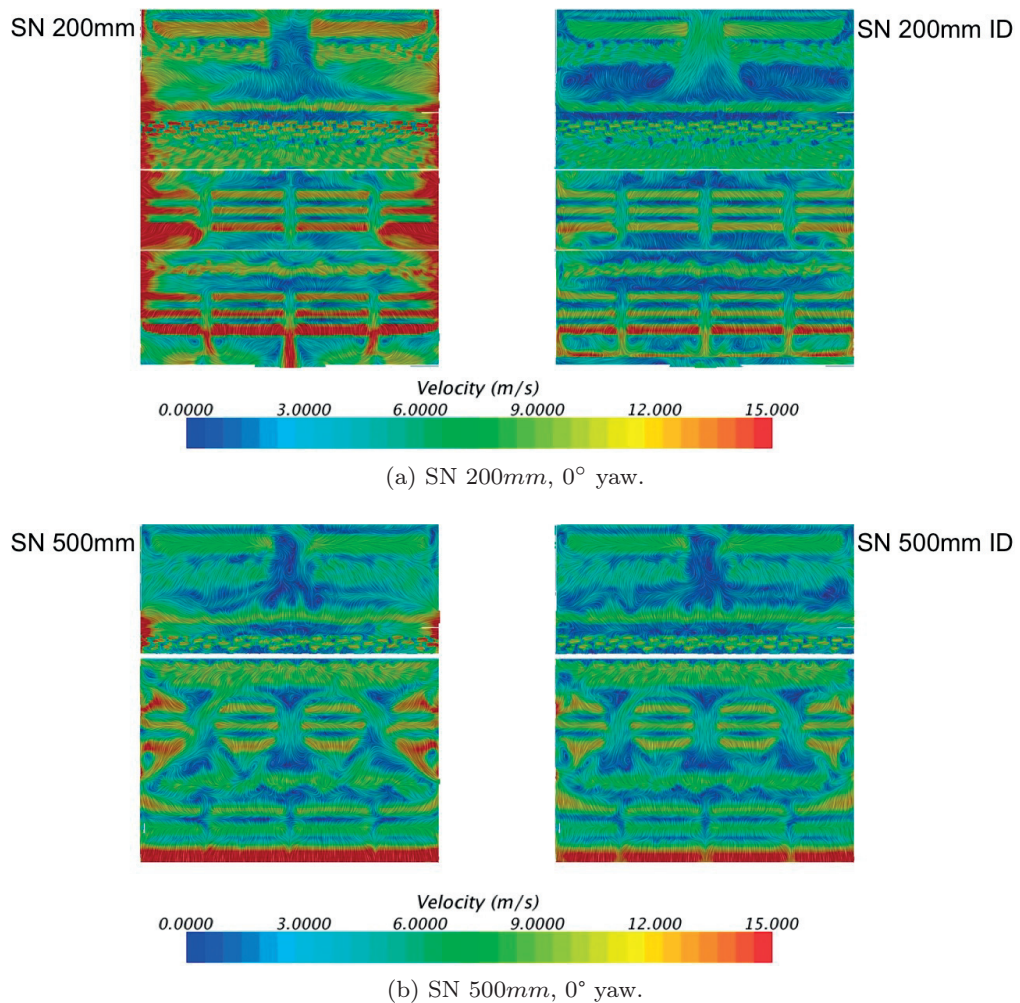
Figure 4.35: Velocity magnitude in an x-plane just behind the grille.

It can be seen that the SN 200mm model without any ID, had significantly higher velocity magnitude on the inside of the grille, also compared to the SN 500mm model, and these results were reflected both in the mass flow of air through the grille, as well as in the total drag decrease obtained for the SN 200mm model. Figure 4.35a emphasizes the benefit of an inlet duct in this configuration; the massive leakage of air on the sides of the cooling module was to a large extent eliminated with an ID.

Not only did the aerodynamic drag decrease by the addition of an ID, also the cooling capacity was improved. This was the case for the SN 200mm model, where the TTT values were reduced by 1°C, as a consequence of the increased mass flow of air through the heat exchangers, the result being valid for both tested yaw angles. For the SN 500mm model the cooling capacity was kept at the same level as without an ID. The magnitudes of the TTT values themselves were very similar for the SN 200mm and 500mm configurations.

Outlet Duct

As previously mentioned, when moving the cooling module towards the grille in the SN concept, there was a longitudinal space released behind the fan, before the engine. In addition to the ID, it was also decided to evaluate possibilities for exiting the cooling air from the fan. As the COE truck is designed today (without any elongation of the cab), the cooling airflow exiting the fan is freely released in the under-hood area, permitting it to interact with the rest of the components in the area. This leads to substantial energy losses, which theoretically could be minimized if a different under-hood layout would be implemented.

For the SN $200mm$ concept, four different OD's were evaluated in terms of aerodynamic resistance and cooling capacity. The same highway-driving scenario as used previously was used for the analysis, with the same targets for the cooling module. OD $1 - 3$ had two channels exiting on each side of the vehicle, dividing the cooling airflow into two parts. OD 4 on the other hand, had one continuous channel from the fan until the outlet of the OD. An overview of the OD's and a short explanation is shown in Figure 4.36.
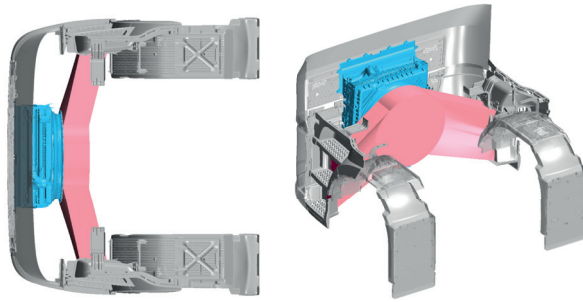
(a) OD 1: Footstep entry. The cooling air is released in the footstep entry on each side of the vehicle.
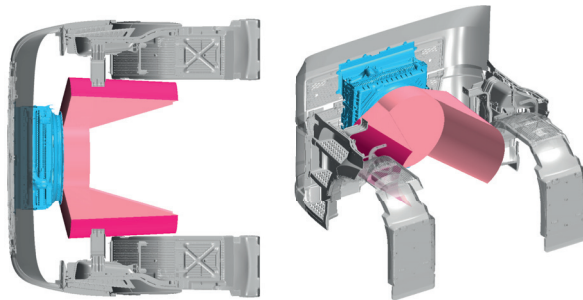
(b) OD 2: Front frame rails. The cooling air is released just outside the front frame rails on each side of the vehicle.
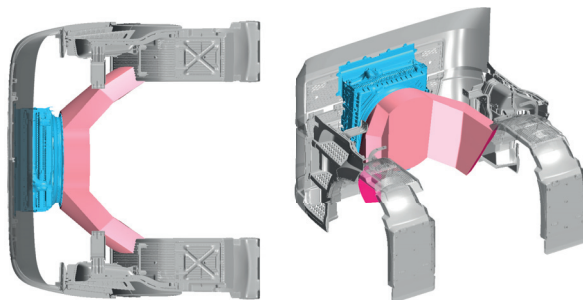
(c) OD 3: Wheelhouse. The cooling air is released in the upstream corner of the wheelhouse, on each side of the vehicle.
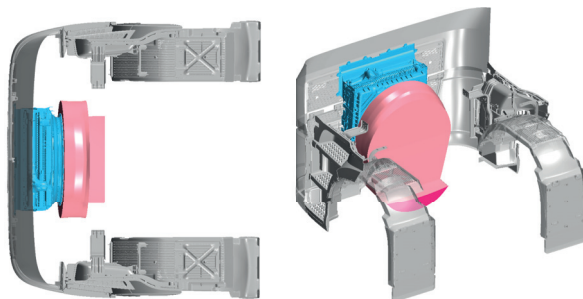
(d) OD 4: Below vehicle. The cooling air is released in one continuous channel, underneath the vehicle and below the engine.

Figure 4.36: Overview of the designs of the OD's evaluated. The ducts are shown in pink, the cooling module in blue colour. The bright pink areas show the outlet area of the duct. Several parts of the under-hood have been excluded, for clarity.

For OD 1, in addition to the OD itself, prolonged door extensions were also added to the model. The aim with the OD 1 design was that the air flowing out from the footstep entry would merge with the exterior flow field in a way that would not create any further flow losses in the vicinity of the door and front wheels. Therefore, the door extensions were further prolonged in the vertical direction and a flap was added downstream, to push the flow through this narrow channel. The door extension and the flap used for OD 1 can be seen in Figure 4.37.
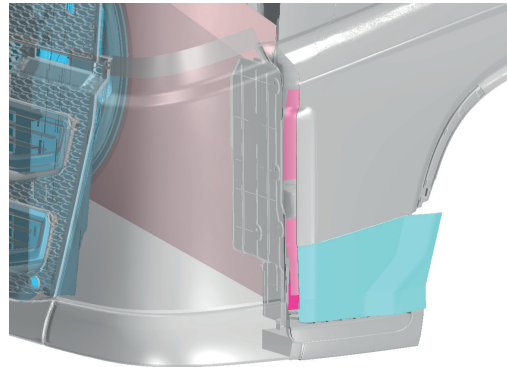
Figure 4.37: Door extension with added flap and elongated in vertical direction to cover almost the entire footstep entry, used for OD 1.

The results from the OD study is shown in Figure 4.38. For comparison, the results for the SN $200mm$ with ID are also presented along with the OD results. Note that all OD simulations also included the ID.
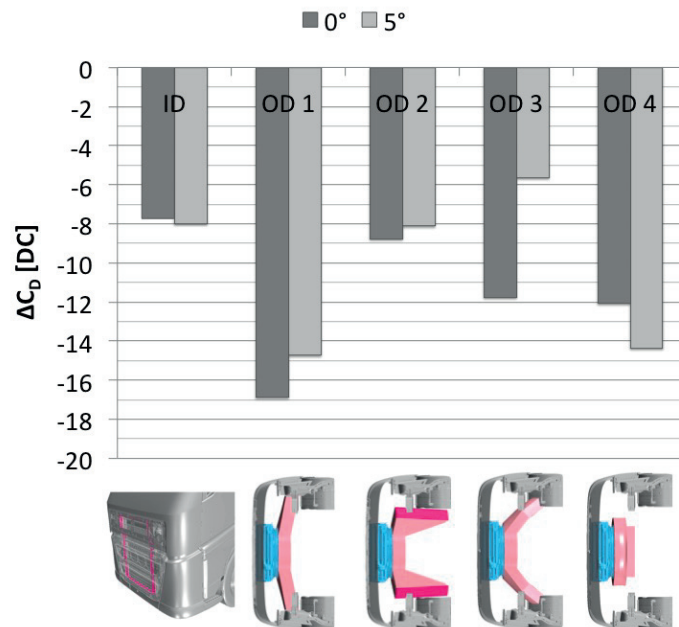
Figure 4.38: Difference in C_D for the ID and OD cases relative to the SN $200mm$ with moved cooling module.

It was seen that the addition of the OD's resulted in reduced aerodynamic resistance for all tested configurations. However, when analyzing the results it would not be enough to only consider the drag levels; it is also necessary to include the cooling airflow aspect in order to achieve a practical, reliable concept. Figure 4.39 shows the mass flow of air through the radiator together with the TTT value for each of the ID and OD configuration. The results presented are from 0° yaw, but the magnitudes were consistent for both tested yaw angles.
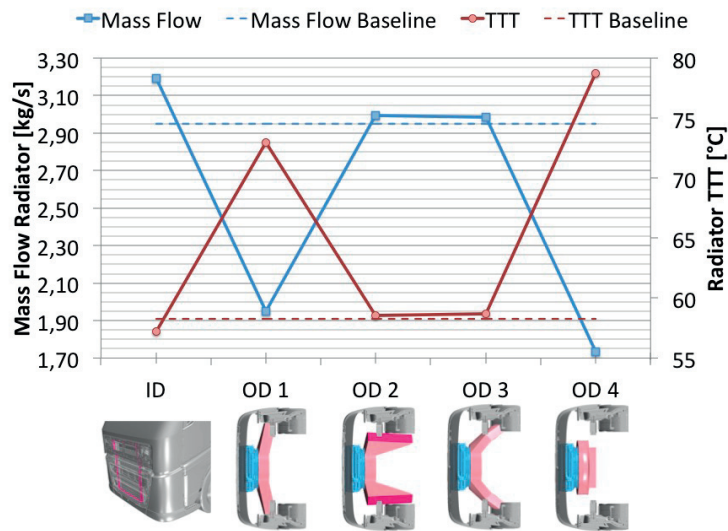
Figure 4.39: Mass flow through the radiator and corresponding TTT values for the ID and OD configurations, 0° yaw.

The results from the analysis of the OD's showed that the drag reductions were rather small; OD 1, the case with the largest drag improvements in terms of aerodynamic drag, resulted in a significantly decreased amount of air through the cooling module and hence a larger TTT value was obtained. Similar results were seen for OD 4, where a rather modest drag reduction yielded very much higher radiator temperatures.

Visualizing the pressure level in a plane cut through the entire vehicle body, the OD itself can be evaluated in terms of pressure-drop between the duct and the exterior flow field. Figure 4.40 shows the static pressure in a z-plane at different heights above the ground for the OD configurations. The reason for using different heights of the planes was to capture the effects occurring at the outlet of the duct.

(a) OD 1 ($z = 680mm$) and OD 2 ($z = 930mm$).

(b) OD 3 ($z = 930mm$) and OD 4 ($z = 330mm$).
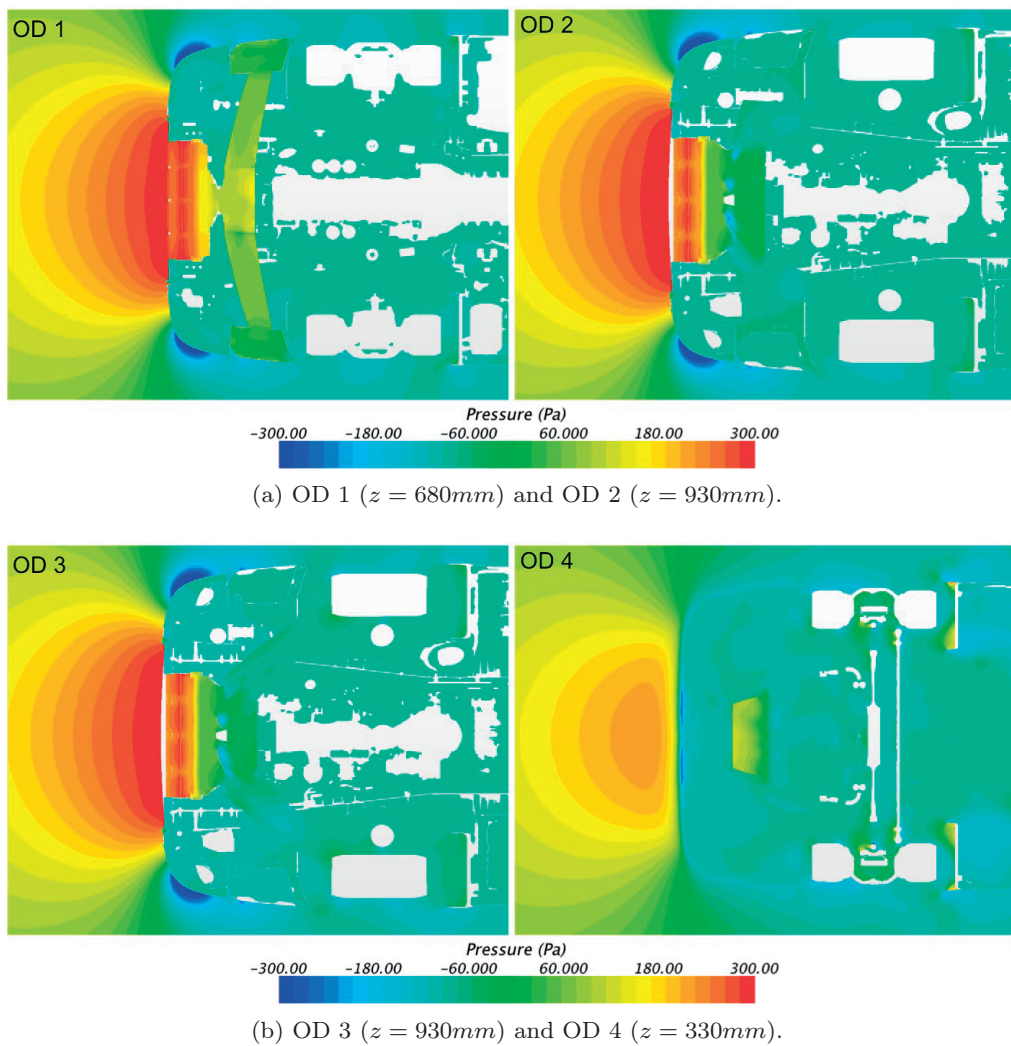
Figure 4.40: Planes of static pressure displayed in a z-plane through the vehicle model.

Figure 4.40 shows that for two OD's the pressure-drops between the duct and the surrounding air were significant, and this was for OD 1 and OD 4. Both these models showed very high pressures in the channel compared to the other two OD's. Hence the designs of these particular OD's, including the outlets, were not ideal. From previous observations, it has been seen that OD 2 and OD 3 were both showing satisfactory results in terms of cooling capacity. By this visualization of the results, it can be further understood. The pressure levels of OD 2 and OD 3 were very similar in the entire under hood, and hence there were less flow losses due to this phenomenon.

4.6   Combined Approach for Complete Vehicle Combination

So far, different approaches of reducing aerodynamic drag and improving the cooling airflow have been evaluated. In this section, some of the concepts have been combined to investigate their total effect on drag and thermal management.

According to the results presented earlier in this thesis, it has been proven that the use of fewer, but longer vehicle combinations, would be efficient from an aerodynamic perspective, as well as the total effect on transport efficiency. The basis for the analysis here was the T2S model discussed in Section 4.3 and modifications to this model were made. As indicated both by the vehicle combinations study in Section 4.1 and the study of drag-reducing devices for trailers in Section 4.3, the gap region between the two cargo-units is a large source of drag. Therefore, the gap between the semi-trailer units was eliminated. The practical gap fairing device, which was evaluated in Section 4.3, was shown to reduce drag, to a greater extent between the cab and the 1st semi-trailer unit, due to the smaller gap between these two parts. Therefore, the gap fairing was also added to the 1st semi-trailer. Furthermore, it is evident that the flow field at chassis level for the trailer units could benefit from improved flow field in this area. The underbodies of the trailers used within the investigations here were very bare, giving possibilities for a massive amount of cross-flow through the chassis, especially in yawed-wind conditions. Hence, chassis skirts for the trailer units were added to the final model. With a covered or eliminated gap between the trailers, the feasibility of such a concept can be questioned. What was aimed for in the investigation presented here was to show the potential for such a transport concept, without having any major limitations with respect to practicality. Regarding the eliminated gap between the trailers, this is something that could be achieved, to certain extent. By an adjustable coupling between the trailers the gap size can be reduced, depending on the truck operation.

By the elongation of the COE cab, and the addition of a SN, an improved flow field around the vehicle was obtained. The potential for both improved aerodynamic drag and cooling capacity was evident, especially for the longer of the two noses evaluated (SN $500mm$). Additional improvements of both aerodynamic drag and cooling capacity was obtained by also adding an ID to guide the flow from the grille to the cooling module and hence these additions were also made to the final model. The vehicle combination is referred to as SN2S $500mm$ ID-GF-EG-CS, according to the previously defined naming convention.

A figure of the final vehicle combination, with all added devices and modifications, is shown in Figure 4.41.
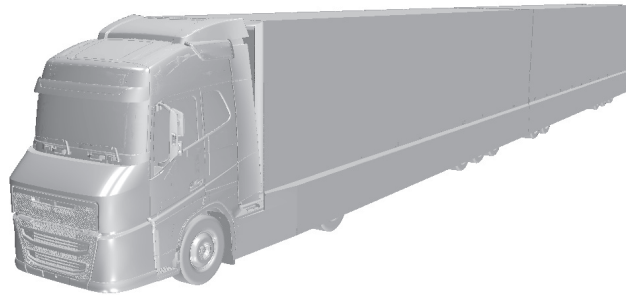
Figure 4.41: Geometry of final vehicle model: SN2S $500mm$ ID-GF-EG-CS.

Comparing the results from the simulations with combined drag-reducing approaches to the previously presented results revealed interesting phenomena. The SN2S $500mm$ configuration was compared together with the SN $500mm$ with ID, and related to the COE configuration without any additional drag-reducing strategies. Figure 4.42 shows the difference in C_D between the configurations.
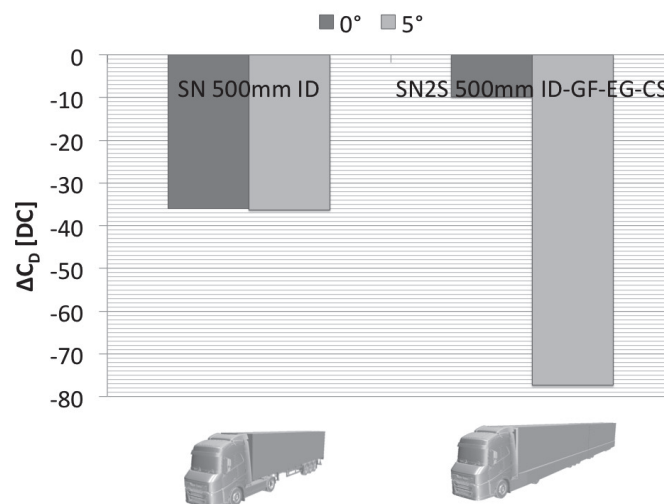
Figure 4.42: Difference in C_D for the SN $500mm$ ID and SN2S $500mm$ ID-GF-EG-CS relative to the COE vehicle combination without any drag-reducing strategies.

Figure 4.42 shows that the addition of an extra semi-trailer unit did not result in any significant drag increase at 0° yaw compared to the other SN $500mm$ model; the SN2S model still showed a $10DC$ reduction in C_D compared to the COE combination, which only had one cargo-unit. The results in 5° yaw

again confirmed that chassis skirts for trailer units was an efficient concept: the addition of chassis skirts, eliminated gap between the trailers and a gap fairing mounted on the 1st trailer unit, a reduction of $80DC$ was found at 5° yaw. Figure 4.43 visualizes the differences in the flow field between the SN $500mm$ and the SN2S $500mm$ models at 5° yaw.
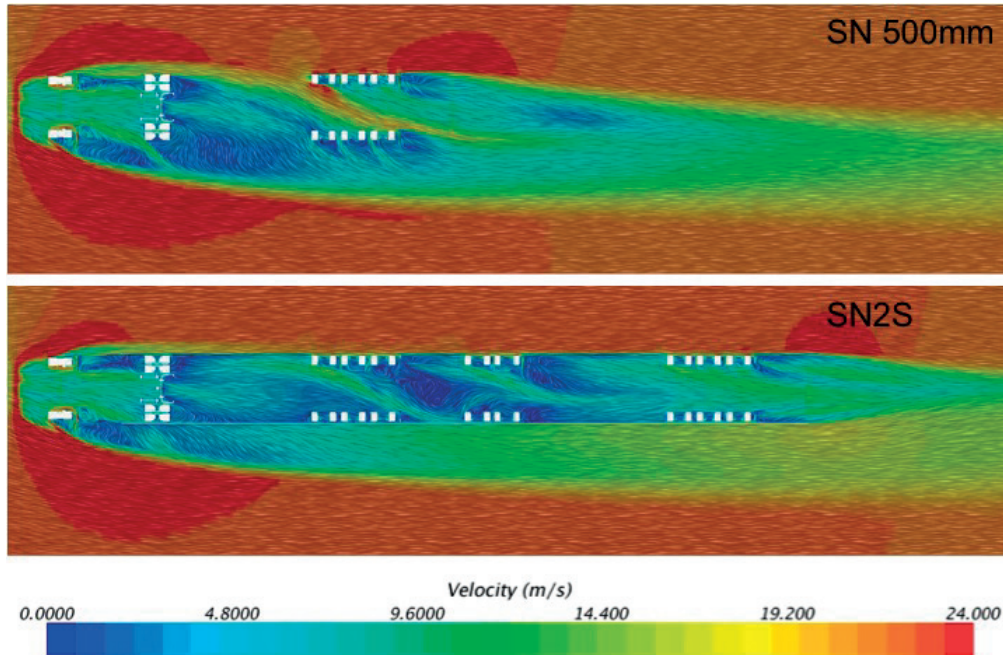
Figure 4.43: Velocity magnitude displayed in a z-plane at $230mm$ above ground, 5° yaw.

As can be seen from Figure 4.43, there were significant differences in the flow field as adding the second semi-trailer unit and the ideal chassis skirts. The plane was positioned $230mm$ above ground; a cut through each of the wheel pairs of the model can hence be seen. It can be seen that the flow field around the cab front, until reaching the front wheelhouse, was very similar between the models. After this point, there were large differences in the flow behaviour along the vehicle, thanks to the chassis skirts along the semi-trailer units. The chassis skirts used for the trailer units were blocking the flow field to a large extent, and instead the flow field stayed attached to the vehicle surface along the windward side of the vehicle. Comparing the velocity fields for the two models along the trailers, there was a strong cross-flow of air through the chassis of the semi-trailer unit for the SN $500mm$. As also has been indicated earlier in the thesis, the design of this particular semi-trailer unit was sensitive for cross-winds due to its exposed underbody. Interestingly, it seemed that there was an equal extension of disturbed flow field in the lateral direction, on the leeward side for the two models analyzed. Though, there were differences in the magnitudes of the velocity in these areas. The SN $500mm$ model clearly showed larger areas of significant flow losses, indicated by the low-velocity areas in Figure 4.43.

What can be concluded from this combined study is that the chassis skirts themselves were the main contributor to the massive reduction in aerodynamic drag seen for this model.

5 Discussion

The answer to where the largest potential for reduced aerodynamic drag is to be found on a complete truck and trailer combination, is not something that can be easily pointed out. There are many factors that have to be included in such an analysis. Apart from the analysis of the airflow and the theoretical possible reductions in air resistance, there must also be considerations regarding the practicality and feasibility of the different concepts. Something that shows large potential from a purely aerodynamic point of view, may be so difficult to solve technically that it loses its potential. For example, if the technical solution of an aerodynamic problem adds extra weight to the vehicle, this has to be included in the total picture since this puts limitations on the total gains associated with the concept. Other examples of limitations to the potential is the degree of change required for the rest of the vehicle in order to obtain the aerodynamic improvements, and also what implications is has on the cost of the vehicle.

It has been shown in this thesis that the use of fewer, but longer vehicle combinations, is something that has large potential from both an aerodynamic and transport efficiency point of view. Only by the use of longer vehicle combinations, without improving the aerodynamic properties of the combinations, shows that the relative power consumption is reduced. By also improving the flow field around the vehicle, in terms of added chassis skirts for the trailer units and improving the flow in the gap between the cargo-units, the overall potential for longer transport concepts is large. It has been shown that a vehicle combination in the range of $30m$ can produce C_D values of the same level, or even lower, as a conventional tractor - semi-trailer unit of 16.5m. The absolutely largest improvements are seen for the longer vehicle combinations that are subjected to some kind of side-wind conditions. It is appreciated the reductions in aerodynamic drag along the chassis level experienced for the trailer-units by adding chassis skirts covering the entire sides of the trailers.

It has been shown that two of the most widely used drag-reducing devices for trucks, the roof deflector and cab side-extenders, are effective in reducing drag for vehicle combinations of different lengths. However, it was clear that for the longer vehicle combinations, a larger portion of the drag reduction that was obtained locally in the flow field where the devices operated, was reduced further downstream. This result was seen due to the fact that the trailer units were not aerodynamically considered. The suggestion here is hence also to consider the aerodynamic behaviour for the trailer units, in order to maintain the positive effects of theses devices.

Considering a design change of the front of the vehicle, both the exterior shape of the cab and the layout of the components in the under-hood area, there is for sure potential for an improved flow field around the vehicle, as well as possibilities for a more efficient cooling airflow. It has been shown that, for a highway driving condition at $80km/h$, the entire cooling airflow could not be shut off permanently since the heat exchangers needed more cooling air than was achieved with an entirely sealed-front configuration. It should, however, be mentioned that the entirely sealed front evaluated in this thesis was really 100% sealed, meaning that absolutely no air could enter the under hood through the grille area. In reality, if having a grille-shutter acting like some kind of throttle device, there will for sure be some leakage of air through the grille-shutter, but the question to pose is how much, and if the leakage air would be sufficient to ensure the right amount of cooling airflow? As a consequence of the result that the 100% sealed-front configuration did not result in proper levels of the TTT's, the partially-opened grille scenarios were evaluated. The configuration with HS was shown to result in a lower opening percentage for an acceptable limit of the TTT value, compared to the CO case. The conclusions from these studies were that it seemed possible to introduce a grille-shutter system to be used for highway-driving conditions, but that proper considerations regarding its design and opening degree must be done. Compared to an opened-grille configuration, the possible drag savings with the 17.5% HS configuration was $26DC$. The corresponding value for the 100% sealed front was $40DC$, so about 1/3 of the possible drag reduction was lost by opening up 17.5% of the grille area. Important to keep in mind is that the $40DC$ reduction would be practically impossible to achieve for this particular configuration since the cooling performance parameters were not of satisfactory levels and hence the $26DC$ result must be seen as a good result; the magnitude of the drag reduction was still significant.

Regarding the cab design itself, it has been seen that the introduction of a SN, where the COE grille was extended in the longitudinal direction, resulted in rather significant aerodynamic improvements. Even though the elongations were rather modest, $200mm$ and $500mm$, there were drag reductions associated to the design change for both evaluated yaw angles. The 5° yaw results showed considerably larger reductions than in 0° yaw, for both the $200mm$ and $500mm$ model. For comparison, the SN $200mm$ model had a $24DC$ drag reduction at 0° yaw, as compared to the COE model with 17.5% HS that showed a $26DC$ reduction, compared to the same reference case. For the SN models though, the under-hood design was seen to be a crucial parameter; there was no need to make changes to the exterior of the cab without also considering the layout of the components in the under hood. The numerical results mentioned above for the SN $200mm$ consider a under-hood design with moved cooling module towards the grille area, to minimize the effects of leakage around the cooling module.

For the SN models, the movement of the entire cooling module, fan and other related geometries, such as the expansion tank, pipes and hoses, is something that is easily done in virtual models. In reality the situation is not as easy. The cooling module has a considerable weight, which would result in higher front-axle loads if moving the entire cooling package forwards. Even for the

$200mm$ nose, the effect on the front-axle load is significant, for the $500mm$ nose the effect would be even larger. A question to pose is whether it would be more practically feasible to keep the cooling module at its original position, and install a duct between the grille and the cooling module. The effect would be the same as when ducting the cooling inlet for the cases with moved cooling module, but the channel itself would be longer. If the gains of having such installation instead would be of the same magnitude as when moving the cooling module, many of the practical issues could be avoided. By a quick study of the comparison for the two different approaches of ducting of the inlet, it did not seem that the differences were large, neither in terms of aerodynamic drag, nor cooling capacity. Hence the suggestion would be to further analyze the longer ducting system for SN models, to ensure proper function and desired levels of drag and cooling performance.

By the movement of the cooling module longitudinally in a SN concept, free space was released behind the cooling fan, before the engine. The layout of the components in the under hood today leaves little room for innovative solutions of where to release the cooling air. As the design is today, the cooling air is simply released behind the fan and freely interacts with the irregular structures present in the under-hood area. The analysis of outlet ducts was then formed, to evaluate possibilities for reducing aerodynamic drag, at the same time keeping the cooling capacity at the same level, or better, than the original. The implications on the results by the introduction of outlet ducts were more difficult to interpret and gave rise to new questions. The approach of where to exit the cooling air seemed crucial for the function of the outlet duct system as such. By introducing a channel between the fan and surfaces at the exterior of the vehicle, a resistance was created and resulted in that less air was pushed through the channels and hence the TTT values were increased for most of the ducts evaluated. The maximum drag reduction achieved was $17DC$, for a configuration which resulted in significantly higher TTT values. It was also seen that the aerodynamic drag was accumulated differently in the under-hood area depending on which kind of outlet duct that was used. It was however the case, that the drag changes were seen most locally in the under hood; the effects on the total flow field was rather small.

The quick answer to where the largest potential for reduced aerodynamic resistance is found on a complete truck and trailer combination, would definitely be on the trailer unit. The potential aerodynamic savings were shown to be very prominent, especially if combining different approaches with each other along the trailer units and thereby creating a some kind of 'optimized' flow structure around the trailer. Among the drag-reducing strategies employed for the trailer units, it can be concluded that working with the chassis level has a large potential for improvements. The approach of using chassis skirts for the trailers has in this thesis been in form of very ideal solutions and meant that all wheels of the trailer units were covered. In reality, such a solution may not be viable for a more practical solution of the chassis skirts: in terms of contamination and dirt deposition, as well as thermal aspects of brake cooling. The impression is, however, that a practical solution of chassis skirts for trailers similar to the ideal chassis skirts would be possible to achieve, and still result in substantial drag reductions.

Even though the largest source of improvements may be found for the trailer units, there is still room for improvements by also work with the design of the cab and an elongation of the tractive unit. Considering the layout of the components in the under hood, possibilities for layouts different from the ones treated in this thesis are seen. One example could be to split the cooling module into smaller components, being able to assign them their own grille inlets. This would result in a more flexible cooling airflow and the potential for such a system would be interesting to evaluate. As the cooling module is commonly arranged in trucks today, the AC condenser is placed in front of the CAC and radiator. The climate system of the truck commonly demands airflow through the AC condenser, even at situations where the CAC and radiator does not require much airflow; hence the potential for redistributing the cooling module components is detected. What also needs to be discussed is the length of the SN, if simply elongating the grille area of a COE cab. In this thesis, two distinct elongations of the grille area have been evaluated, $200mm$ and $500mm$, and their respective potential has been pointed out. In order to more specifically be able to state the potential for design changes made to the tractive unit front, a wider range of the elongations needs to be analyzed to distinguish the specific implications on aerodynamic drag and cooling capacity.

Another discussion that is relevant for the area of studies performed here is the aspects of tractive unit and trailer OEM's. The most common scenario today is that the tractive units and trailers are developed by separate OEM's. Hence, the truck OEM's do not know what kind of trailer that will be used by the fleet owner afterwards, and therefore the possibility for adaptation of the respective tractive unit to the different trailers is not very large. The truck owner can adjust the height of the roof deflector depending on the height of the trailer, but other than that the possible adjustments are small. It would be a big step for the truck business to merge the development processes for tractive units and trailers, but the potential gains are, from an aerodynamic perspective, very large. In such case, it would be possible to optimize each vehicle combination to ensure proper aerodynamic function of the vehicle. The truck OEM's would by this commonality approach be able to market themselves as an even more environmental-friendly company, which is a rather desirable aspect nowadays.

6   Conclusions

The total driving resistance can be reduced by the use of fewer, but longer vehicle combinations. Their aerodynamic properties change by the addition of more cargo-units and show large areas of energy losses at ground level along the trailers and in the gap between the units. By working with these two problem areas, the total aerodynamic drag for longer vehicle combinations can be reduced by considerable amounts.

A properly designed $30m$ long vehicle combination can produce C_D values of the same magnitude or lower than a $16.5m$ tractor - semi-trailer combination with no additional devices added to the trailer unit.

For the longer vehicle combinations, it has been shown that a large portion of the drag-reduction obtained by the roof deflector and cab-side extenders in the cab region, are lost as moving downstream along the trailer. This indicates that the trailers are not properly designed and the total drag levels would benefit from a mutual design approach for both the tractive unit and the trailer.

By restricting the airflow through the under hood at highway driving conditions, to simulate the function of a grille shutter device, it was found that a 100% sealed front did not result in sufficient amount of cooling airflow for the specified conditions. It was shown that a 17.5% opening of the grille area yielded TTT values below the approved level of 100°C. There was certainly a potential for fuel savings by a covered grille; however the levels of drag reduction needs to be confirmed by test data.

By the introduction of a soft nose, simply by an elongation of the COE grille area by $200mm$ and $500mm$, it has been shown that the under hood of the model also needs to be reconsidered in order to obtain any major aerodynamic reductions and desired amounts of cooling airflow. Either this can be done by also moving the cooling module and related components towards the grille, reducing the distance between the grille and cooling package, or by a inlet duct between the inside of the grille and the cooling module, guiding the flow.

It has been seen that the overall potential for adding outlet ducts was rather low, compared to the other approaches evaluated in the thesis. The introduction of outlet ducts would require an extensive re-design of the entire under-hood area, with only small aerodynamic gains in return. It is still recommended to further examine the possibilities for outlet ducts, since only a few designs were evaluated in this thesis.

As a final conclusion, it can be stated that it would be beneficial, from an aerodynamic point of view, for tractive units and trailers to be developed by the same OEM's, or at least being developed in close cooperation between companies. It is seen as a natural continuation in the design process to optimize the aerodynamic properties of the entire vehicle combination together with the other aspects of a truck, in the strive for the most energy-efficient truck and trailer on the market.

7 Further Work

Truck and trailer aerodynamics focusing on the possibilities seen with reconsidered length legislation, is a wide-spread area of research and naturally, there are no possibilities to cover all aspects within a PhD study. For following work within the area, a few recommendations can be made.

It was concluded in this thesis that the trailer unit itself has a largest potential for substantial aerodynamic improvements, by proper re-design or by introducing add-on devices. It should however be emphasized that the tractive unit also still has potential for further improvements, even though the development curve for current design have flattened out compared to the trailer. In this thesis, two distinct elongations of the COE cab have been investigated. For future work, it is suggested to evaluate different elongations, in terms of lengths and designs, to investigate the development curve for elongated tractive units.

Regarding the study of outlet ducts, the results presented in this thesis are design-specific for the particular outlet ducts evaluated. Also, the size of the outlet duct longitudinally was something set by the elongation of the COE cab, in this case $200mm$, which is a relatively small distance for being able to introduce a duct. It would hence be of interest to unconditionally investigate the area of outlet ducts in more detail, to be able to point out their potential without external boundary conditions.

An interesting continuation of the study regarding ducted cooling airflows would be to investigate possibilities and potential gains with splitting the cooling module into smaller parts and placing them differently in the under hood, with separate inlets and outlets for the cooling air. By this approach, a more customized cooling situation can be achieved and the possibilities for reduced aerodynamic drag is seen by being able to restrict the airflow to certain heat exchangers at non-critical operating conditions.

8 Summary of Papers

Paper I

Influence of Different Truck and Trailer Combinations on the Aerodynamic Drag

Presented at SAE World Congress 2011*, Detroit.*

The first paper treated the aerodynamics of truck-trailer combinations. Six different vehicle combinations were used in the computational study, where they differed both in terms of total length, type of tractive unit, types of cargo-units and the associated gap sizes between them. Important parameters were the dependence of yaw angle on the drag coefficient, and the dependence of gap size between two cargo-units on the drag associated to the model.

The main results from the paper was that the longer vehicle combinations yielded considerably more aerodynamic drag than the shorter vehicles. They were also especially sensitive to yawed-wind conditions. It was also concluded that the gap size between two cargo-units appeared to be an important factor determining the total drag of the vehicle combination. However, it was also found from the study that it may be favourable from a transport efficiency point of view to use fewer, but longer vehicle combinations. The simplified study performed in the paper showed that the longest vehicle combinations produced approximately 80% of the power requirements per loading length compared to a traditional tractor-semi-trailer combination.

Paper II

Aerodynamic Effects of Roof Deflector and Cab Side Extenders for Truck-Trailer Combinations

Presented at SAE Commercial Vehicle Engineering Congress 2011*, Chicago.*

The second paper considered the efficiency of roof deflector and cab side-extenders for three different vehicle combinations, with a rigid truck as the tractive unit. Three configurations of each vehicle combination were analyzed in order to determine the aerodynamic efficiency of the drag-reducing devices. One important aspect was how the drag accumulation developed whilst moving downstream, to see how well the possible drag reductions performed along the vehicle.

The results showed that the two drag-reducing devices were efficiently reducing drag for all vehicle combinations. However, the results varied depending on whether the results in 0° yaw or 5° yaw were considered: for straight-ahead wind conditions the shortest vehicle combinations appeared to gain the most in terms of absolute drag reduction when adding both devices; whereas the side wind simulations showed that the longest vehicle combination gained the most. The flow fields were rather similar for all cases with identical set-up of drag-reducing devices; for example there was a large area of energy losses on the leeward side at chassis level for the cases without any roof deflector and cab side-extenders. Another interesting result was that the drag reductions that were obtained upstream in the cab area were somewhat lost when moving downstream. The main conclusion from the study was that it is important to make improvements of the entire vehicle combination, in order to maintain the positive effects produced by the drag-reducing devices upstream.

Paper III

Aerodynamic Investigation of Gap Treatment- and Chassis Skirts Strategies for a Novel Long-Haul Vehicle Combination

Published in SAE International Journal of Commercial Vehicles 5 (2) , pp. 616 − 627, 2012.

Previous studies have indicated that the use of longer, but fewer vehicle combinations, would be beneficial from a transport efficiency point of view. It has also been seen that the effect of two of the most common drag-reducing devices, the roof deflector and cab-side extenders, are reduced as moving downstream of the vehicle. This effect was particularly strong for the longer vehicle combinations, indicating that the non-aerodynamic nature of the trailers have to be improved to better maintain the effects of the drag-reducing devices obtained in the cab region. In this paper, a novel vehicle combination was analyzed in terms of aerodynamic properties; the vehicle was $31.60m$ long and consisted of a tractor and two semi-trailer units in tandem. Ideal design changes of the trailers were made, such as chassis skirts covering the entire chassis of the trailers, a covered or eliminated gap between the trailer units, and combinations of the devices. Additionally, a more practical solution to improving the gap flow was evaluated.

The results showed that by the use of the ideal design changes, the aerodynamic drag was reduced to a large extent. The combined gap treatment and chassis skirts were especially successful; the total drag coefficient was reduced significantly. It was seen that the chassis skirts were far more efficient compared to gap treatment; as a consequence of blocking the main part of the airflow at chassis level in yawed-wind conditions. The practical solution with a gap fairing was shown to be efficient, if used for both semi-trailer units.

Paper IV

Comparative Studies between CFD and Wind Tunnel Measurements of Cooling Performance and External Aerodynamics for a Heavy Truck

The fourth paper included two comparative studies between CFD and measurements. The first one is a comparison between cooling performance simulations and chassis dynamometer measurements; the second study is a comparison between external aerodynamics simulations and wind-tunnel measurements. The purpose of this study was to evaluate and develop methods and models for determining aerodynamic drag and cooling performance, for the future development of more energy-efficient cooling of heavy trucks.

The results from the two studies showed that there was in general good agreement between CFD and wind-tunnel measurements. For the cooling performance simulations, the analyzed parameters were very close to the measured values. For the external aerodynamics simulations, the results were not easy to analyze. The overall results were still satisfactory; for the simulated yaw angles, the values of the drag coefficient were less than 4.1% different from measured data.

Paper V

Aerodynamic Analysis of Cooling Airflow for Different Front-End Designs of a Heavy-Duty Cab-over-Engine Truck

The fifth paper concerned the front-end design of a COE truck, where the aerodynamic properties and cooling airflow were evaluated. Two different front-end shapes were evaluated; one was a Volvo FH COE model, and one configuration where the COE front was extended $200mm$ in the longitudinal direction, to evaluate the difference in aerodynamic properties and cooling airflow. Also, the potential for implementing a grille-shutter device for highway-driving conditions was evaluated for the COE model.

The results showed that there were possibilities for drag reductions associated with the elongated front; however, careful considerations have to be taken regarding the under-hood design to be able to benefit from the new exterior shape. It was seen that, without making any changes to the under hood of the elongated model, there was a considerable amount of leakage of air around the cooling module. Hence, a large portion of the air was flowing around the cooling module, instead of through it. Considering the possibility for closing the grille at highway driving, the simulations showed that it would not be possible

to entirely seal the front of the vehicle and still obtain sufficient amount of cooling air. By opening up slots in the grille area, it was found that an opening degree of 17.5% of the grille area resulted in radiator temperatures below the target value of 100°C. One of the main conclusions from the investigation was that, if considering making an elongation of the cab front, the layout under-hood components needs to be reconsidered.

Paper VI

Perspectives of Aerodynamic Drag and Thermal Management for an Elongated Heavy-Duty Cab-over-Engine Truck with Ducted Cooling Air Inlets and Outlets

Submitted to SAE International Journal of Commercial Vehicles, 2016.

The sixth paper was a direct continuation of the fifth paper. In this paper, the elongated COE model was evaluated with a different layout of the components in the under hood. The cooling module, fan and related components was moved $200mm$ towards the front of the vehicle, to reduce the amount of leakage of air around the cooling module. Also, an inlet duct was added between the grille and cooling module, with the aim of further improving the aerodynamics and cooling capacity. By the movement of the cooling module towards the grille area, free space was created longitudinally between the fan and the engine. This space was used to lead the cooling air out from the engine bay. Four different designs of outlet ducts were evaluated, to investigate their implications on the aerodynamic drag, and the cooling capacity of the vehicle.

The results showed that by the movement of the cooling module towards the grille, the aerodynamic drag was reduced and the cooling capacity was increased. By the addition of the inlet duct these parameters were further improved, avoiding any leakage of air around the cooling module. The addition of an outlet duct did not result in any major improvements with respect to aerodynamic drag and cooling capacity; difficulties with the geometrical design is considered as one explanation for this. Design changes of the outlet duct could improve the results, but the overall potential for this kind of duct implementation is considered rather low, given that the layout of the components in the under hood would need to be heavily re-designed.

References

[1] `http://ec.europa.eu/eurostat/statistics-explained/index.php/Freight_transport_statistics/`, April 2016.

[2] `http://www.bp.com/en/global/corporate/energy-economics/statistical-review-of-world-energy/oil/oil-prices.html`, August 2016.

[3] `http://www.dieselnet.com/standards/eu/hd.php`, April 2016.

[4] Wong J.Y. *Theory of Ground Vehicles.* John Wiley and Sons, Inc., 3 edition, 2001.

[5] Barnard R.H. *Road Vehicle Aerodynamic Design.* MechAero Publishing, 2 edition, 2001.

[6] `http://ec.europa.eu/transport/road_safety/specialist/knowledge/speed/speed_limits/current_speed_limit_policies.htm`, October 2011.

[7] `http://www.iihs.org/laws/speedlimits.aspx`, October 2011.

[8] Aurell J. and Wadman T. *Vehicle Combinations Based on the Modular Concept.* Nordiska Vägtekniska Förbundet, 2007.

[9] Åkerman I. and Jonsson R. *European Modular Concept for Road Freight Transport - Experiences and Possibilities.* ISBN 13:978-91-85665-07-5, 2007.

[10] Odhams AMC., Roebuck RL., Lee YJ., Hunt SW., and Cebon D. *Factors Influencing the Energy Consumption of Road Freight Transport.* Journal of Mechanical Engineering Science, 2009.

[11] Backman H. and Nordström R. *Improved Performance of European Long Haulage Transport.* ISBN 91-88752-38-0, 2002.

[12] Burgess A., van der Engel A.W., Kindt M.R.J., Schoemaker J.T., Groen R.J., and Gützkov P. *European Modular System Paper.* R20100085/31238000/MKI/LJO, 2010.

[13] Hjelm L. and Bergqvist B. *European Truck Aerodynamics - A Comparison Between Conventional and CoE Truck Aerodynamics and a Look into Future Trends and Possibilities.* The Aerodynamics of Heavy Vehicles II: Trucks, Buses, and Trains, 2007.

[14] `http://ops.fhwa.dot.gov/freight/publications/size_regs_final_rpt/index.htm#length`, October 2011.

[15] `http://www.volvotrucks.com/trucks/sweden-market/sv-se/trucks/Bildbank/Pages/image_bank.aspx`, June 2016.

[16] `http://eur-lex.europa.eu/legal-content/EN/TXT/HTML/?uri=CELEX:32015L0719&from=FR`, April 2016.

[17] Hucho W.H. *Aerodynamics of Road Vehicles*. Society of Automotive Engineers, Inc., 4 edition, 1998.

[18] Tritton D J. *Physical Fluid Dynamics*. Clarendon Press, 2nd edition edition, 1988.

[19] Cooper K.R. *The Effect of Front-Edge Rounding and Rear-Edge Shaping on the Aerodynamic Drag of Bluff Bodies in Ground Proximity*. SAE Technical Paper 850288, 1985.

[20] Söderblom D. *Investigation of Wheel Housing Flow on Heavy Trucks*. Licentiate Thesis, Chalmers University of Technology, 2009.

[21] Saltzman E.J. and Meyer Jr. R.R. *A Reassessment of Heavy-Duty Truck Aerodynamic Design Features and Priorities*. NASA/TP-1999-206574, 1999.

[22] Cooper K.R. *Truck Aerodynamics Reborn - Lessons from the Past*. SAE Technical Paper 2003-01-3376, 2003.

[23] Håkansson C. and Lenngren M. *CFD Analysis of Aerodynamic Trailer Devices for Drag Reduction of Heavy Duty Trucks*. Master's Thesis, Chalmers University of Technology, 2010.

[24] Gullberg P. *Optimization of the Flow Process in Engine Bays - 3D Fan Modeling Strategies*. Licentiate Thesis, Chalmers University of Technology, 2009.

[25] Larsson L. and Martini H. *Aerodynamic Drag Reduction of a Heavy Vehicle with Variable Cooling Air Intake Area*. Master's Thesis, ISSN 1652-8557, Chalmers University of Technology, Sweden, 2009.

[26] Pfeifer C. *Evolution of Active Grille Shutters*. SAE Technical Paper 2014-01-0633, 2014.

[27] Hallqvist T. *The Cooling Airflow of Heavy Trucks – a Parametric Study*. SAE Technical Paper 2008-01-1171, 2008.

[28] Williams J. *Aerodynamic Drag of Engine-Cooling Airflow With External Interference*. SAE Technical Paper 2003-01-0996, 2003.

[29] Larsson L. *Investigation of Rear-Mounted Cooling Module Installations for Heavy Vehicles*. Licentiate Thesis, Chalmers University of Technology, 2011.

[30] Gilhaus A., Hau E., Künstner R., and Potthoff J. *Über den Luftwiderstand von Fernlastzügen, Ergebnisse aus Modellmessungen im Windkanal – Teil I*. Number 3/79. Automobil-Industrie, 1979.

[31] Gilhaus A., Hau E., Künstner R., and Potthoff J. *Über den Luftwiderstand von Fernlastzügen, Ergebnisse aus Modellmessungen im Windkanal – Teil II*. Number 3/80. Automobil-Industrie, 1980.

[32] Göhring E. and Krämer W. *Auswirkung aerodynamischer Massnahmen auf Kraftstoffverbrauch und Fahrleistung moderner Nutzfahrzeuge – Teil 2*. Number 87. Automobiltechnische Zeitschrift, 1985.

[33] Göhring E. and Krämer W. *Auswirkung aerodynamischer Massnahmen auf Kraftstoffverbrauch und Fahrleistung moderner Nutzfahrzeuge – Teil 3*. Number 88. Automobiltechnische Zeitschrift, 1986.

[34] Watkins S. and Vino G. *The Effect of Vehicle Spacing on the Aerodynamics of a Representative Car Shape*. Journal of Wind Engineering and Industrial Aerodynamics, 2008.

[35] Browand F. and Hammache M. *The Limits of Drag Behaviour for Two Bluff Bodies in Tandem*. SAE Technical Paper 2004-01-1145, 2004.

[36] Castellucci P. and Salari K. *Computational Simulation of Tractor-Trailer Gap Flow with Drag-Reducing Aerodynamic Devices*. SAE Technical Paper 2005-01-3625, 2005.

[37] Schoon R. and Fongloon P.P. *Practical Devices for Heavy Truck Aerodynamic Drag Reduction*. SAE Technical Paper 2007-01-1781, 2007.

[38] Barnard R.H. *Theoretical and Experimental Investigation of the Aerodynamic Drag due to Automotive Cooling Systems*. Proc Institute of Mechanical Engineers Vol. 214 Part D. IMechE, 2000.

[39] Kuthada T. and Wiedemann J. *Investigations in a Cooling Air Flow System under the Influence of Road Simulation*. SAE Technical Paper 2008-01-0796, 2008.

[40] Baeder D., Indinger T., Adams N., and Decker F. *Comparison of Numerical Simulations with Experiments of Bluff Bodies Including Under-Hood Flow*. SAE Technical Paper 2011-01-0171, 2011.

[41] Larsson L., Wiklund T., and Löfdahl L. *Cooling Performance Investigation of a Rear Mounted Cooling Package for Heavy Vehicles*. SAE Technical Paper 2011-01-0174, 2011.

[42] Larsson L., Löfdahl L., Dahl E., and Wiklund T. *Continuing Cooling Performance Investigation of a Rear Mounted Cooling Package for Heavy Vehicles*. SAE Technical Paper 2011-01-2285, 2011.

[43] Panton R.L. *Incompressible Flow*. John Wiley and Sons, Inc., 2005.

[44] White F.M. *Fluid Mechanics*. 5th Edition, McGraw-Hill, New York, 2005.

[45] `http://www.cfd-online.com/Wiki/Navier-Stokes_equations`, April 2016.

[46] CD-Adapco, STAR-CCM+ Manual, Version 9.06.009 Edition.

[47] `http://www.cfd-online.com/Wiki/Favre_averaged_Navier-Stokes_equations`, May 2016.

[48] `http://www.cfd-online.com/Wiki/Boussinesq_eddy_viscosity_assumption/`, May 2016.

[49] Shih T-H., Liou W.W, Shabbir A., Yang Z., and Zhu J. *A New K-Epsilon Eddy Viscosity Model for High Reynolds Number Turbulent Flows*, volume 24. Computers Fluids, 1995.

[50] *Best Practise Guidelines for Handling Automotive External Aerodynamics with FLUENT*. FLUENT, 2005.

[51] `http://www.beta-cae.gr/`, May 2016.

[52] `http://www.cd-adapco.com`, April 2016.

[53] `http://www.ilight.com/en/`, May 2016.

[54] `http://www.svenskanarko.com/index1024.html`, June 2011.

[55] `http://www.parator.com/`, June 2011.

[56] `http://www.volvogroup.com/`, May 2016.

[57] `http://www.nrc-cnrc.gc.ca/eng/solutions/facilities/wind_tunnel/nine_metre.html`, May 2016.

[58] Martini H., Gullberg P., and Löfdahl L. *Comparative Studies between CFD and Wind Tunnel Measurements of Cooling Performance and External Aerodynamics for a Heavy Truck*. SAE Int. J. Commer. Veh. 7(2):2014, 2014.

[59] Martini H., Bergqvist B., Hjelm L., and Löfdahl L. *Influence of Different Truck and Trailer Combinations on the Aerodynamic Drag*. SAE Technical Paper 2011-01-0179, 2011.

[60] Martini H., Bergqvist B., Hjelm L., and Löfdahl L. *Aerodynamic Effects of Roof Deflector and Cab Side Extenders for Truck-Trailer Combinations*. SAE Technical Paper 2011-01-2284, 2011.

[61] Martini H., Bergqvist B., Hjelm L., and Löfdahl L. *Aerodynamic Investigation of Gap Treatment- and Chassis Skirts Strategies for a Novel Long-Haul Vehicle Combination*. SAE Int. J. Commer. Veh. 5(2):2012, 2012.

[62] Chronéer Z. Volvo GTT, Personal Communication, May 2011.

[63] Bergqvist B. Volvo GTT, Personal Communication, September 2011.

[64] `http://www.euro4m.eu/downloads/euro4m_CIB_temperature.pdf`, May 2016.

[65] Gullberg P. Volvo GTT, Personal Communication, May 2016.

[66] Gullberg P., Löfdahl L., Adelman S., and Nilsson P. *An Investigation and Correction Method of Stationary Fan CFD MRF Simulations.* SAE Technical Paper 2009-01-3067, 2009.

[67] Martini H., Gullberg P., and Löfdahl L. *Aerodynamic Analysis of Cooling Airflow for Different Front-End Designs of a Heavy-Duty Cab-over-Engine Truck.* Submitted to SAE Int. J. Commer. Veh., 2016.

[68] Martini H., Gullberg P., and Löfdahl L. *Perspectives of Aerodynamic Drag and Thermal Management for an Elongated Heavy-Duty COE Truck with Ducted Cooling Air Inlets and Outlets.* Submitted to SAE Int. J. Commer. Veh., 2016.

[69] Landman D., Wood R., Seay W., and Bledsoe J. *Understanding Practical Limits to Heavy Truck Drag Reduction.* SAE Technical Paper 2009-01-2890, 2009.

[70] `www.duo2.nu`, June 2016.